The study of primary production in plankton blooms driven by riverine inputs of nutrients and fresh water in ROFI (region of freshwater influence)

Yasuhiro Hoshiba

Division of Ocean and Atmospheric Science,
Graduate School of Environmental Science,
Hokkaido University

Abstract

Rivers transport nutrients and suspended sediment matter (SSM) as well as fresh water from land to coastal regions, where the biological productivity is high. In the coastal area, the buoyancy of fresh water leads to the formation of horizontal anticyclonic gyres and vertical circulations, which affect the variation of biological production such as plankton blooms. However, the primary production caused by the three-dimensional dynamics have not been quantitatively discussed, and observations can hardly capture the daily temporal variations of phytoplankton blooms. We developed an ocean general circulation model (OGCM) including a simple ecosystem model, to investigate the three-dimensional and temporal changes in phytoplankton blooms caused by riverine input such as flooding.

We first conducted ideal setting-simulations. The distribution patterns of nutrients and phytoplankton differ significantly from that of fresh water. The phytoplankton maxima shift from the downstream (right-hand side of the river mouth) to the upstream regions (left-hand side of the river mouth). The shift from the downstream to the upstream region (D-U Shift) is categorized by the different nitrate origins: (1) river-originated nitrate (RO-nitrate) is dominant in the downstream region; (2) subsurface-originated nitrate (SO-nitrate) is dominant in the upstream region, and is transported by upwelling associated with vertical circulation and horizontal anticyclonic gyre; and (3) regenerated nitrate (R-nitrate) is dominant in the upstream region. The total primary production in phytoplankton blooms is maintained not only by RO-nitrate but also by SO-nitrate that is 1.5 times larger than the river-originated.

Next, we conducted the realistic simulation of Ishikari Bay and a few ideal setting-simulations. The phytoplankton maxima shift toward the left-hand side of the river mouth during the early time, but the shift does not keep going to the left-hand side all the time. This is because much SO-nitrate does not come from the subsurface to the surface layer after the middle simulated time, due to weak upwelling forced by vertical circulation in the left-hand side. The gentle angle of bottom slope weaken the vertical circulation and SO-nitrate supply from the subsurface, and the NPP is small.

It is natural that D-U Shift of phytoplankton maxima often occurs in the real situation like Ishikari Bay when high riverine input such as flooding. The conclusion that the shift is categorized into three stages by the different nitrate origins, RO-, SO- and R-nitrates in turn depends on the bottom slope angle and the way of inputs and the amounts of fresh water and nutrients. Bottom slope angle and the way of fresh water input change the behaviour of plumes, nutrient supply from the subsurface with the change of vertical circulation, and the rate of regeneration.

Contents

Chapter 1 General Introduction

1.1 Region Of Freshwater Influence (ROFI)

Nutrients and suspended sediment matter (SSM) are derived from river discharge (Le *et al*., 2006; Usui *et al*., 2006). River discharge has influence on coastal areas, where biological productivity is high (Costanza *et al*., 1997). Fresh water is supplied as a buoyant input into large areas of the shelf seas adjacent to estuaries where was termed regions of freshwater influence (ROFIs) by Simpson (1997). In ROFI, freshwater inputs induce horizontal river plumes with anticyclonic gyres due to geostrophic adjustment, and vertical circulation composed of the surface water flows from the coast to offshore and a subsurface counter-flow with upwelling occurs near the coast (Rattray and Hansen, 1962). The strength of circulation depends on the density difference between the river derived fresh water input and the coastal sea water. These horizontal and vertical flows transport nutrients and SSM from the river mouth into ROFI. ROFIs in the subarctic regions have seasonal changes in nutrients in the surface water, which are abundant from winter to spring but depleted from summer to autumn (Kudo *et al*., 2007; Yoshimura and Kudo, 2011). Phytoplankton blooms occur due to regularly large amounts of riverine discharge by snowmelt and/or a few days pulse of riverine discharge due to heavy rains (*e.g*., Agboola *et al*., 2009).

1.2 Anticyclonic gyres spreading and propagating towards the upstream region

In this study, when we look offshore from the river mouth, we call the left-hand side ‘upstream’ and the right-hand side ‘downstream’ the same as in previous studies (*e.g.*, McCreary *et al*., 1997; Yankovsky, 2000; Magome and Isobe, 2003). The downstream is the propagated direction of the Kelvin wave.

The buoyant inflow from the river mouth in flooding forms an anticyclonic gyre that often spreads and propagates towards the upstream region. Propagations of river plumes to the upstream area have been reported in various river systems (*e.g.*, the Changjiang River; Beardsley *et al.*, 1985, major Siberian rivers in the Arctic; Weingartner *et al.*, 1999, the Mississippi River; Walker *et al.*, 1994, the Ganges River; Murty *et al.*, 1992, the La Plata River; Piola *et al.*, 2008, some rivers in the Suo-Nada in Japan; Magome and Isobe, 2003). The Figure 1 in Matano and Palma (2010) showed chlorophyll-a observed by satellite propagating to the upstream. The prerequisite condition of propagating to the upstream occurring is that the width of the river mouth is smaller than the internal deformation radius calculated from the density difference between the river and the sea waters. Propagating to the upstream generally does not occur if the river mouth width is wider than the internal deformation radius (*e.g.*, the exp.1 of Chao and Boicourt, 1986; the width of the river mouth is 15 km). The gyre propagating can be explained by the method of mirror image (Kubokawa, 1991). McCreary *et al*. (1997) also explains that the proceeding to the upstream results from the downward frontal current generated by geostrophic adjustment, and the upward coastal jet established by Kelvin-wave propagation from the plume nose thining the layer within the plume. The strength of propagating depends on the outflow amount from the river mouth, the density difference between the river and the sea waters, topography around the river mouth, and so on. There are a lot of previous studies

related to this propagating of anticyclonic gyres (*e.g.*, Chapman and Lentz, 1994; Yankovsky, 2000).

1.3 Objective of this study

There are a lot of previous studies discussing the physics of horizontal anticyclonic gyres (*e.g*., Garvine, 2001; Nof and Pichevin, 2001; Pimenta *et al*., 2011), but limited quantitative studies focusing on the primary production increased by gyres. The relationship between the vertical circulation and primary production has been studied using a box model (Yamamoto and Hashimoto, 2007). Observations of phytoplankton blooms in ROFI have been also conducted (*e.g.*, Beman *et al*., 2005; Agboola *et al*., 2009; Yoshimura and Kudo, 2011). However, box models cannot represent three-dimensional dynamics, and observations can hardly capture the daily temporal variations of phytoplankton blooms.

In this study, we applied an OGCM with simple ecosystem model to investigate three-dimensional and temporal variations of plankton bloom caused by flooding in ROFI. The OGCM was set to have fine resolution (~1 km) near the river mouth to represent the spatial variation in detail, although conventional models have been often had coarse resolution (about 10 km). The sensitivity of ecosystem process depends on each region, and we assume the region as a subarctic, due to the affinity to Hokkaido, Japan. In the next chapter, we discuss the phytoplankton bloom in the case of a simple rectangular simulation. In chapter 3, we also present the simulation results based on the real situation such as the Ishikari Bay in the spring, 2007. In chapter 4, we have the general conclusion.

Chapter 2 Along-coast shifts of plankton blooms driven by riverine inputs of nutrients and fresh water onto the coastal shelf

2.1 Introduction

Simpson (1997) termed large areas of the shelf seas adjacent to estuaries as regions of freshwater influence (ROFI) and classified into them four types: open coast, corner source, gulf and gulf with sill. Open coast ROFI, assumed in this study, is the simplest situation that the estuarine discharge enters the sea on a straight coast. The Tokachi River, for example of the open coast ROFI, the second largest discharge in Hokkaido, had steady large amounts of discharge in spring (April to June) and two pulses of discharge in August and October in 2006 (Figure 2.1), and the river mouth of 1 km width. The daily mean discharge on 19th August, 2006 amounted to 1865 m^3/s. In the ROFI of Tokachi River, the Oyashio current flows off the Hokkaido coast from northeast to southwest. The Oyashio flow and wind-driven flow have influences on the temporal and spatial variations of river plumes (Lihan *et al.*, 2008), but effects of background flows were not considered in this chapter. Before applying the realistic simulation, we introduce a simple simulation such as no tides and background flows, as a first step, in order to focus on the response of ecosystem and biogeochemical cycles to river flows.

Fresh water from the river is muddy due to SSM (*e.g.*, sand, silt, and other terrestrial

inorganic particles). The relationship between river discharge and turbidity is well known as the empirical L-Q equation: the SSM concentration from the river is larger as the flux of river discharge becomes larger. When SSM in fresh water mixes with the sea water, SSM particles aggregate due to the pH difference between the river and the sea water, and are removed from the sea water as settling sediment particles (Kusuda, 2003). The rate of removal from the water as settling sediment particles is larger with larger particle-size of SSM, according to Stokes' law. High turbidity (*i.e.*, SSM concentration increases with freshwater flux) tends to shade sunlight and prevent phytoplankton from photosynthesis, when the freshwater flux is larger (Kaiser *et al*., 2005). The case study introducing SSM is conducted in the discussion part (2.4.4) to investigate the response of ecosystem and biogeochemical cycles to river flows.

2.2 Model and Method

2.2.1 Model

The model used in this study is an OGCM, the Center for Climate System Research (CCSR) Ocean Component Model (COCO) version 4.0 (Hasumi, 2002). We dealt with fresh water and nutrient flowing from a river into the ocean which has the simplified rectangular domain on f-plane (about 43°N, Figure 2.2). The domain was large enough not to affect the river plume. The horizontal grid sizes are approximately 1 km (x-direction) and increasing from 1 km near river mouth to 20 km far from the river mouth (y-direction). The model has ten vertical layers with thickness increasing from 10 m at the surface to 40 m at the bottom. The depth to the ocean floor varied from 30 m near shore to 200 m for the offshore (Figure 2.2). We used the Quadratic

Upstream Interpolation for Convective Kinematics with Estimated Streaming Terms (QUICKEST; Leonard, 1979) and the Uniformly Third-Order Polynomial Interpolation Algorithm (UTOPIA; Leonard *et al*., 1993) as the vertical and horizontal tracer advection schemes, respectively. The diffusion coefficient along and across the isopycnal was set to 1.0×10^6 cm^2/s with a maximum slope of 0.01. The horizontal diffusion coefficient was set to 1.0×10^6 cm^2/s and the vertical diffusion coefficient was 0.5 cm^2/s. These values are defaults in the model (COCO ver.4) except the vertical diffusion coefficient. The somewhat large coefficient relative to the default value (about 0.1 cm^2/s; Tsujino *et al.,* 2000) was determined due to the effects of vertical mixing in coastal regions. A biharmonic friction with a Smagorinsky-like viscosity (Griffies and Hallberg, 2000) was used for momentum with a scaling constant C = 3.0 in their notation. The initial salinity was assumed to be constant (33.5 g/kg) throughout the region, and the initial temperature was constant horizontally (Figure 2.4 (e)).

We incorporated a simple ecosystem part, based on the four-compartment version in Yoshikawa *et al*. (2005), into OGCM (Figure 2.3). The four state variables are composed of nutrient assumed to nitrate, phytoplankton, zooplankton and detritus. The concentrations of components are calculated by individual biological processes (*i.e.*, photosynthesis, grazing, etc.) as nitrogen fluxes, except physical processes of diffusion and advection. The biological parameters used in this study are summarized in Table 1, most of which were based on those in Yoshikawa *et al*. (2005). The time step of the hydrodynamic model was 2 minutes. After a spin-up of 10 years with the ecosystem model, we used the distributions of nitrate, phytoplankton, zooplankton and detritus as initial conditions of the experiments driven by river input (Figure 2.4 (a)-(d)). The 10

years were enough that the distributions of NPZD became a quasi-steady state due to the diffusion and the ecosystem cycle in the model.

In all experiments except experiment #4 (Table 2), we put the freshwater input as 2,000 m^3/s (the peak discharge rate from Fig. 2.1), with the same surface temperature, into river mouth region of 20 km × 3 km for the first 2 days and no discharge for the other 98 days. Nitrate concentration of 1.0 mg/l, a typical value representative of rivers in Hokkaido, Japan (Tachibana *et al*., 2001; Ileva *et al*., 2009), in the fresh water was also used. In experiment #4, we put the freshwater input as 100 m^3/s for 40 days with a nitrate concentration of 1.0 mg/l, which is the same total freshwater volume and nitrate amount discharged as in the other experiments but a long-term input, and no discharge for the other 60 days. We confirmed that the results in the two experiments; an averaged discharge of 100m^3/s instead of no discharge as the initial condition, and the averaged 100m^3/s discharge instead of no discharge after high discharge were almost the same as those in the experiment #1 (not shown).

In experiment #5, we also give SSM input given by an empirical equation for the Tokachi River, Hokkaido (T. Irino, *personal communication*),

$$[\mathrm{SSM}] = 0.00331 \times \mathrm{MF}^{1.685} \qquad (1)$$

where [SSM] (g/m^3) is the concentration of SSM, MF (m^3/s) is the mass flux of freshwater input. SSM is transported as a passive tracer and is gradually removed from the sea water according to the following equation:

$$\frac{\partial[\mathrm{SSM}]}{\partial \mathrm{t}} = (\mathrm{Adv.}) + (\mathrm{Dif.}) - \frac{1}{\tau}[\mathrm{SSM}] \qquad (2)$$

where (Adv.) and (Dif.) represent advection and diffusion terms as physical processes, and τ is the removal time for SSM. SSM is faster removed as its size is bigger. Following Kusuda *et al*. (1978), aggregated clay particles (0.2 to 0.5 mm diameter) in

salty water have precipitated at the sinking speed of 0.2 to 0.5 mm/s. As this sinking speed is approximately equivalent to the removal time of τ = 0.5 to 2.0 days, we conducted four parameter studies as τ = 0.5, 1.0, 1.5, 2.0 days. The effect of shading sunlight due to SSM was included as follows: light intensity (*I*) at the depth *z* is

$$I = I_0 \exp(-\int_0^z \kappa dz) \quad (3)$$

$$\kappa = \alpha_1 + \alpha_2[PHY] + \alpha_{SSM}[SSM] \quad (4)$$

where I_0 is the isolation at the sea surface (I_0 = 135 W/m^2), imposed as the boundary condition, and α_{SSM} (Table 2.1) is the coefficient of shading light due to SSM.

2.2.2 Numerical experiments

We conducted five experiments for 100 days (Table 2.2). In experiment #1 (hereafter referred as the control case), we initiated the model with freshwater and nutrient inputs for two days but no SSM input. Experiment #2 (no flux-case) without all inputs was conducted as the base line condition, and we discussed most of simulation results as differences from those in the no flux-case. Experiment #3 was designed to clarify the direct effect of river-originated nutrient comparing with Experiment #1. Experiment #4 demonstrates the different pattern of river input, *i.e.*, long-term input of 40 days instead of two days. In experiment #5, we dealt with SSM to demonstrate the shading effect by SSM.

2.3 Results

The buoyant inflow from the river mouth forms an anticyclonic gyre due to

geostrophic adjustment. The horizontal salinity distributions with current velocity in the surface layer (5 m depth) in the control case are shown in Figure 2.5 (a). The buoyant water in the anticyclonic gyre continues downstream as a coastal current trapped against the wall as a Kelvin Wave (*e.g.*, Bowden, 1983). The anticyclonic gyre spreads and propagates towards the upstream region with time. It is natural to propagate to the upstream occurring, because the width of the river mouth is 3 km in this study, which is smaller than the internal deformation radius (~ 10 km). The flow of gyres determines both distributions of salinity and nitrate (Figure 2.5 (b)). Both distributions are similar until Day 6. Nitrate-rich freshwater spreads from the river mouth, bends to the right, and is transported to the downstream while being trapped against the coast. However, the distribution pattern of nitrate gradually becomes different from that of salinity as time progresses. Nitrate maxima tend to locate in the upstream region rather than the river mouth. This is because upwelling, forced by vertical circulation, occurs in the upstream region due to the anticyclonic gyre. The upwelling supplies nutrient-rich water from the subsurface layer to the surface (Figure 2.6 (a), (b)). As an advantage of the three-dimensional model, we can obtain upwelling in the upstream region as a combination of horizontal anticyclonic gyre and vertical circulation. The horizontal anticyclonic gyre transports coastal surface water to the offshore in the upstream region where upwelling forced by vertical circulation is formed. Therefore, upwelling occurs mainly in the upstream region, and the coastal upwelling region spreads to the upstream with horizontal anticyclonic gyre propagating toward the upstream region (Figure 2.7).

Phytoplankton bloom occurs (Figure 2.5 (c)), which is maintained by nitrate supplied from the river at its first stage and from the subsurface layer at its subsequent stage, as

discussed in the next section. This shift of nutrient supply causes a location shift of phytoplankton maxima from the downstream to the upstream regions (hereafter we call this 'Downstream-to-Upstream shift (D-U Shift)'). Zooplankton bloom follows phytoplankton bloom with D-U Shift (Figure 2.5 (d)).

2.4 Discussion

2.4.1 Introducing nitrate colored by its origins

To clarify the dynamics of D-U Shift, we increased the number of nutrient-tracers and introduced nitrates categorized into three origins from the river, the subsurface layer, and via regeneration (hereafter we term these as river-originated nitrate, RO-nitrate; subsurface-originated nitrate, SO-nitrate; and regenerated nitrate, R-nitrate, respectively). RO-nitrate is the river nutrient input integrated over time, and the three nitrates are used by the ecosystem and recycled as R-nitrate (*i.e.*, there are no RO-nitrate and R-nitrate as initial condition). Net primary production (NPP) is also divided into three components, RO-NPP, SO-NPP and R-NPP, in proportion to the three origins of nitrates in nutrient uptake.

Total nutrient uptake occurs as a sequence of RO-NPP, SO-NPP and R-NPP with time (Figure 2.8 (a)). This time sequence is categorized into three stages by the primary origin of nitrate: RO-nitrate as the first stage (Day 0 to 7), SO-nitrate as the second stage (Day 8-19), and R-nitrate as its final stage (after Day 20). RO-NPP and SO-NPP decrease gradually in order, and are replaced by R-NPP. After Day 40, total NPP consists only of R-NPP.

D-U Shift can be explained by the shift of nitrate origins as the geographically different sources. D-U Shift is observed in total NPP (Figure 2.9 (a)). The maximum of total NPP located in downstream region is mainly made up of the RO-NPP in the first stage (Day 2 and 6 in Figure 2.9 (b)), which is caused by nitrate-rich freshwater spreading from the river mouth and transported to downstream by the anticyclonic gyre. There is a small area where the SO-NPP is less than that in the no flux-case in the first stage (the purple-colored region in Day 2 in Figure 2.9 (c)), due to the spread of discharged water without phytoplankton near the river mouth. In the second stage (after Day 6), the SO-NPP mainly appears in the upstream region. The bloom in the upstream region is dependent on SO-NPP associated with upwelling, as discussed in the previous section (Figure 2.10). In general, the R-NPP gradually increases where the concentration of phytoplankton is high. Therefore, the distribution of R-NPP follows the plankton bloom with D-U Shift (Figure 2.9 (d)): the R-NPP maxima are located in the downstream region in Day 10, and shifts to the upstream region in Day 22. As a result, D-U Shift is induced by the different nitrate origins: RO-nitrate in downstream at the first stage, SO-nitrate at the second, and SO- and R-nitrates in the upstream region.

The accumulated RO-, SO-, and R-NPP until Day 40 are 0.84, 1.26, and 1.42, respectively, to the total amount of river nitrate input. It is interesting that SO-NPP is 1.5 times larger than RO-NPP, *i.e.*, NPP in ROFI is maintained not only by RO-nitrate but also by SO-nitrate which is transported by vertical circulation, also with R-nitrate.

2.4.2 The case of freshwater flux without nutrient input

Even without a nutrient input, a phytoplankton bloom occurs caused by the vertical circulation (Figure 2.8 (b)), although the NPP maximum is less than that in the control case. Note that SO-NPP is also smaller than that in the control case, because the vertical circulation is the same as the control case but the phytoplankton concentration is lower. R-NPP is also less than that in the control case. The R-NPP is greater than the SO-NPP after Day 26 (Figure 2.8 (b)).

We found no local maximum NPP in the downstream region without nutrient discharge from river. That is, the local maximum of NPP is located in the upstream region all the time with a gradual propagating towards the more upstream region with time (Figure 2.11 (a)). Total NPP almost consists of SO-NPP until Day 14 (Figure 2.11 (a), (b)). High R-NPP domain appears after Day 10 due to R-nitrate increased by biological production where NPP is high at that time or was 4-5 days before that time, and propagates with time in the upstream region (Figure 2.11 (c)). Comparing these results with those in the control case, the phytoplankton bloom in the first stage of D-U Shift is made by nutrient-rich water input from the river mouth. Even without nutrient input from the river, vertical circulation and anticyclonic gyre forced by freshwater inputs make propagation of NPP distributions in the second stage of D-U Shift.

2.4.3 The difference between long and short durations of river discharge

Rivers in the subarctic zone often have flooding due to snowmelt and heavy rain in spring. D-U Shifts in the long-term input case are much slower than that in the control case (Figure 2.12 (a), (b)). In the case of long-term input, river input keeps a quasi-steady large flow until Day 40. High NPP region (over 4.0 mmol/m^2/day)

accompanied by the anticyclonic gyre expands bigger and propagates toward a more upstream region than that in the control case. In the near coast upstream region, the gyre has the along coastal flows to the upstream (*e.g.* Figure 9 in McCreary *et al.*, 1997), and therefore river water is transported towards the upstream region via turned to the left at the river mouth (‘initial left turn’). Total NPP is slowly increasing in the long-term input case (Figure 2.8 (c)), compared with that in the control case. The steady river input produces a gradual increase in RO-NPP, and the development of vertical circulation leads to a gradual increase in SO-NPP. Therefore, the phytoplankton maxima are smaller than that in the control case, but the duration of bloom is longer.

NPP is higher in upstream region than that in downstream, and high NPP domain is spreading towards a more upstream region with time (Figure 2.12 (a)). The initial left turn transports RO-nitrate to the upstream region, where NPP increases. As a result, the total accumulated NPPs in the long-term input case are higher in the upstream region (red-shaded) and lower in the downstream region (blue-shaded) than those in the control case, although these differences are small, about 5~7 % at most (Figure 2.12 (c)).

2.4.4 Introducing Suspended Sediment Matter (SSM) from river

What kind of impact does SSM have on the marine ecosystem in ROFI? SSM is introduced with freshwater input from river, and removed SSM from the water column for 1 day, as an example of the middle removal time of parameters (0.5 to 2 day).

High concentrations of SSM tend to shade sunlight and prevent phytoplankton from photosynthesis, as mentioned in the introduction.

During the first week (Day 0 to Day 8), NPP in SSM case is significantly lower than that of the no flux-case (Figure 2.8 (d)). This is because river-originated water with SSM spreads over the sea surface near the river mouth and covers phytoplankton already existing in the subsurface water. As a result, NPP in SSM case is low due to the effect of shading sunlight. The shift of the maximum peak of phytoplankton concentration to the upstream is delayed compared to that of the control case (Figure 2.13 (a), (b)), and the maximum peak arrives at the upstream region on day 24 (not shown). D-U Shift also occurs in the SSM case, but the shift differs from the control case as follows. As shown in Figure 2.8 (d), phytoplankton mainly utilize RO-nitrate, and do not exhaust it until the concentration of SSM is very low (Figure 2.14). Therefore, the duration of the first stage in D-U Shift is extended by around 4 days, and the situation of the high phytoplankton concentration in the downstream region is also kept for more days (Figure 2.13 (a)). Sunlight shading occurs due to high concentration of SSM (Day 2 and Day 6 in Figure 2.14 (a)). The surface concentration of phytoplankton is lower than that of the no flux-case near the river mouth and in the downstream region (Day 2), and the relatively low region (*i.e.*, the concentration of phytoplankton is lower than that of the no flux-case) spreads towards a more downstream region in Day 6. In Figure 2.14 (a) during Day 2 to Day 6, the domain where light reaches deeper (A-region; yellow ~ green) occurs surrounded by high shading domain (B-region; blue ~ purple), because the subsurface clear water comes due to strong upwelling. After Day 14, the small shading domain remains close to the river mouth associated with the high concentration of SSM in river water. The area

where the phytoplankton concentration is higher than 0.25 μgchl-a/l (light red in Figure 2.13) is smaller than that in the control case, but the bloom duration is longer and D-U Shift is delayed, as increasing rate of NPP in the surface is also slow.

We estimated how the removal time of SSM from sea water impacts the phytoplankton bloom in ROFI. As SSM removal time increases, NPP decreases because SSM inhibits photosynthesis. Thus when tau in equation (2) is longer, SSM settles out much later, the time to recover from the low NPP is delayed more, and the peak of the plankton bloom is delayed (Figure 2.15).

2.5 Conclusion and Remarks

In this study, we incorporated a simple ecosystem into an OGCM to investigate three-dimensional and temporal variations of plankton bloom in ROFI. Nutrient-rich river discharge drives phytoplankton bloom in ROFI. River also indirectly supplies nutrients with saline water from the subsurface to the surface by vertical circulation driven by the freshwater input.

The direct and indirect nutrient supplies produce the shift of phytoplankton maximum concentration from downstream to upstream regions (D-U Shift). D-U Shift is categorized into three stages by the different nitrate origins as follows: (1) phytoplankton increases using river-originated nitrate in downstream, (2) after river-originated nitrate is exhausted, phytoplankton increases mainly using subsurface-originated nitrate in the upstream region, where nitrate is supplied by the upwelling as a part of vertical circulation associated with horizontal anticyclonic gyre,

and (3) after subsurface-originated nitrate is also exhausted, NPP (Net Primary Production) is kept high by regenerated nitrate in upstream region.

In the case of freshwater input without nutrient, the maximum peak of phytoplankton concentration in the downstream part of D-U Shift does not occur, although a weak phytoplankton bloom occurs. Nutrient-rich water input has a significant impact on phytoplankton bloom in the first stage of D-U Shift. The buoyant flows due to freshwater input play an important role in the second stage. The vertical circulation by buoyant flows generates the upwelling from the nutrient-rich subsurface layer.

In the case of SSM input, NPP is significantly low during the first week, because river-originated water with high concentrations of SSM spreads over the sea surface near the river mouth, shades sunlight and prevents phytoplankton from photosynthesis. As SSM removal time form sea water increases, the time to recover from the low NPP is delayed more, and the peak of plankton bloom is delayed. D-U Shift occurs in the SSM case, although the shift to the upstream is delayed.

Effects of tide and background flow were not included in this chapter. If tide is included, the river plume spreading and propagating is horizontally suppressed, but the NPP is higher (see Appendix).

As the sensitivity of tide and background flow much depends on each region, we need the observation data *in situ* about tides and background flows in order to conduct more realistic simulations in specific ROFI.

Table 2.1 Biological parameters.

V_{max}	Phytoplankton Maximum Photosynthetic Rate at 0°C	0.5	/day
K_{NO3}	Phytoplankton Half Saturation Constant for Nitrate	2	μmolN/l
k	Phytoplankton Temperature Coefficient for Photosynthesis	0.0693	/°C
I_{opt}	Phytoplankton Optimum Light Intensity	104.7	W/m^2
M_{p0}	Phytoplankton Mortality Rate at 0°C	0.04375	l/μmolN/day
k_{Mp}	Phytoplankton Temperature Coefficient for Mortality	0.0693	/°C
R_{p0}	Phytoplankton Respiration Rate at 0°C	0.03	/day
k_R	Phytoplankton Temperature Coefficient for Respiration	0.0519	/°C
γ	Phytoplankton Ratio of Extracellular Excretion to Photosynthesis	0.135	(nodim.)
G_{Rmax}	Zooplankton Maximum Grazing Rate at 0°C	0.3	/day
k_G	Zooplankton Temperature Coefficient for Grazing	0.0693	/°C
l	Zooplankton Ivlev Constant	1.4	l/μmolN
P^*_Z	Zooplankton Threshold Value for Grazing	0.04	μmolN/l
α	Zooplankton Assimilation Efficiency	0.7	(nodim.)
β	Zooplankton Growth Efficiency	0.3	(nodim.)
M_{z0}	Zooplankton Mortality Rate at 0°C	0.0585	l/μmolN/day
k_{Mz}	Zooplankton Temperature Coefficient for Mortality	0.0693	/°C
α_1	Light Dissipation Coefficient of Sea Water	0.04	/m
α_2	Self Shading Coefficient	0.04	l/μmolN/m
α_{SSM}	Shading Coefficient due to SSM	0.6	m^2/g
S_{DET}	DET Sinking Velocity	20	m/day
V_{DN0}	Remineralization Rate of DET to Nitrate at 0°C	0.2	/day
K_{DN0}	Temperature Coefficient for DET Remineralization to Nitrate	0.0693	/°C

All values are based on those of Yoshikawa *et al*. (2005), except α_{SSM} is newly introduced in this study.

Table 2.2 Experiments in Chapter 2.

Experiment No.	1	2	3	4	5
Name	control	no flux	only fresh water	long-term input	SSM
Freshwater input	Yes	No	Yes	Yes	Yes
Nutrient input	Yes	No	No	Yes	Yes
SSM input	No	No	No	No	Yes
Duration of discharge	2 days	-	2 days	40 days	2 days

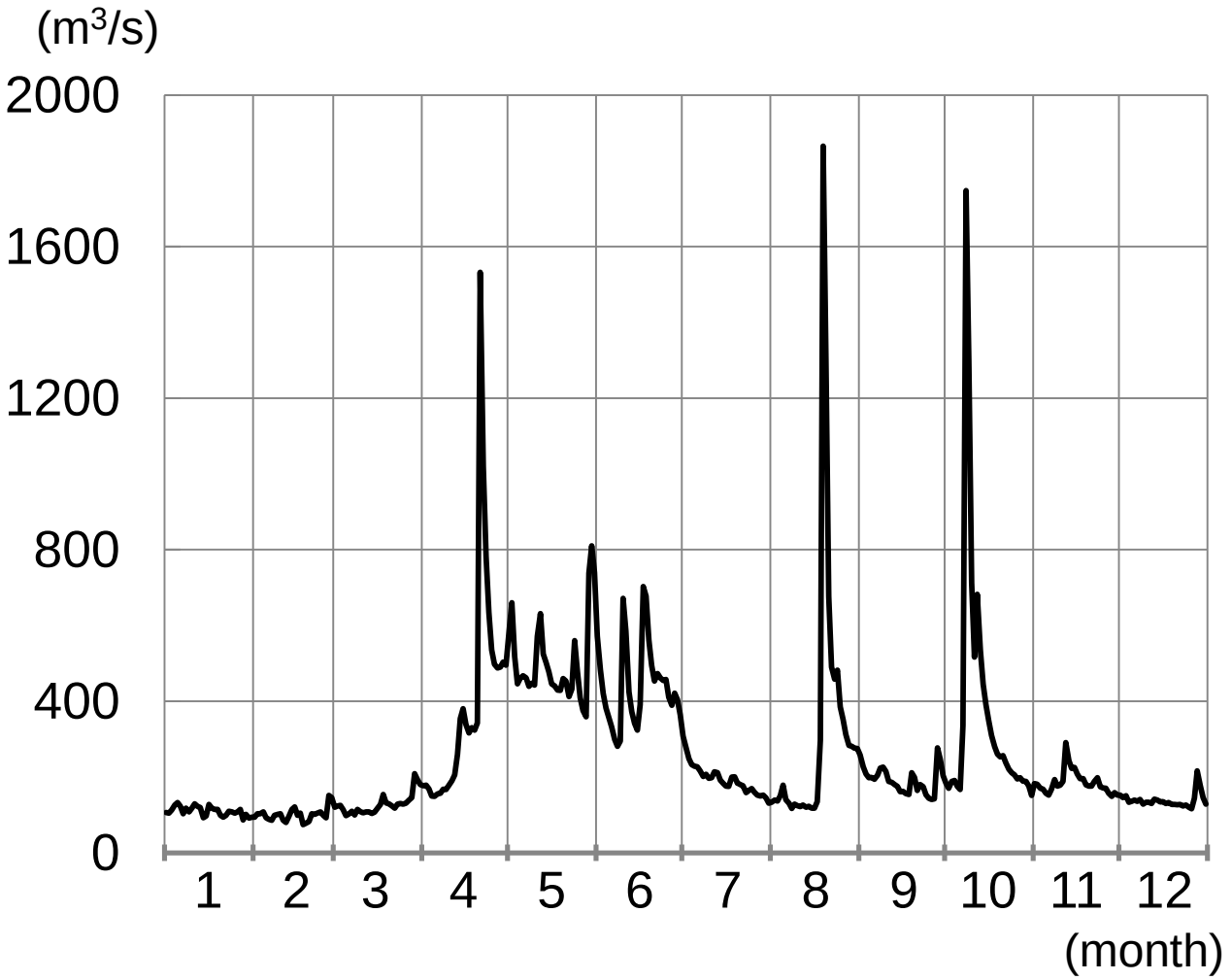

Fig. 2.1: River discharge at Moiwa near the river mouth of the Tokachi River in Hokkaido, Japan observed in 2006 (Ministry of Land, Infrastructure and Transport, Japan: http://www1.river.go.jp/).

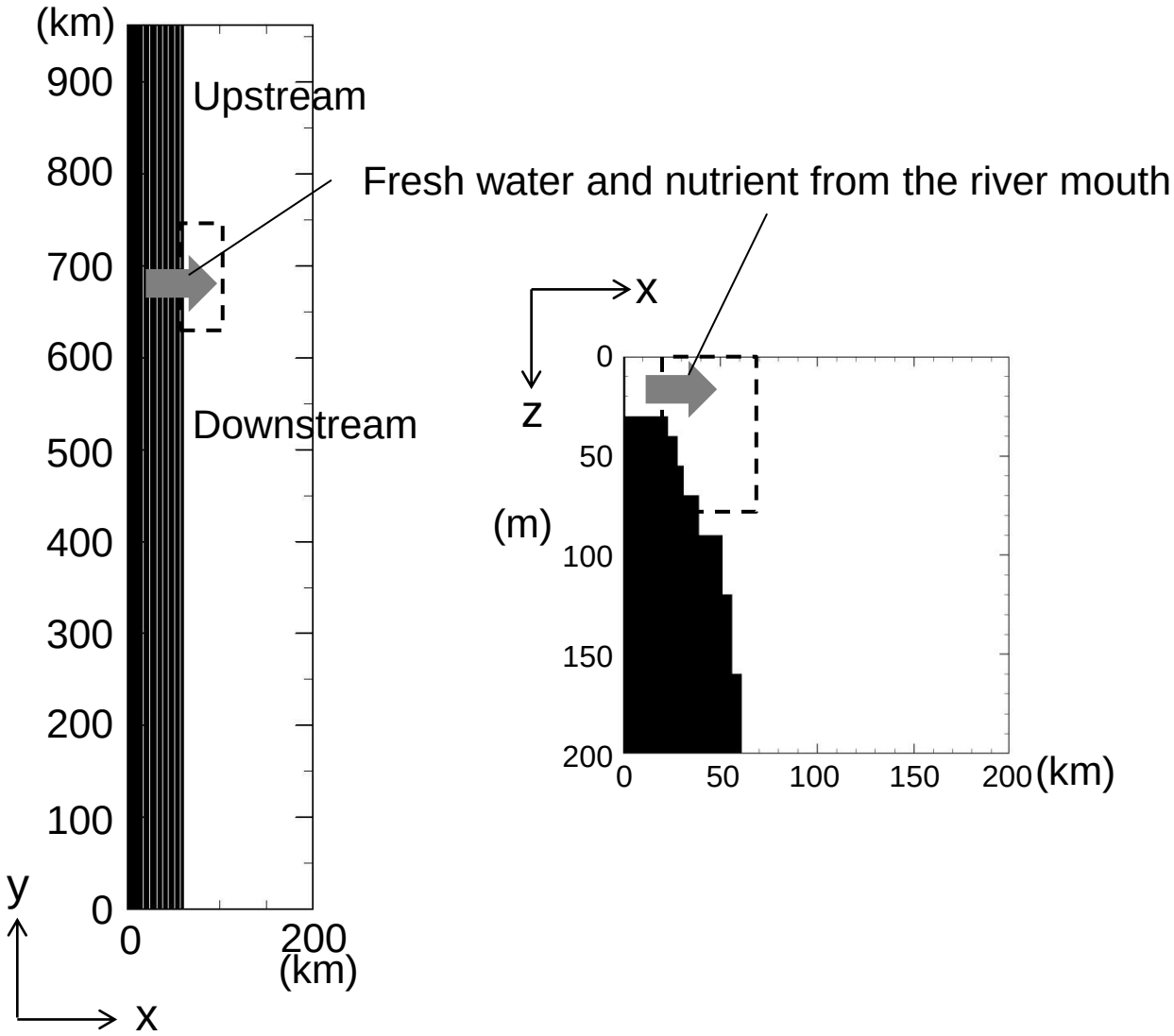

Fig. 2.2: Horizontal geography and vertical topography used in the model. The width of the river mouth is about 3km, the depth of ocean floor varied from 30 m near shore to 200 m in the offshore area. The dashed area shows the area drawn in figures 2.5, 2.6, 2.7, 2.9, 2.10, 2.11, 2.12, 2.13 and 2.14.

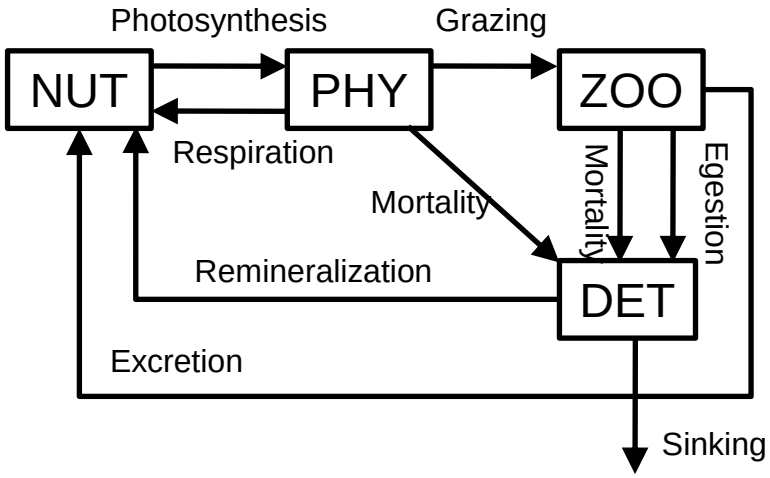

Fig. 2.3: Schematic view of interactions among the four components. The symbol NUT indicates the nitrate concentration, PHY phytoplankton, ZOO zooplankton, DET detritus.

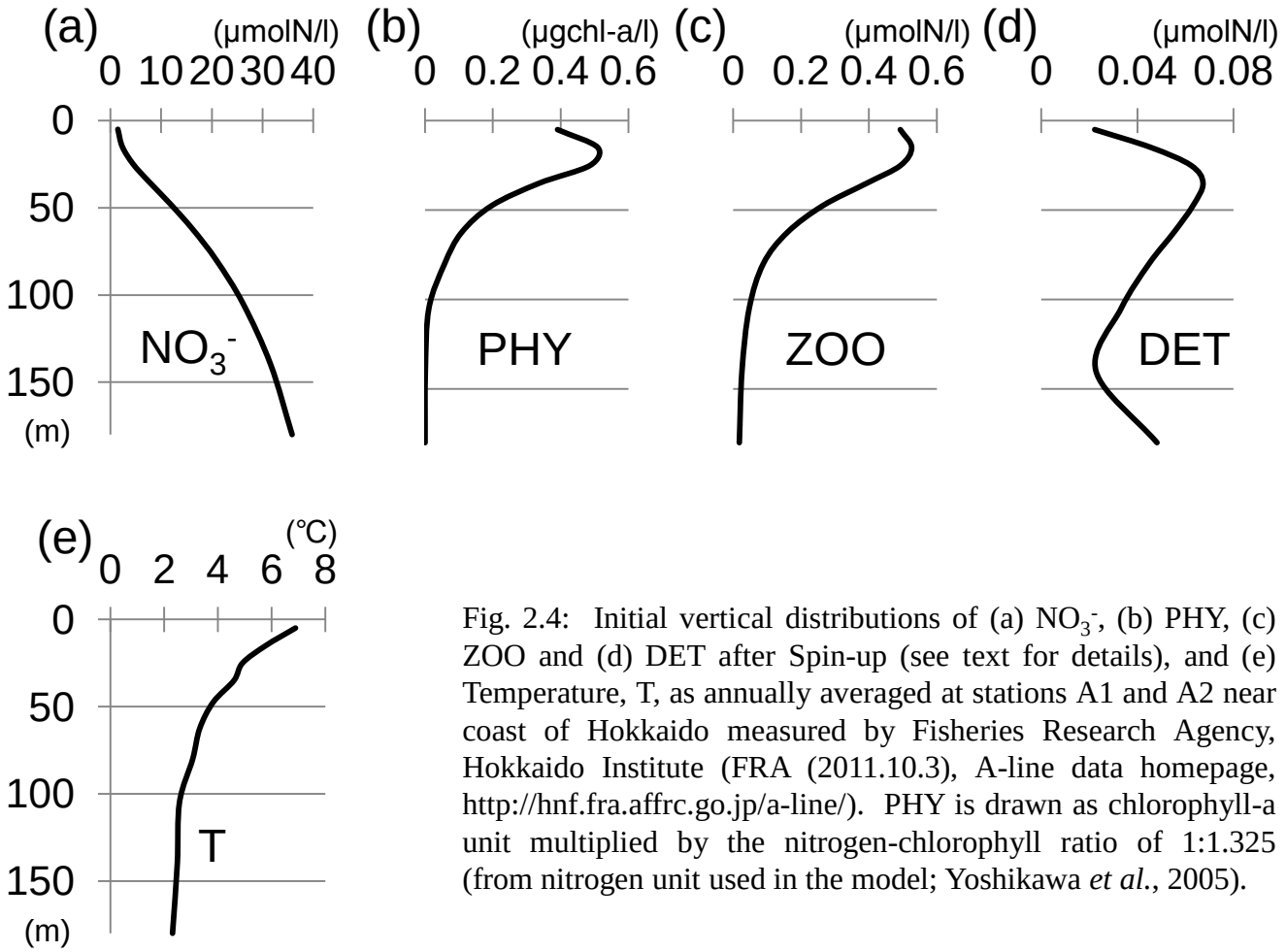

Fig. 2.4: Initial vertical distributions of (a) NO_3^-, (b) PHY, (c) ZOO and (d) DET after Spin-up (see text for details), and (e) Temperature, T, as annually averaged at stations A1 and A2 near coast of Hokkaido measured by Fisheries Research Agency, Hokkaido Institute (FRA (2011.10.3), A-line data homepage, http://hnf.fra.affrc.go.jp/a-line/). PHY is drawn as chlorophyll-a unit multiplied by the nitrogen-chlorophyll ratio of 1:1.325 (from nitrogen unit used in the model; Yoshikawa *et al.*, 2005).

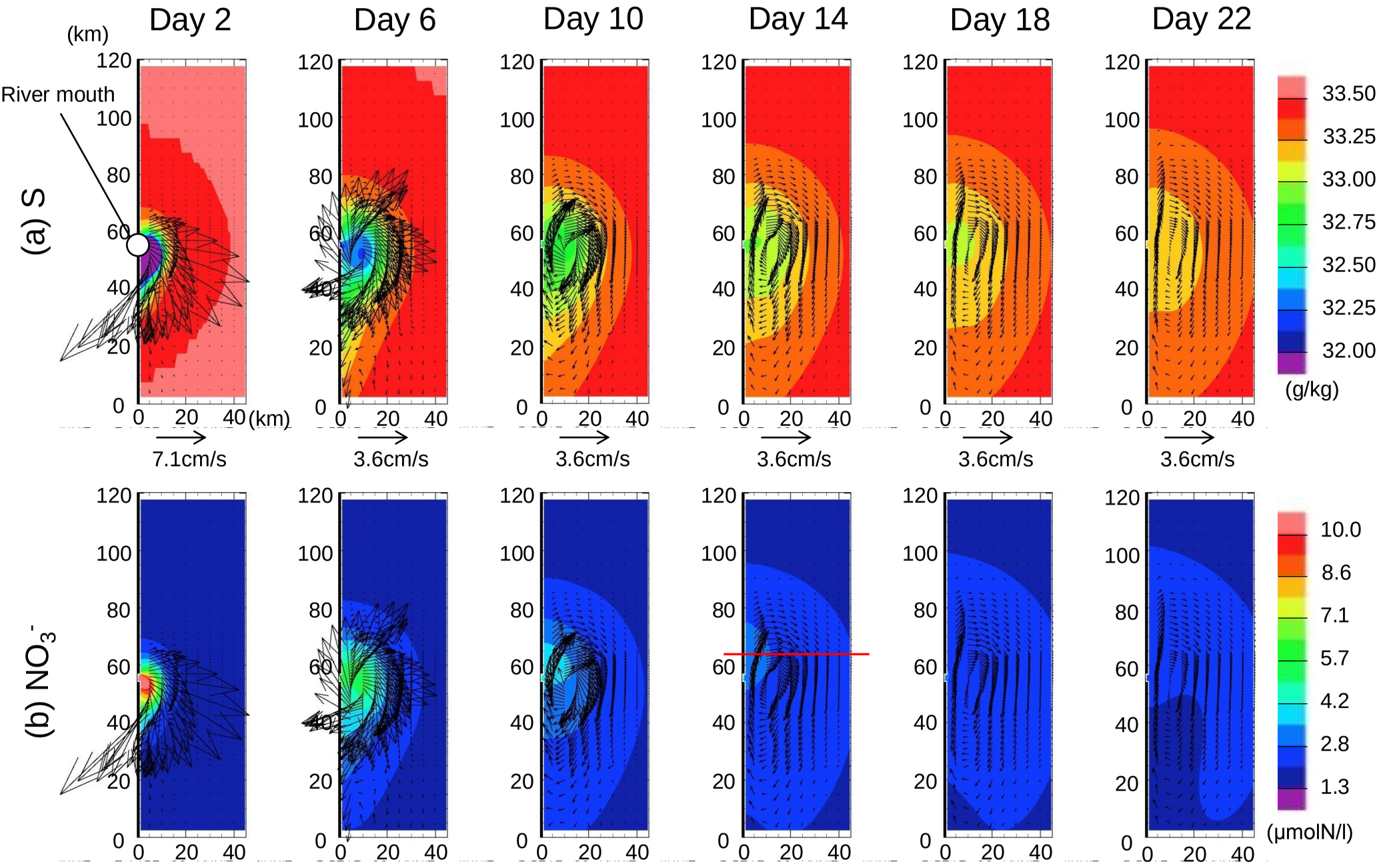

Fig. 2.5 (1): In the control case, the horizontal distributions of (a) salinity and (b) nitrate in the surface layer (5 m depth), with current velocity field whose vectors are drawn at intervals of five grids. Red line in (b) Day 14 shows the location of the vertical nearshore-to-offshore section detailed in Fig. 2.6.

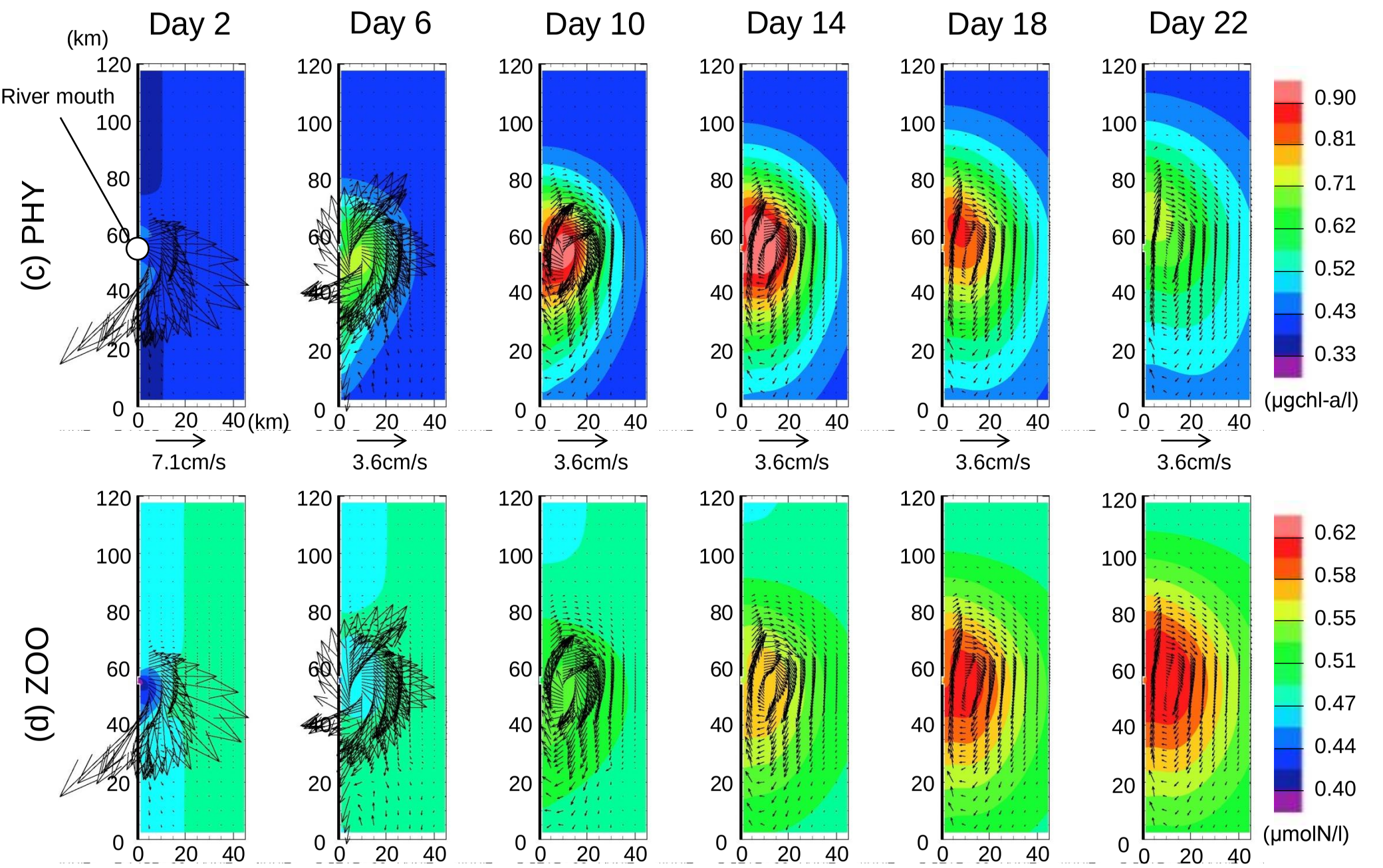

Fig. 2.5 (2): In the control case, the horizontal distributions of (c) phytoplankton and (d) zooplankton in the surface layer (5 m depth), with current velocity field whose vectors are drawn at intervals of five grids.

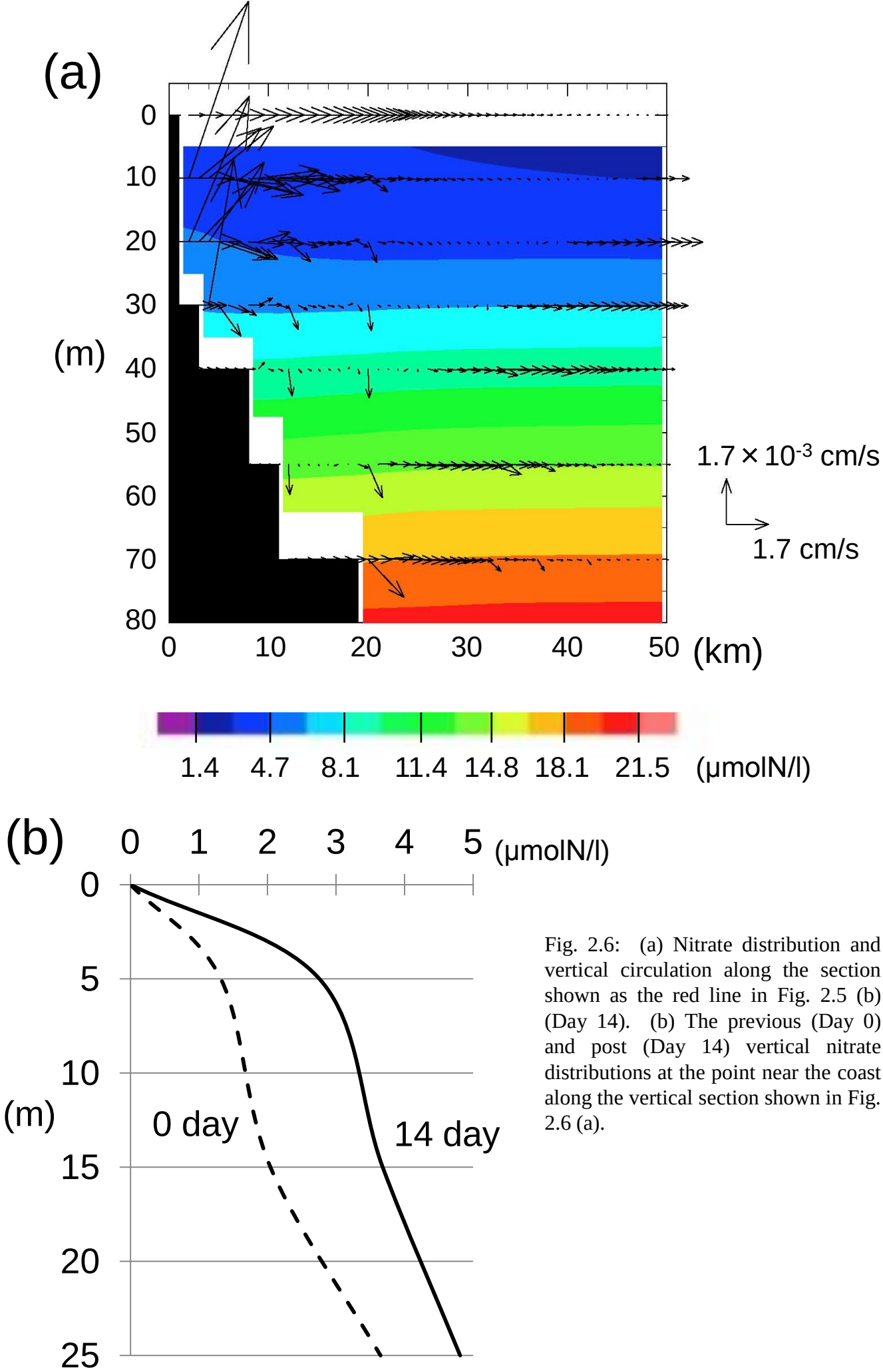

Fig. 2.6: (a) Nitrate distribution and vertical circulation along the section shown as the red line in Fig. 2.5 (b) (Day 14). (b) The previous (Day 0) and post (Day 14) vertical nitrate distributions at the point near the coast along the vertical section shown in Fig. 2.6 (a).

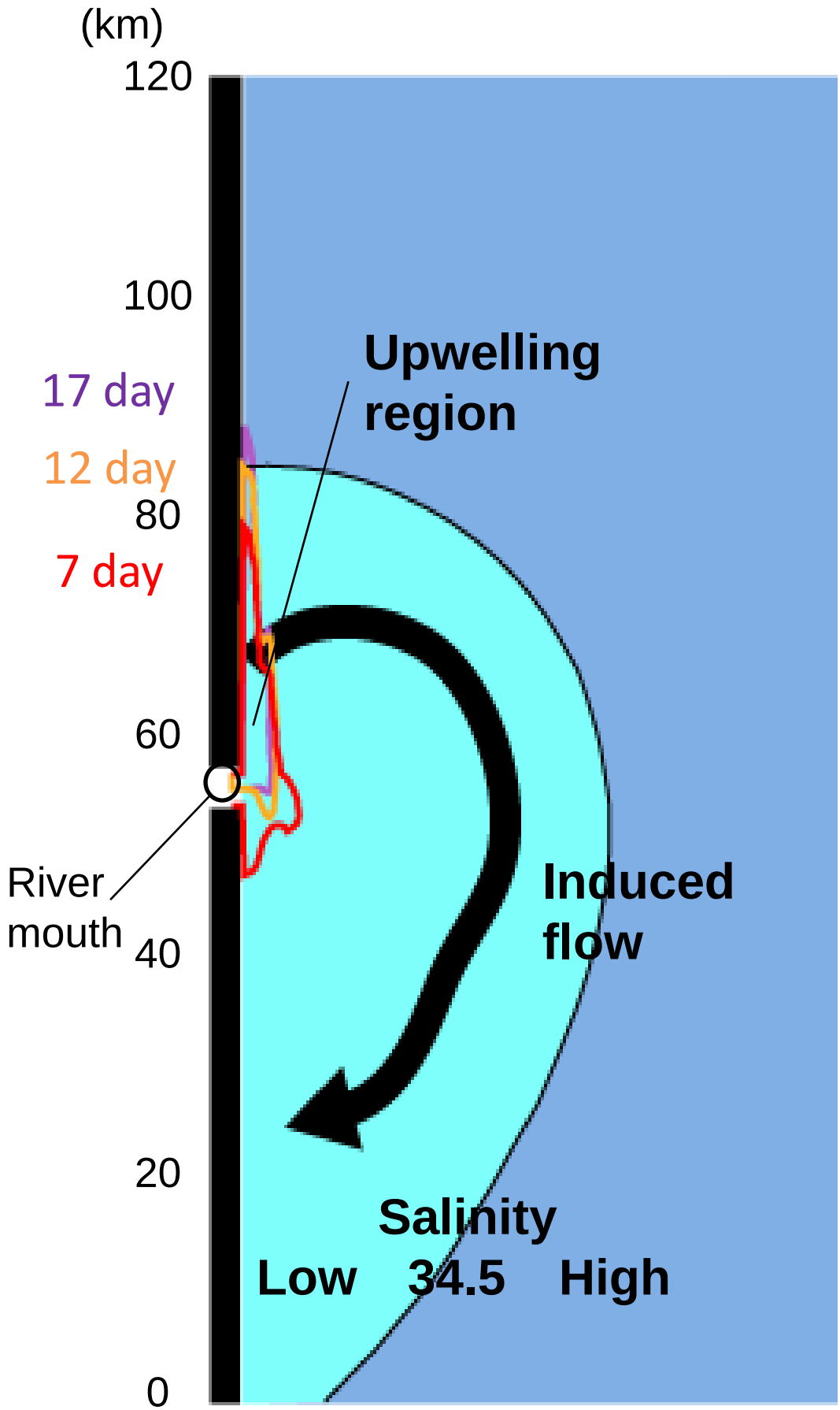

Fig. 2.7: Simulated image of the river-plume front, upwelling region, and induced flow by horizontal anticyclonic gyre in the surface layer in the control case, respectively. The black contour shows the salinity of 34.5 g/kg at the depth of 10 m on 12 day. The regions surrounded by color contours (red; 7 day, orange; 12 day, purple; 17 day) show vertical upwelling at the depth of 10 m of over a speed of 0.001 cm/s. The arrow shows the main stream of horizontal gyre on 12 day at the depth of 5 m. Upwelling region spreads to the upstream with horizontal anticyclonic gyre propagating toward the upstream.

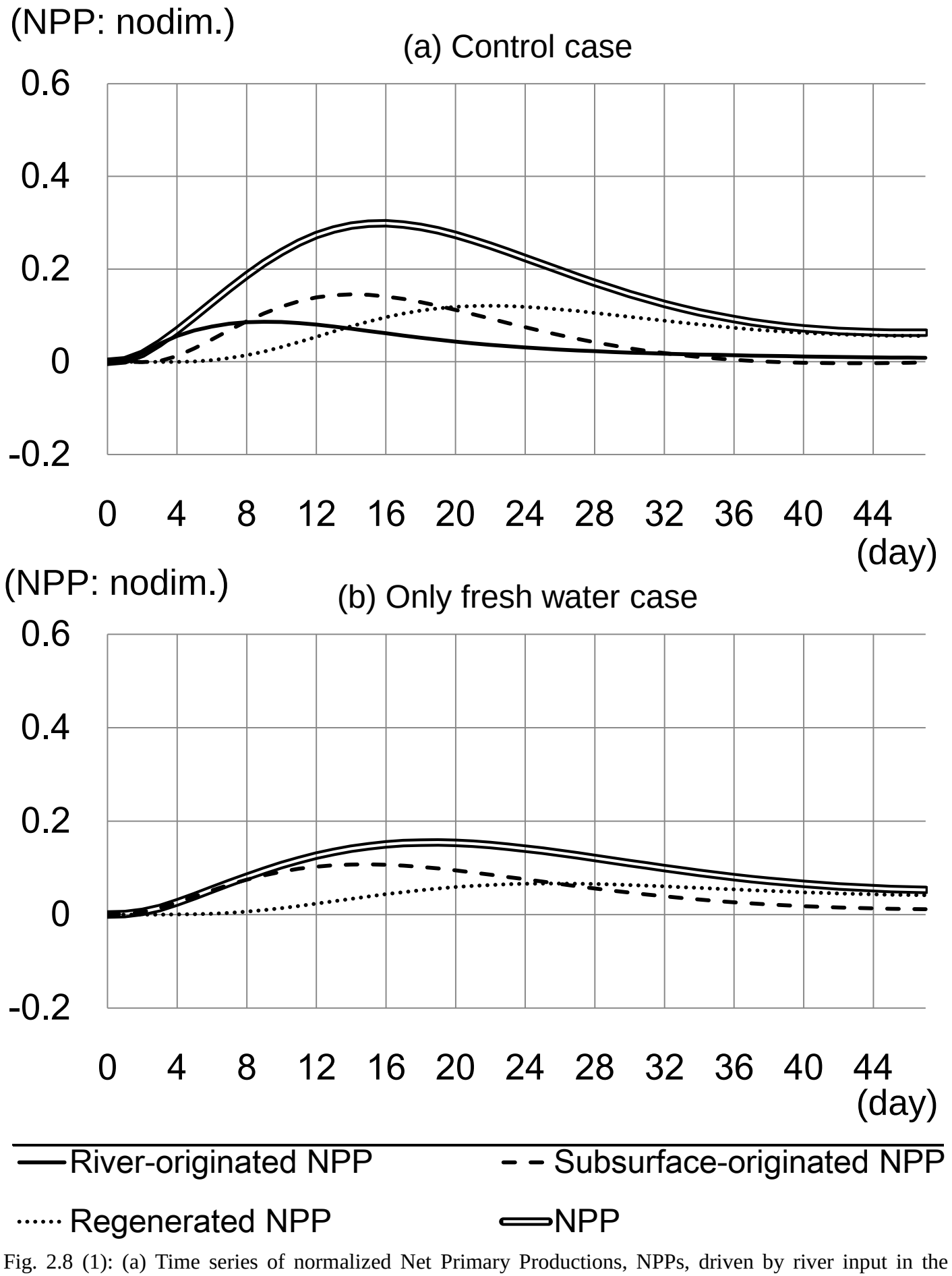

Fig. 2.8 (1): (a) Time series of normalized Net Primary Productions, NPPs, driven by river input in the calculation domain, that is, NPPs in the control case subtracted by that in the no flux case. NPPs are categorized into three origins: river-originated (solid line), subsurface-originated (dashed line), and regenerated (dotted line) and normalized by the nitrate input, *i.e.*, nitrate of 1.0 mg/l in fresh water of 2000 m^3/s in Day 1 in the control case. (b) Same as (a) except those in the only freshwater case.

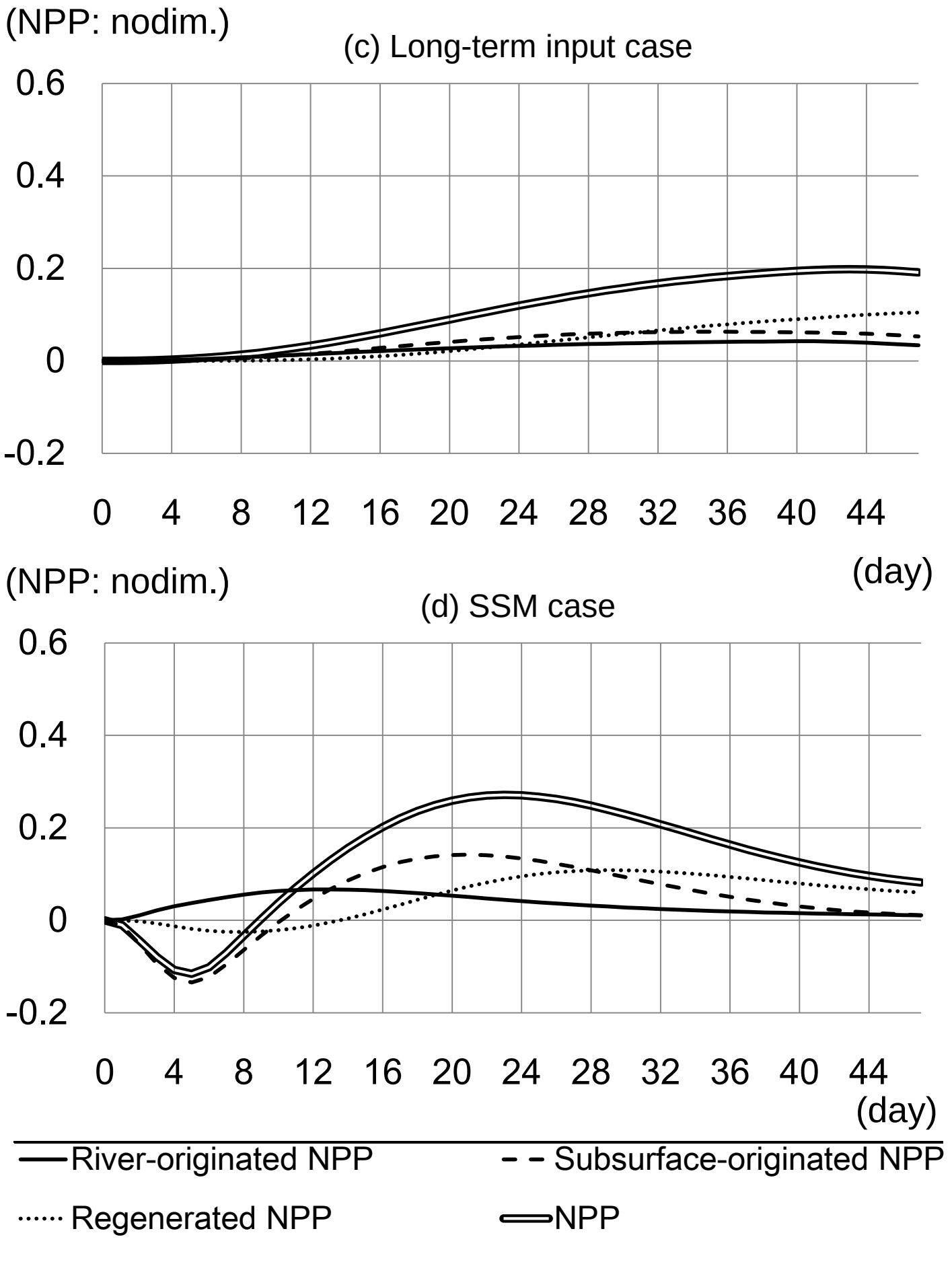

Fig. 2.8 (2): (c) Same as (a) except those in the long-term input case. (d) Same as (a) except those in the SSM case.

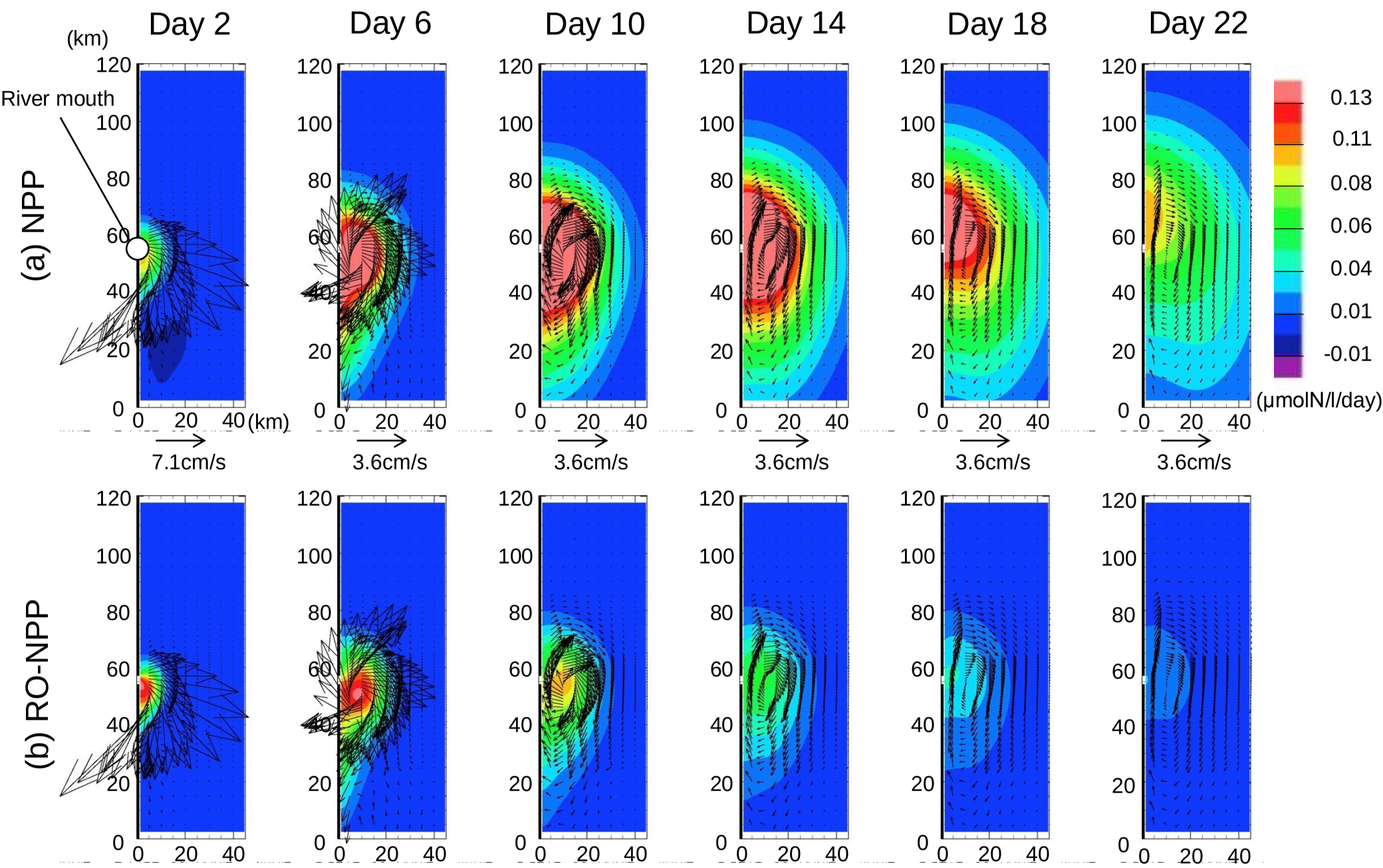

Fig. 2.9 (1): Horizontal distributions of the NPPs driven by river input in the surface layer (5 m depth): (a) NPP and (b) River-originated NPP subtracted by that in the no flux-case, with current velocity field at intervals of five grids.

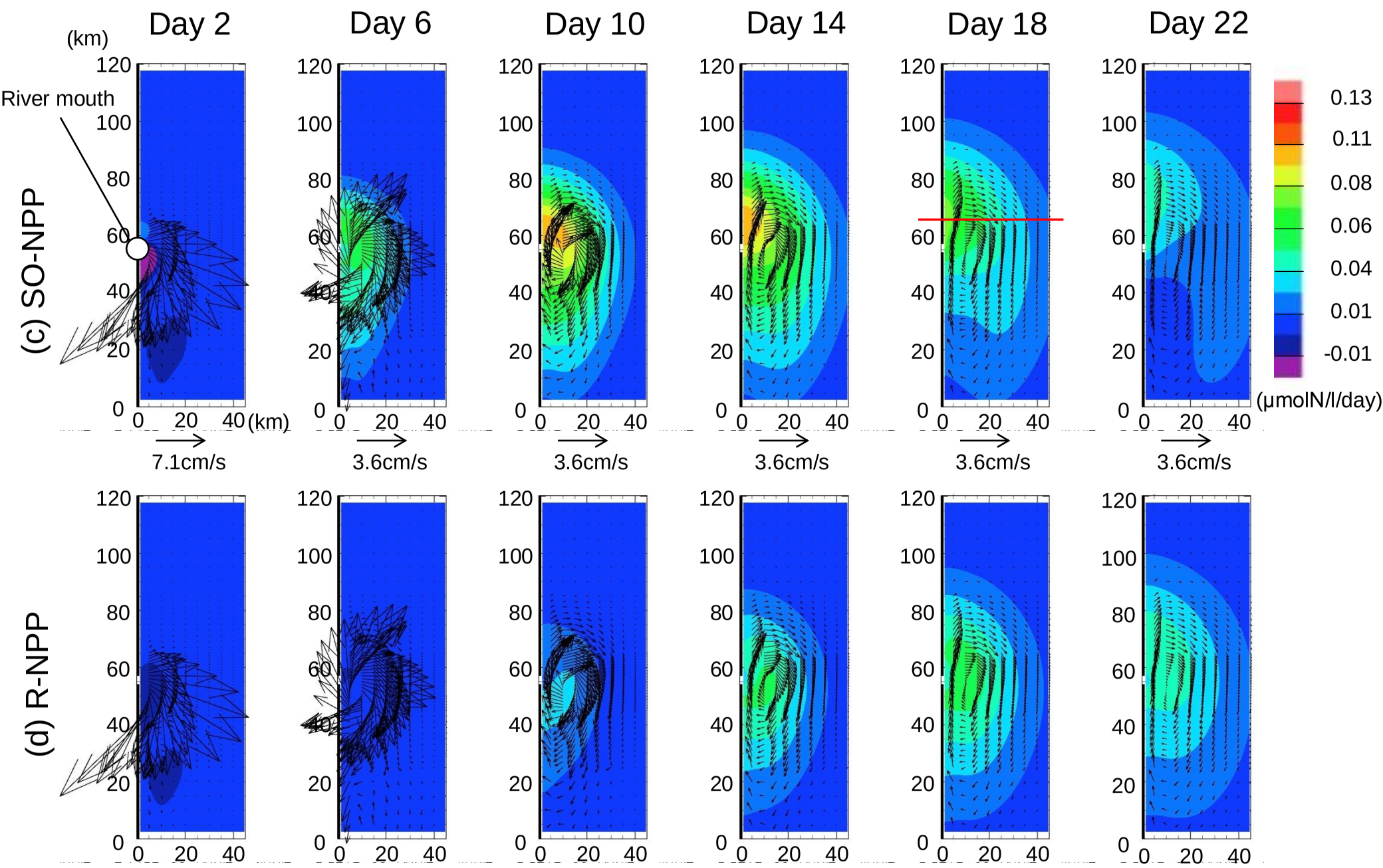

Fig. 2.9 (2): Horizontal distributions of the NPPs driven by river input in the surface layer (5 m depth): (c) Subsurface-originated NPP and (d) Regenerated NPP subtracted by that in the no flux-case, with current velocity field at intervals of five grids. Red line in (c) Day 18 shows the location of the vertical nearshore-to-offshore section detailed in Fig. 2.10.

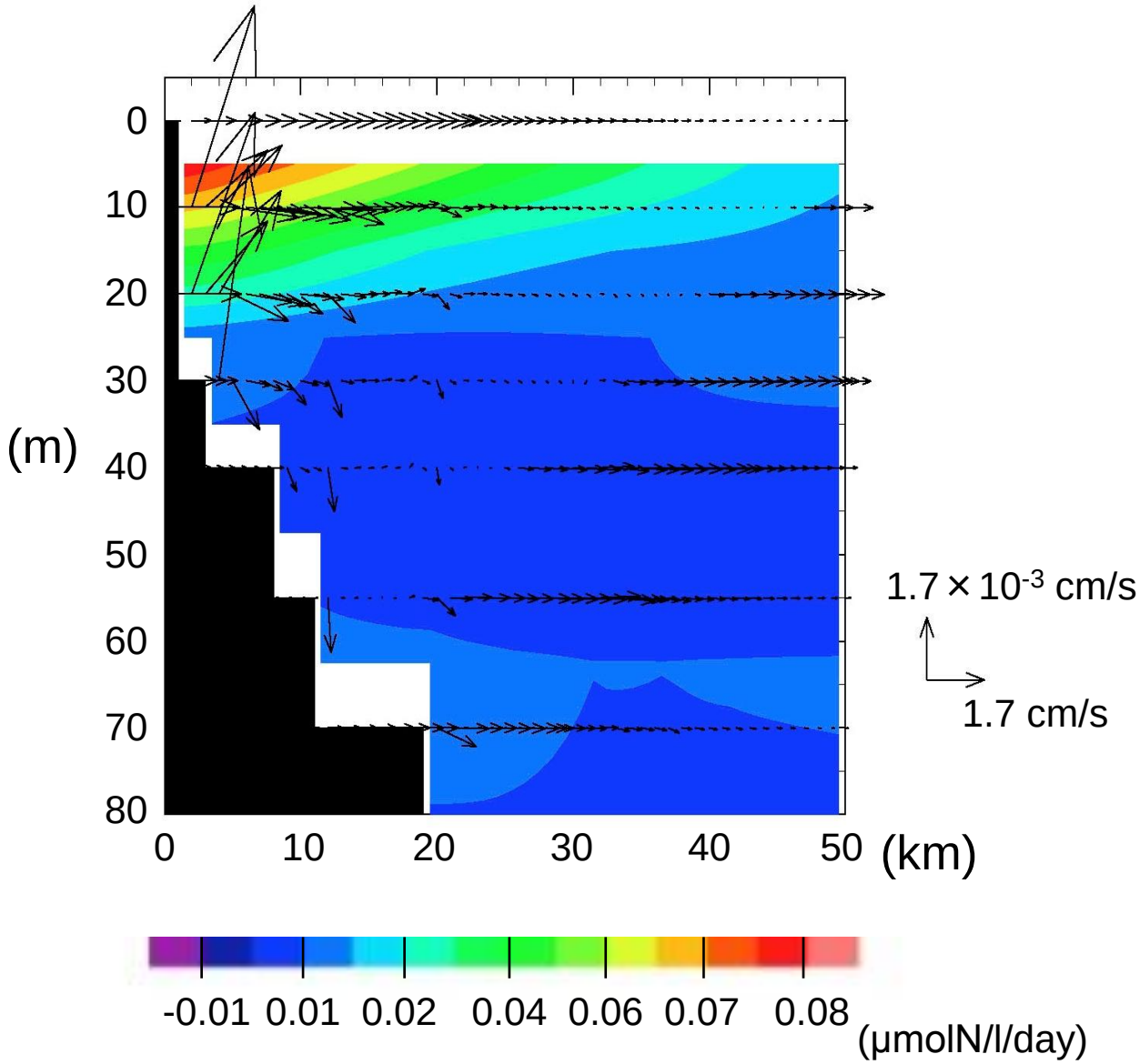

Fig. 2.10: SO-NPP distribution subtracted by that in the no flux-case and vertical circulation along the section shown as the red line in Fig. 2.9 (c) (Day 18).

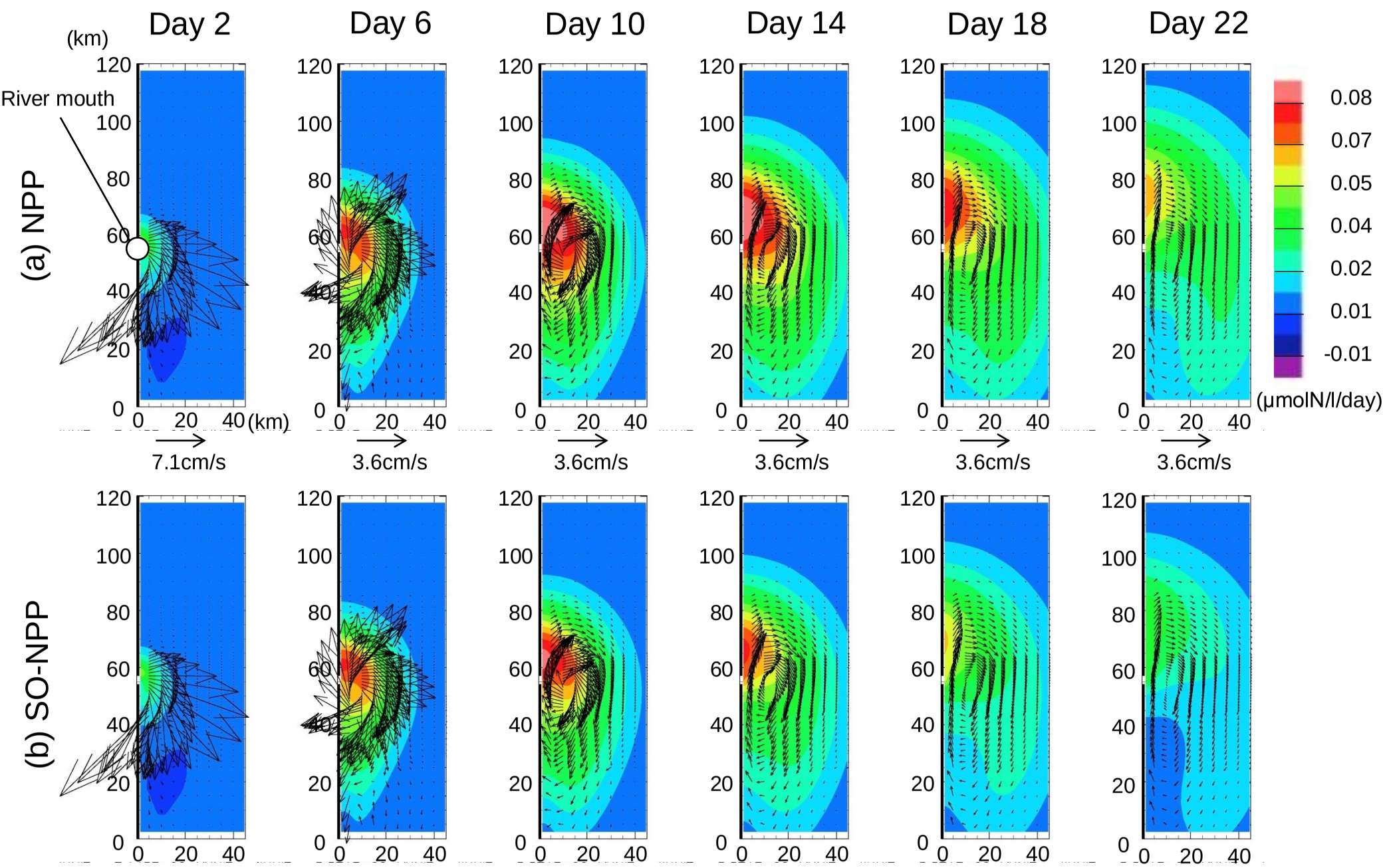

Fig. 2.11 (1): Same as Fig. 2.9 except NPP and Subsurface-originated NPP in the only freshwater case.

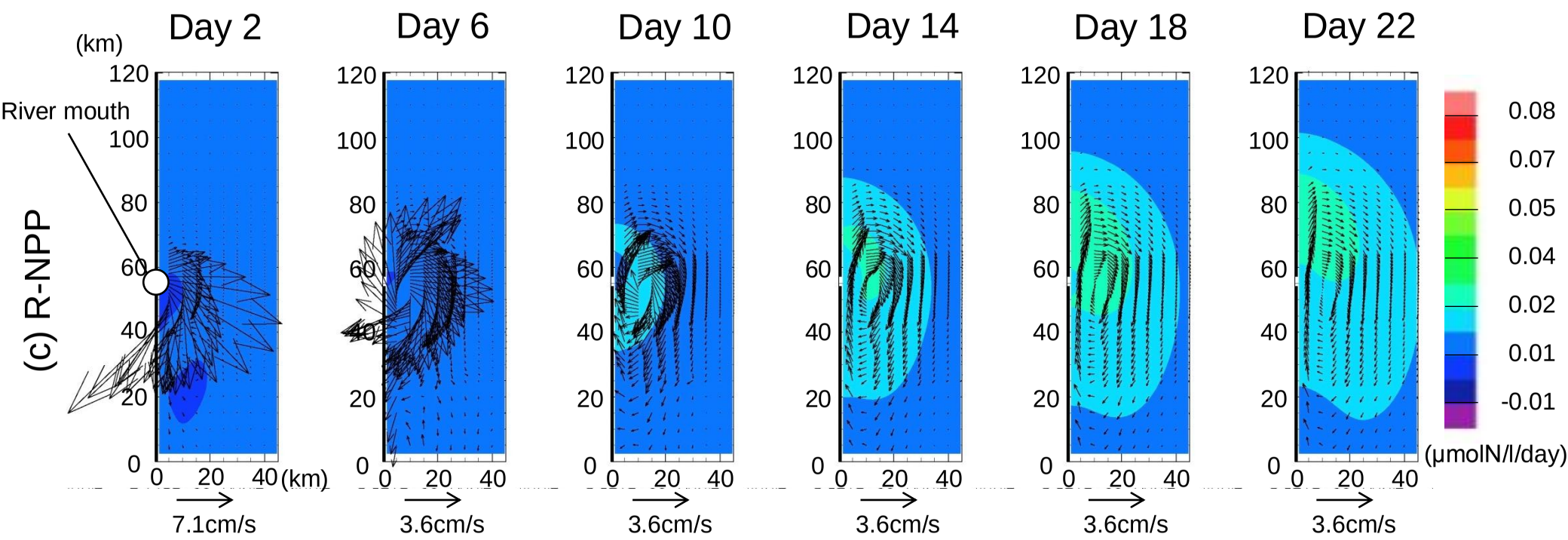

Fig. 2.11 (2): Same as Fig. 2.9 except regenerated NPP in the only freshwater case.

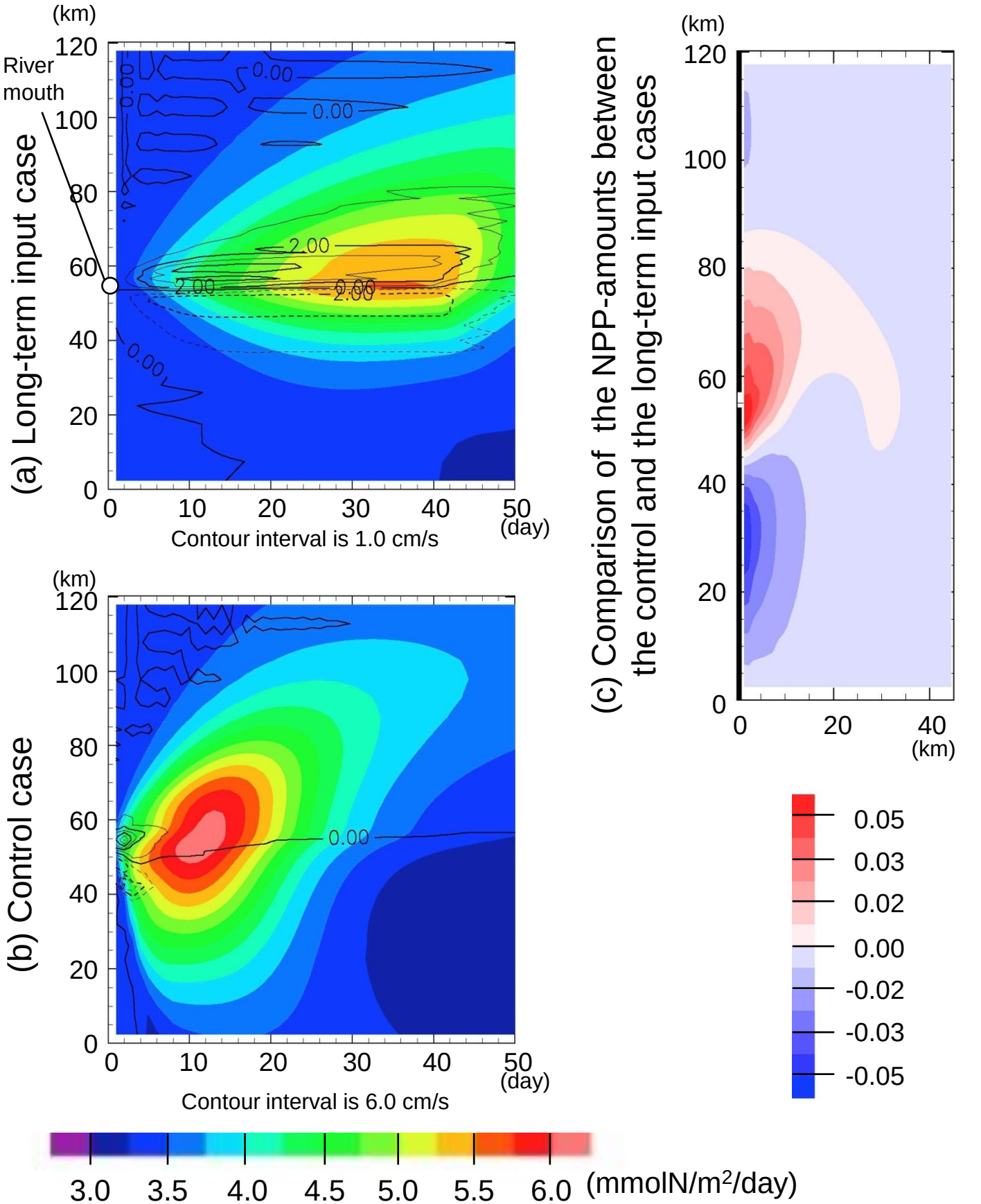

Fig. 2.12: Time series of NPP in (a) the long-term input case, (b) the control case, along the coast with 1.5 km distance with contour of velocity along the coast (solid and dashed lines are toward upstream and downstream, respectively). (c) the ratio of NPP as $(NPP_{long\text{-}term} - NPP_{control})/(NPP_{long\text{-}term}+NPP_{control})$ accumulated from Day 0 to Day 50, where $NPP_{control}$ is NPPs driven by river input in the control case and $NPP_{long\text{-}term}$ is NPPs driven by river input in the long-term input. Red shaded area shows the NPP in the long-term input is higher than that in the control case (blue shaded shows lower values than the control case).

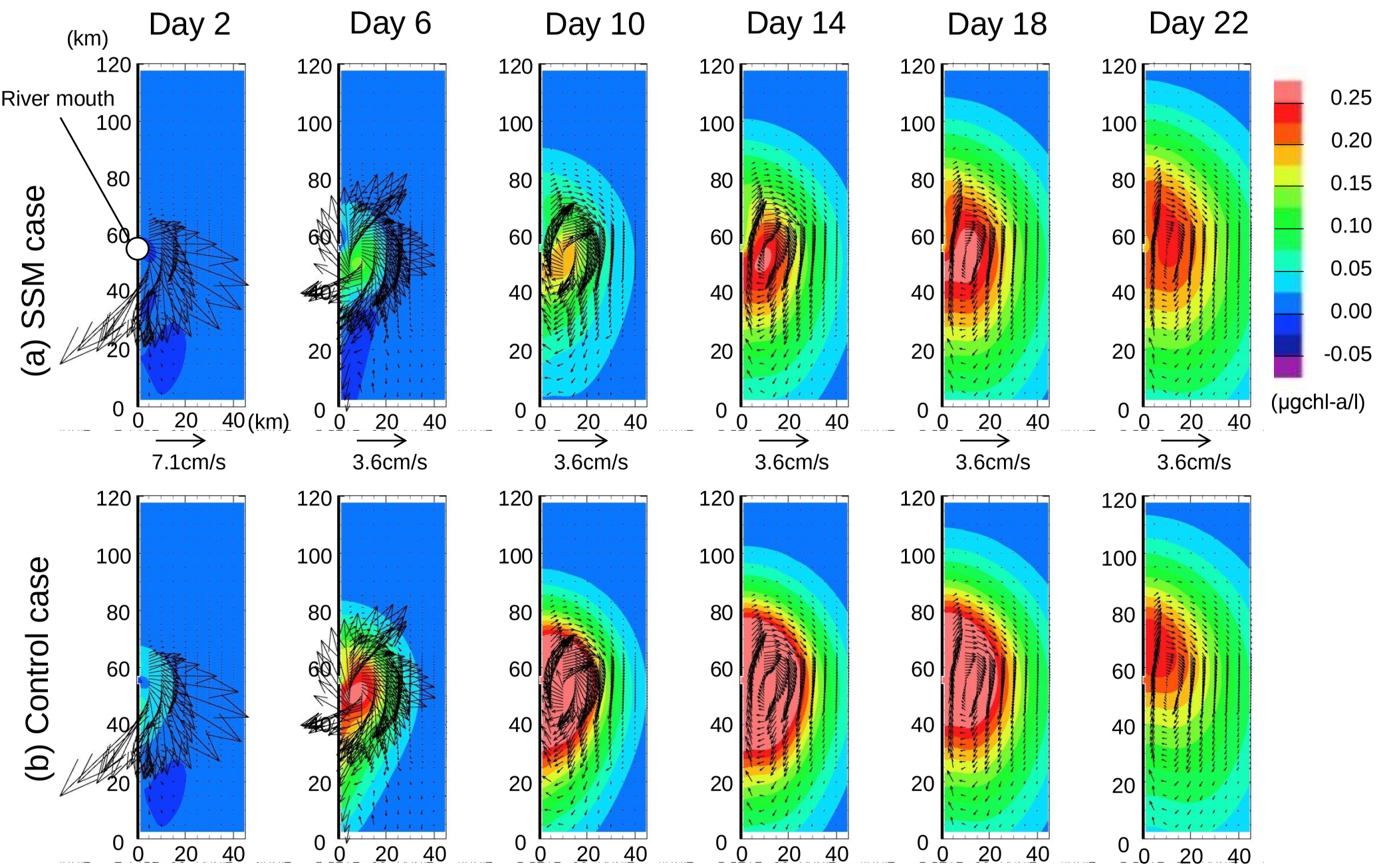

Fig. 2.13: Horizontal distributions of phytoplankton driven by river input in the surface layer (5 m depth) in (a) the SSM case and (b) the control case subtracted by that in the no flux-case, with current velocity field at intervals of five grids.

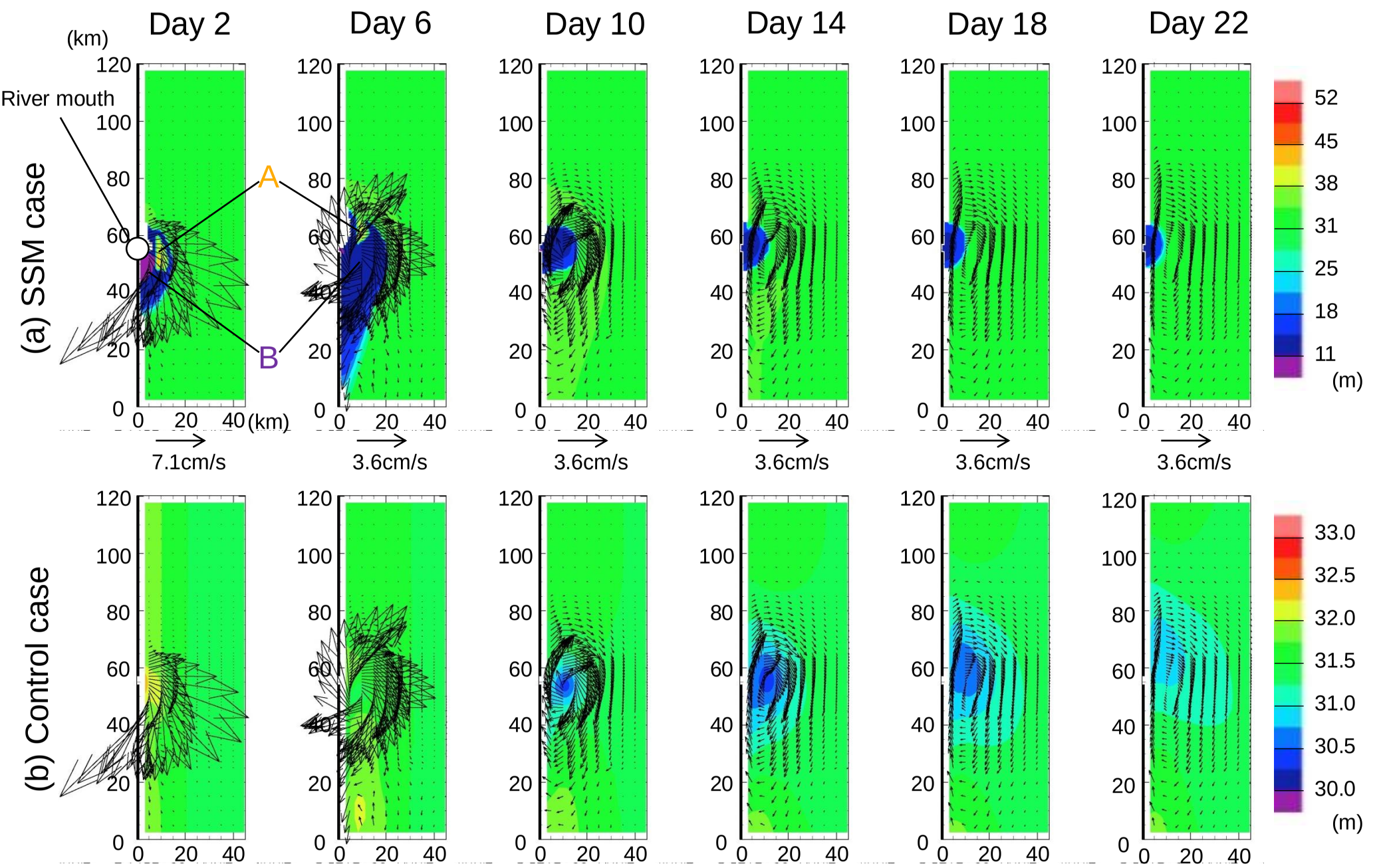

Fig. 2.14: Same as Fig. 2.13 except those in the depth of 20 % of the surface insolation. White colored area shows that light intensity on the floor has over 20% to the surface insolation.

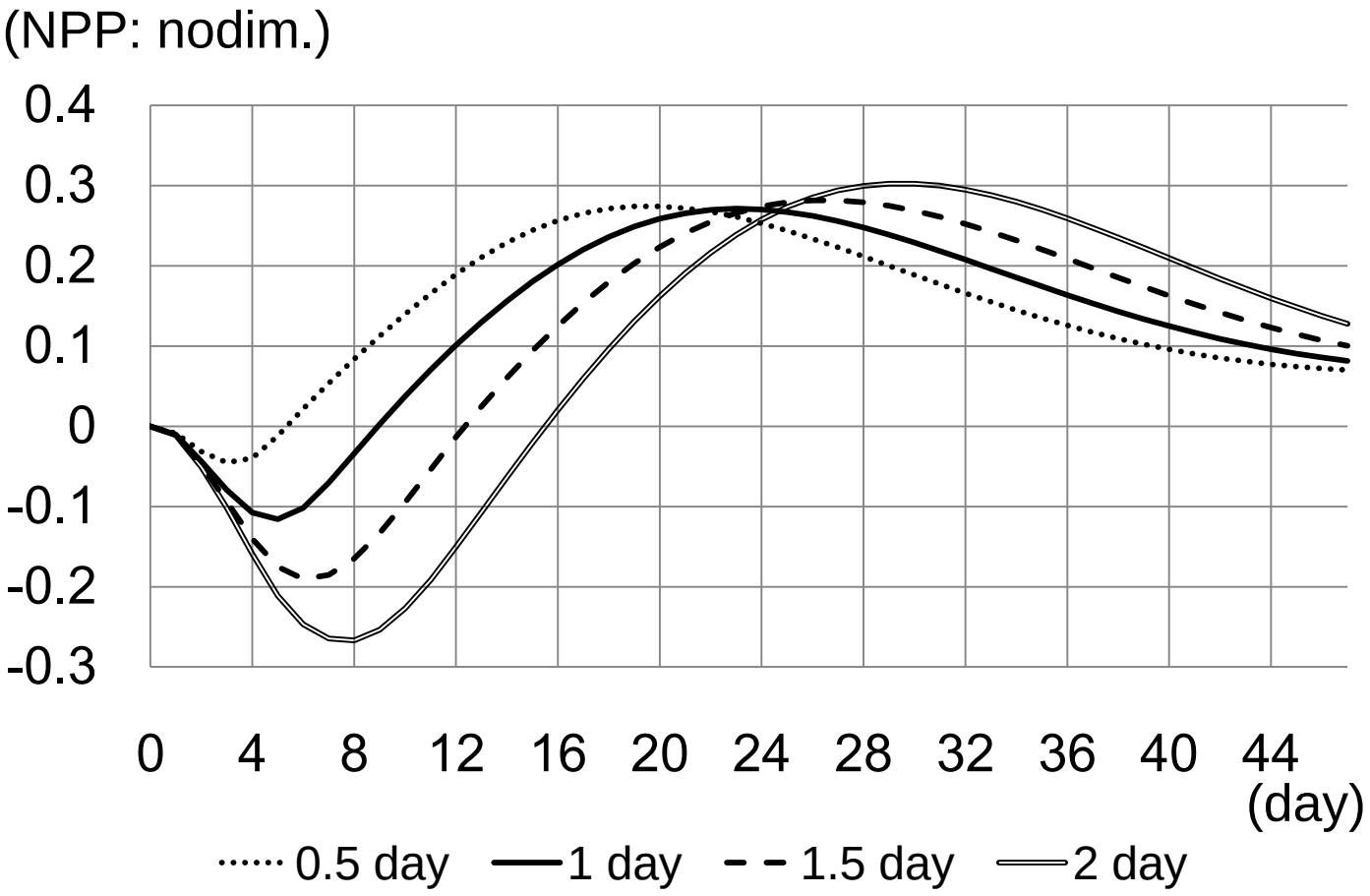

Fig. 2.15: Time series of normalized NPP driven by river input in the calculation domain, changing in the SSM removal time: t=0.5, 1.0, 1.5, and 2.0 days.

Chapter 3 A model simulation of phytoplankton blooms of the Ishikari Bay in May, 2007

3.1 Introduction

Ishikari Bay in Hokkaido, Japan is one of the ROFIs in subarctic region, and nutrients and fresh water is discharged from the Ishikari River to the Ishikari Bay. Ishikari Bay is identified as the inside of the line linked from Cape Ofuyu to the Syakotan Peninsula (Figure 3.1). The bay inside of the line has gentle coastal shelf composed of less than 100 m depth, and the bottom depth rapidly deepen toward the outside of the line. In the offshore of Ishikari Bay, Tsushima Warm Current flows along the steep continental slope from southwest to northeast. Ishikari Bay receives a little nutrient fluxes from oligotrophic Tsushima Warm Current (Yoshida *et al.*, 1977). Only a few chemical and biological studies are carried out in Ishikari Bay (*e.g.*, Agboola *et al.*, 2009; Agboola *et al.*, 2010). Ishikari Bay is characterized as oligotrophic coastal water with a considerable influence of the Ishikari River.

The Ishikari River has the largest discharge in Hokkaido and the second largest total catchment area in Japan. The mean discharge in 2007, for example, was 343.96 m^3/s. The mean water depth of the river is 2.8 m at “Ishikari Ohashi” located on 22.6 km above from the river mouth, and the river mouth is about 1.5 km width.

The amplitude of tide is generally small along coast of Japan Sea (Unoki, 1993). The effect of tide in Ishikari Bay is also small; the sum of major four tide components

(M_2+S_2+K_1+O_1) is only 17 cm at most. Effect of tide was not included in this chapter.

In this chapter, we investigate three-dimensional and temporal variations of plankton bloom by the realistic simulation of the Ishikari Bay on the spring in 2007, and compare the conclusion in Chapter 2 to the primary production of the Ishikari Bay by the different nitrate origins. The similar ideal settings as Chapter 2 are also used to discuss the effects of bottom slope angle on primary production in ROFI.

3.2 Model and Method

3.2.1 Model setting of the Ishikari Bay

The model used in this chapter is the same OGCM as Chapter 2. We dealt with realistic topography of Ishikari Bay, fresh water and nitrate flowing from the river into the Ishikari Bay on β-plane (Figure 3.2). The horizontal grid sizes are approximately 1 km in the dashed area. We took huge outside area out of Ishikari Bay area whose size is a square of 110 km; the north and west boundaries were at 1900 km north and 450km west from Ishikari Bay area, which was large enough that Tsushima Warm Current could keep flowing in the simulation. The model has 43 vertical layers with thickness increasing from 2 m at the surface to 50 m at the bottom. The physical setting and values are the same in Chapter 2 except the vertical viscosity and diffusivity that are determined by the turbulence closure level 2.5 scheme (Mellor and Yamada, 1982). The initial salinity and temperature were determined with Gaussian interpolation of observation data (Figure 3.3 (a), (b)). The observed data is during 9^{th} to 15^{th} May, 2007 in the Ishikari Bay and the west coast of Hokkaido, and has detailed vertical resolution per 1 m. The simulation was started after a spin-up of 2 days with the

salinity and temperature to form geostrophic background flow, and the time step was 1.4 minutes. The region except the Ishikari Bay was restored to the observed salinity and temperature value for 4 days during all the simulated time.

We incorporated the same ecosystem part in Chapter 2 into the OGCM. The initial concentrations of phytoplankton and nitrate were determined from the complemented observation data (Fig. 3.3 (c), (d)). The observation data have vertical resolution per 5 m at least. The concentration of chlorophyll-a at the nearest point from the river mouth (point A in Fig. 3.3 (c)) is smaller than that of the left-hand side of the river mouth (point B). The situation is consistent with the result of D-U Shift in Chapter 2. After a spin-up of 3 months with the ecosystem model simulated with the above fixed nitrate and phytoplankton value, we also used the distributions of zooplankton and detritus as initial conditions of the experiments driven by river input.

In the Ishikari Bay case (Table 3.1), we put the freshwater input as the real Ishikari River discharge in May to June, 2007 (Figure 3.4), with the same surface temperature, into river mouth region of 2 km × 2 km for 50 days. Regularly large amounts of riverine discharge by snowmelt occur in the spring season, and it rained a few days ago from the initial day (5/9). The same nitrate concentration of 1.0 mg/l in the Chapter 2, in the fresh water was also used, and the case demonstrated above was called experiment #1.

3.2.2 Ideal settings

The similar ideal settings in Chapter 2 are introduced to discuss the effects of bottom slope angle and to compare the conclusion in Chapter 2 with primary production of the

Ishikari Bay. The physical setting, ecosystem part and initial state are the same in Chapter 2 except that the model has 28 vertical layers with thickness increasing from 2 m at the surface to 40 m at the bottom, and the river mouth is about 2 km width.

We conducted four ideal setting cases for 50 days (Table 3.1). In experiment #2 (hereafter referred as the I-I case), we initiated the model with the similar slope angle to that in the Ishikari Bay and the same riverine inputs as the Ishikari Bay case (Fig. 3.4). Experiment #3 (S-I case) was the similarly steepen slope angle to that in Chapter 2 and the same riverine inputs as the Ishikari Bay case. Experiment #4 (I-P case) demonstrates the similar slope angle to that in the Ishikari Bay and the same riverine input as the control case in Chapter 2 (2000 m^3/s), *i.e.*, for the first 2 days of pulse input and no discharge for the other 48 days. The total amount of freshwater discharge for 50days was 3.5×10^8 m^3 in the pulse case, but the amount in the Ishikari Bay case was 1.8×10^9 m^3 five-times larger than that of the pulse case. Experiment #5 (S-P case) was the similarly steepen slope angle to that in Chapter 2 and the same riverine pulse inputs as the control case in Chapter 2.

3.3 Results

Tsushima Warm Current forced by geostrophic balance of the temperature and the salinity flows from southwest to northeast in the offshore of the Ishikari Bay (Figure 3.5 (a)). The main axis does not penetrate into the inside of the Ishikari Bay. Anticyclonic gyre exists in the Ishikari Bay, and low salinity water from the Ishikari River spread with the clockwise flows to left-hand side of the river mouth. The low salinity region (~ 25.3 g/kg) spreads with the time until Day 13, but the region becomes

smaller after Day 17 due to the decreasing in river discharge (Fig. 3.4). Horizontal distribution pattern of high nitrate concentration is similar to that of low salinity, and the concentration maximum is located near the river mouth all the time (Figure 3.5 (b)). The maxima of phytoplankton concentration shift towards the more left-hand direction of the river mouth with time until Day 13 (Figure 3.5 (c)). The area where the phytoplankton concentration is higher than 2.39 μgchl-a/l expands clockwise to the offshore after Day 13, but the extent of the area toward the downstream of the anticyclonic gyre reduct on Day 25.

The same riverine inputs as the Ishikari Bay case are applied to the similar ideal setting in Chapter 2 (I-I case). The salinity minimum and the nitrate maximum are located near the river mouth all the time (Figure 3.6 (a), (b)). The low salinity and the high nitrate regions spread to the left-hand side of the river mouth (the upstream) until Day 9 and become smaller after Day 13. The sequence of the I-I case is similar to that of the Ishikari Bay case in that the low salinity and the high nitrate regions spread until Day 13 and reduce after Day 17 (Fig. 3.5 (a), (b)). The phytoplankton maxima shift toward the upstream region and expand to the offshore, but the extent reduces after Day 21 (Figure 3.6 (c)). The sequence is also similar to that of the Ishikari Bay case in that the maximum region shifts to the left-hand side, expands to the offshore until Day 21 and reduces after Day 25 (Fig. 3.5 (c)). The sequences of the I-I and the Ishikari Bay cases are consistent with each other, although the each initial states are different. The I-I case is also used to discuss in the next section.

3.4 Discussion

3.4.1 Small nitrate supply from the subsurface layer

In the Ishikari Bay case, horizontal distribution pattern of nitrate is similar to that of salinity all the time. On the other hand, in Chapter 2 (Fig. 2.5 (a) and Fig. 2.5 (b)), these distribution patterns become different from each other with time. This is because upwelling of subsurface water with high nitrate concentrarion in the upstream region causes the difference, as discussed in Chapter 2.

We also introduced nitrates categorized into three origins as same as Chapter 2. High concentration of SO-nitrate is widely distributed over the surface in the Ishikari Bay on Day 1 (Figure 3.7). The surface SO-nitrate is used by phytoplankton, and gradually decreases with time. The SO-nitrate maximum shifts toward the left-hand side of the river mouth (around x = 60 km) until Day 5, because SO-nitrate is supplied from the subsurface layer to the surface near the coast in the left-hand side region of the river mouth on Day 5 (Figure 3.8 (a)). The concentration maximum in the left-hand side reduces with time, due to small SO-nitrate coming from the subsurface (Figure 3.8 (b)), and the maximum shifts to the right-hand side of the river mouth after Day 9 (Fig. 3.7). The SO-nitrate is supplied to the surface layer only for the early time in the left-hand side region.

The net primary pruduction (NPP) is mainly made by river-originated NPP (RO-NPP) until Day 24, and is mainly made by R-NPP (regenerated NPP) after Day 25 (Figure 3.9). The rate of subsurface-originated NPP (SO-NPP) is much smaller than that of the control case in Chapter 2 (Fig. 2.8 (a)). The accumulated RO-, SO-, and R-NPP until Day 34 are 0.87, 0.07, and 0.61, respectively, to the total amount of river nitrate input. Fig. 3.9 is drawn by the same as Fig .2.8 except NPPs in the Ishikari case subtracted by that in another case without riverine flux case from the river mouth. The negative

SO-NPP from Day 9 to Day 18 in Fig. 3.9 suggests that the SO-NPP in Ishikari case is smaller than that in the case without riverine flux. This may be because the growth rates of phytoplankton in the Ishikari Bay in both the cases are close to the saturation rate (*i.e.*, NPPs in two cases are almost the same for each other), and the percentage of SO-nitrate in the Ishikari case becomes relatively smaller due to additional RO-nitrate than that in the case without riverine inputs.

3.4.2 Effects of bottom slope

Why do the nitrate-supply from the subsurface layer become smaller in the Ishikari Bay? We conducted two cases changing in bottom slope: the similar slope angle to that in the Ishikari Bay (I-I case) and the same as Chapter 2 (S-I case). In the I-I case, we did not find the shift in the three stages by the different nitrate origins: RO-, SO- and R-nitrates, as seen in Chapter 2 (Figure 3.10 (a) and Fig. 2.8 (a)). The rate of SO-NPP in the NPP is smaller than that of the S-I case (Figure 3.10 (a), (b)), which is consistent with that in the Ishikari Bay case. The NPP maximum of the I-I case is also smaller than that of the S-I case, due to the smaller SO-NPP.

Small amount of nitrate comes from the subsurface in the I-I case, because the vertical circulation is weaker. The area of strong upward flux (over 0.033 m^3/s) is limited on the bottom near the coast in the I-I case, and the subsurface water with high concentration of SO-nitrate is not supplied to the surface (Figure 3.11 (a)). Strong upwelling driven by deeper vertical circulation occurs in the S-I case, which induces much SO-nitrate supply from the subsurface layer (Figure 3.11 (b)). This result is consistent with the previous study of that the strength of vertical circulation is

proportional to the cube of water depth (Unoki, 1993).

NPP maxima shift from the downstream to the upstream region in the both cases as time progresses (Figure 3.12 (a), (b)), except Day 23 and 28 of the I-I case. The maxima exist in the downstream region on Day 28 of the I-I case, due to weak upwelling to the surface and nitrate-depletion in the upstream region. Horizontal anticyclonic gyre of the I-I case more expands into the upstream and is suppressed to the offshore. McCreary *et al*. (1997) explains that the downward frontal current generated by geostrophic adjustment transport the front water of the plume nose, and the gyre proceeds to the upstream. The deficiency of the water in front of the gyre due to the weaker upwelling in the upstream is compensated by horizontal water from the river mouth, so that the anticyclonic gyre more spreads to the upstream than that of the S-I case. It implies that the influence of river discharge and RO-nitrate is more important for NPP of the upstream region in the case of shoal ROFI.

The same riverine inputs of fresh water and nitrate in the control case in Chapter 2 was applied to I-P case and S-P case. The dominant source in the NPP is shifted from RO-, SO- to R-NPP in turn, though the dominant duration by SO-NPP is only Day 11 in the I-P case (Figure 3.13 (a)). In the S-P case, the SO-NPP is larger than that in the I-P case as discussed above, which induces larger NPP (Figure 3.13 (b)) than that of the I-P case. The three stage's shift of the dominant sources depends on the way of freshwater and nitrate inputs.

Although the total NPP of the I-P case is smaller than that of the S-P case, the R-NPP of the I-P case is larger than that of the S-P case after Day 25 (Fig. 3.13 (a), (b)). The accumulated R-NPP of the I-P case until Day 50 is 4.06 that is more than the value 3.59 of the S-P case, to the total amount of river nitrate input. This is because R-nitrate

supply to the surface layer in I-P case is higher than that in S-P case, due to high concentration of detritus converted into R-nitrate on the bottom that is shallower in I-P case than that in S-P case (Figure 3.14).

3.5 Conclusion and Remarks

We conducted the realistic simulation of the Ishikari Bay to investigate three-dimensional and temporal variations of phytoplankton bloom, and compared the phytoplankton bloom in the Ishikari Bay to the conclusion in Chapter 2. The regions of salinity minimum and nitrate maximum are located near the river mouth all the time. The phytoplankton maxima shift toward the left-hand side of the river mouth until Day 13, but the shift does not keep going to the left-hand side. This is because subsurface-originated nitrate (SO-nitrate) is supplied from the subsurface to the surface layer only for the early time in the left-hand side region, but small SO-nitrate coming to the surface after the middle simulated time. The rate of subsurface-originated net primary production (SO-NPP) is also much smaller than that of the control case in Chapter 2, and the shift of the three stages by the different nitrate origins, RO- (river-originated), SO- and R (regenerated) –nitrates in turn, is not found.

Several ideal settings were used to discuss why the nitrate-supply from the subsurface layer is much small in Ishikari Bay. Upwelling forced by the vertical circulation in the upstream is weak in the case of gentle bottom slope angle, which does not maintain much SO-nitrate supply from the subsurface layer.

Horizontal anticyclonic gyre in the gentle bottom slope case tends to expand into the upstream and be suppressed to the offshore. It implies that the influence of river

discharge and RO-nitrate is more important for NPP of the upstream region in the case of shoal ROFI.

R-NPP is large in the shallow case, because R-nitrate supply to the surface layer is large, due to high concentration of detritus converted into R-nitrate on the bottom.

We need to investigate the relationship between the effects of bottom slope angle and NPPs in detail; how angles bottom slope are influenced on SO-NPP and R-NPP amounts. Horizontal distribution of RO-NPP also varies with bottom slope angle.

The three stage's shift of the dominant sources by RO-, SO- and R-nitrates depends on the way of fresh water and nitrate inputs. The way of inputs and the amounts of fresh water and nutrients affect the shift, which might be estimated.

Table 3.1 Experiments in Chapter 3.

Experiment No.	1	2	3	4	5
Name	Ishikari Bay	I-I	S-I	I-P	S-P
Geography	Realistic	Ideal	Ideal	Ideal	Ideal
Angle of bottom slope	Ishikari	Ishikari	Steep	Ishikari	Steep
Freshwater input	Ishikari	Ishikari	Ishikari	Pulse	Pulse
Duration of discharge	50 days	50 days	50 days	2 days	2 days

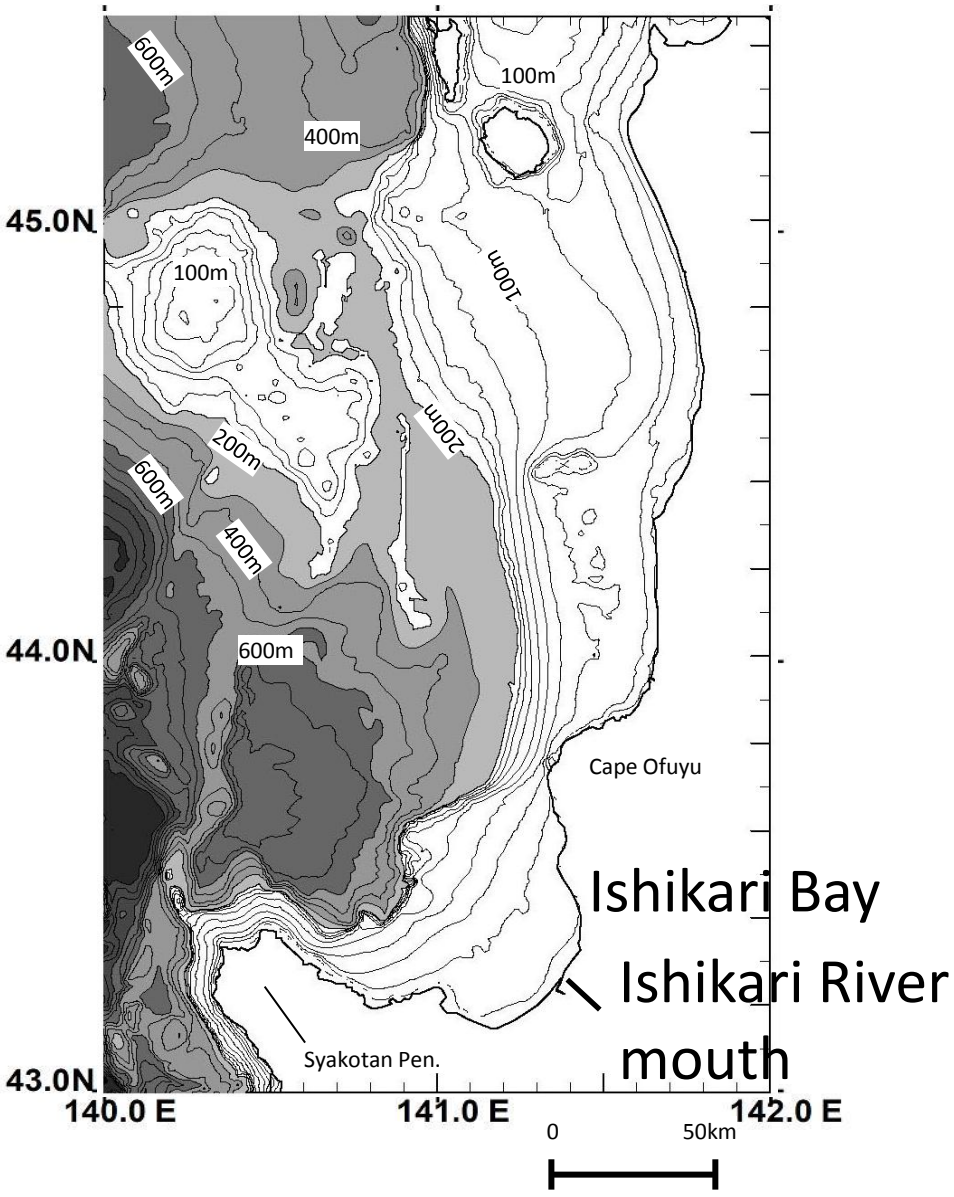

Fig. 3.1: Geography and topography off the west coast of Hokkaido.

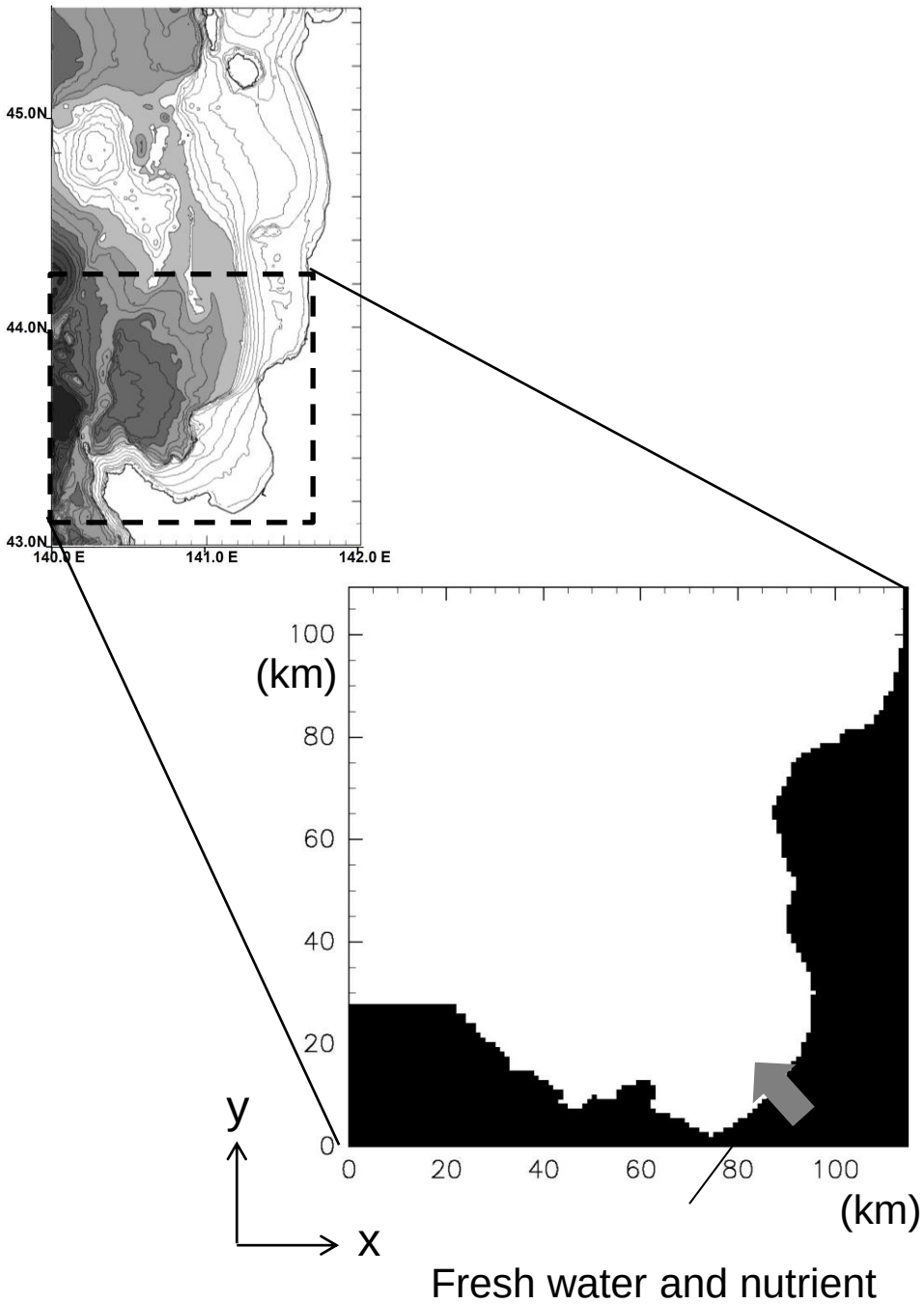

Fig. 3.2: Horizontal geography of Ishikari Bay used in the model. The dashed area shows the area drawn in figures 3.5 and 3.7.

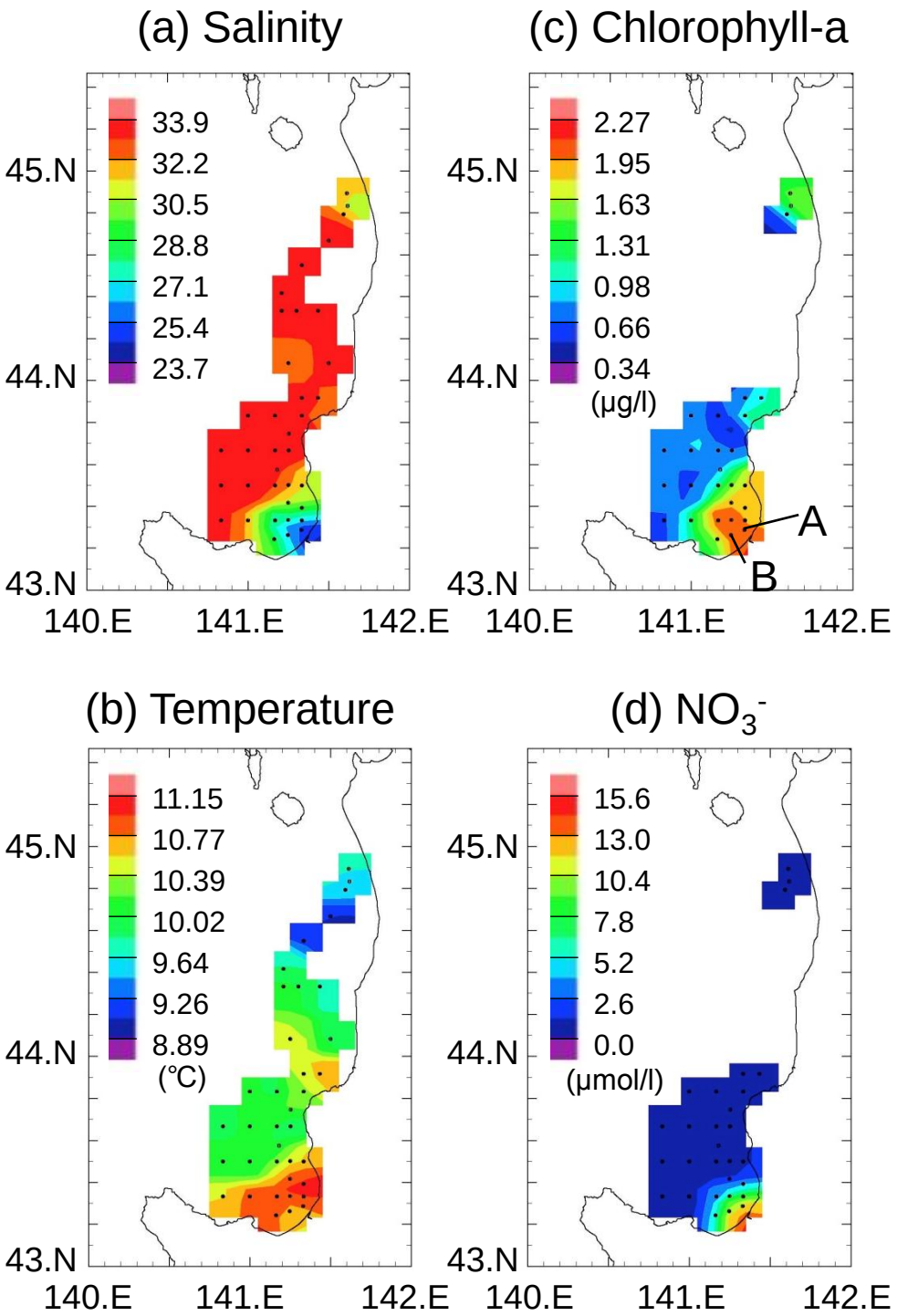

Fig. 3.3: In Gaussian interpolation of observation data in May, 2007, the horizontal distributions of (a) salinity, (b) temperature, (c) chlorophyll-a and (d) nitrate in the surface layer ((a) and (b); 2 m depth, and (c) and (d); 0 m), with dots that shows observation points.

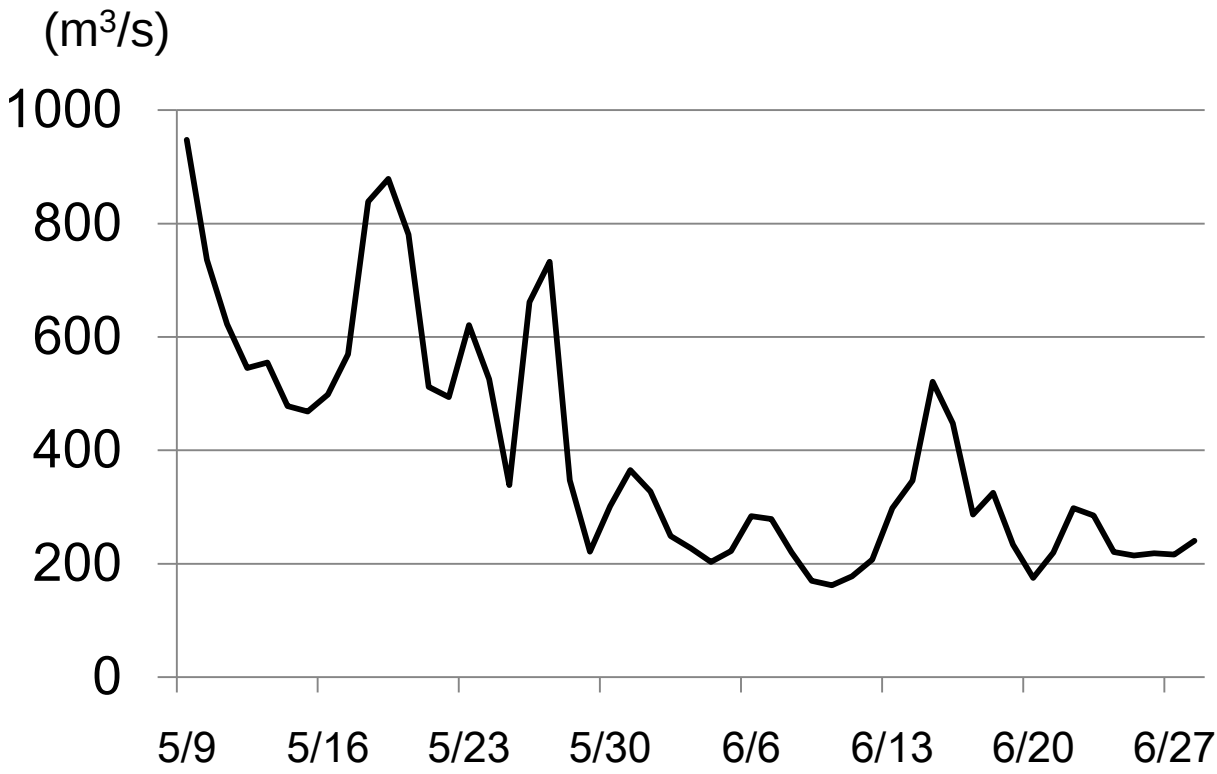

Fig. 3.4: River discharge at Ishikari Ohashi located on 22.6 km above from the river mouth of Ishikari River in Hokkaido, Japan observed in May to June, 2007 (Ministry of Land, Infrastructure and Transport, Japan: http://www1.river.go.jp/).

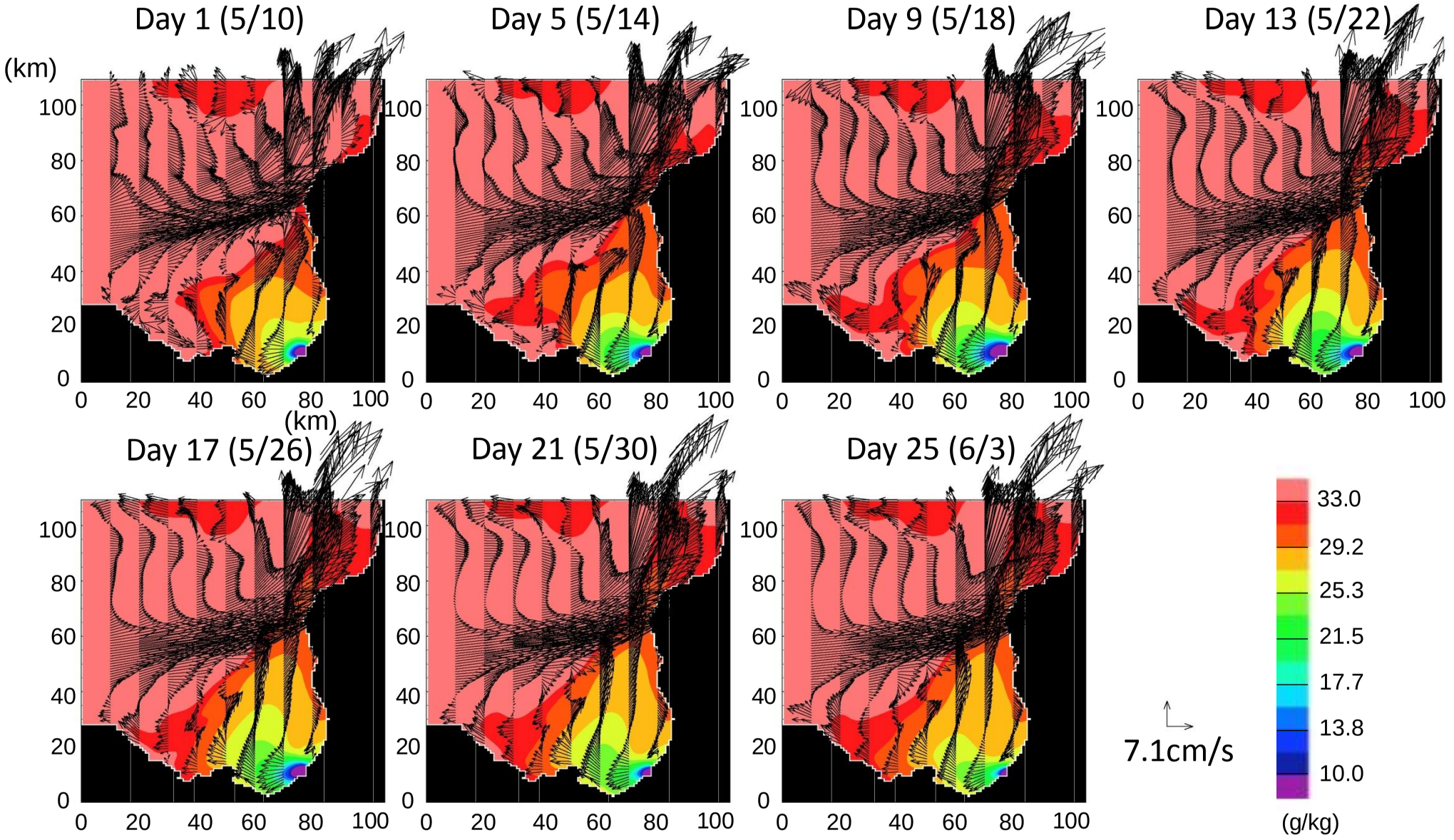

Fig. 3.5 (a): In the Ishikari Bay case, the horizontal distributions of salinity in the surface layer (1 m depth), with current velocity field whose vectors are drawn at intervals of ten grids.

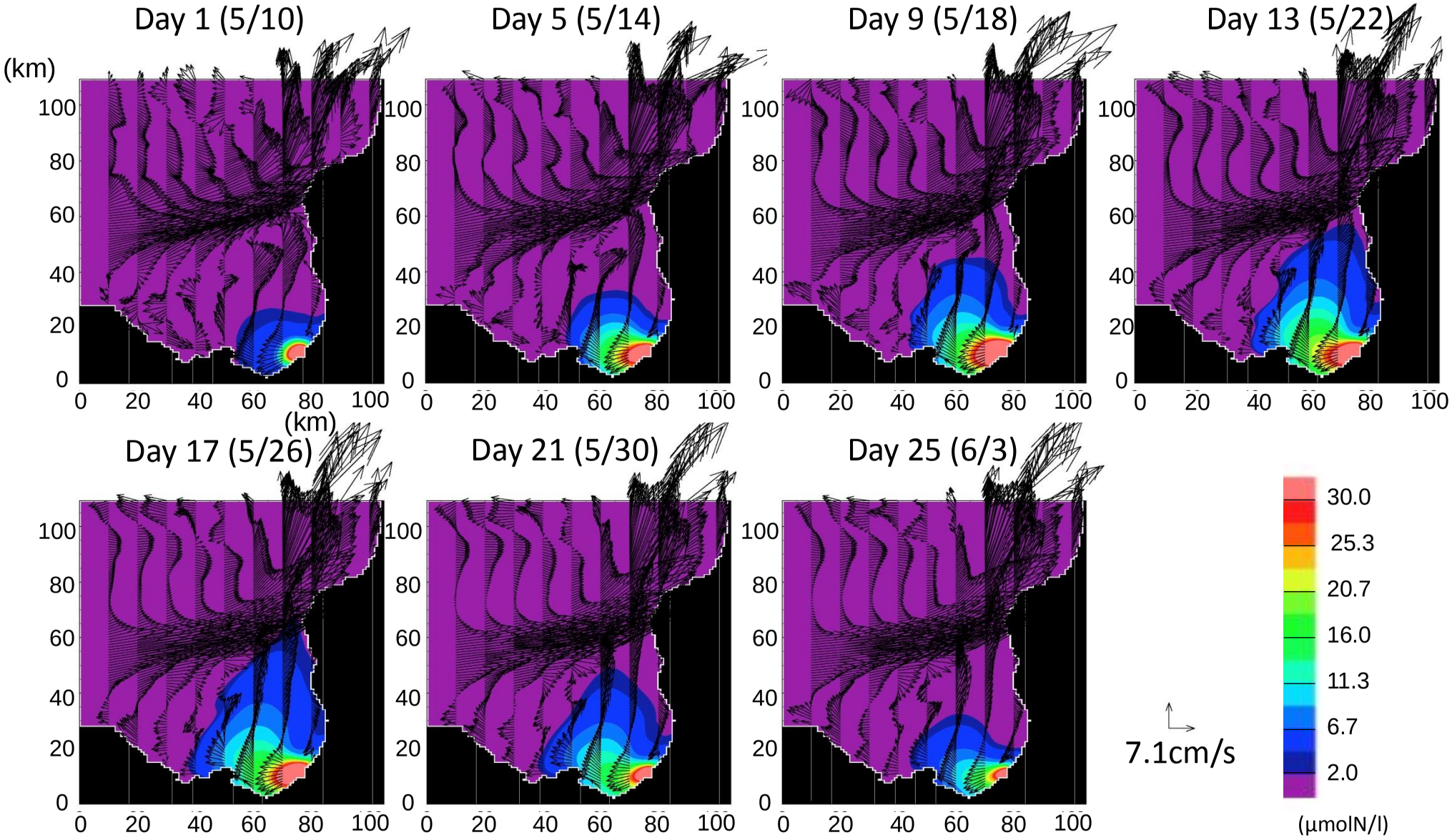

Fig. 3.5 (b): Same as (a) except that of nitrate.

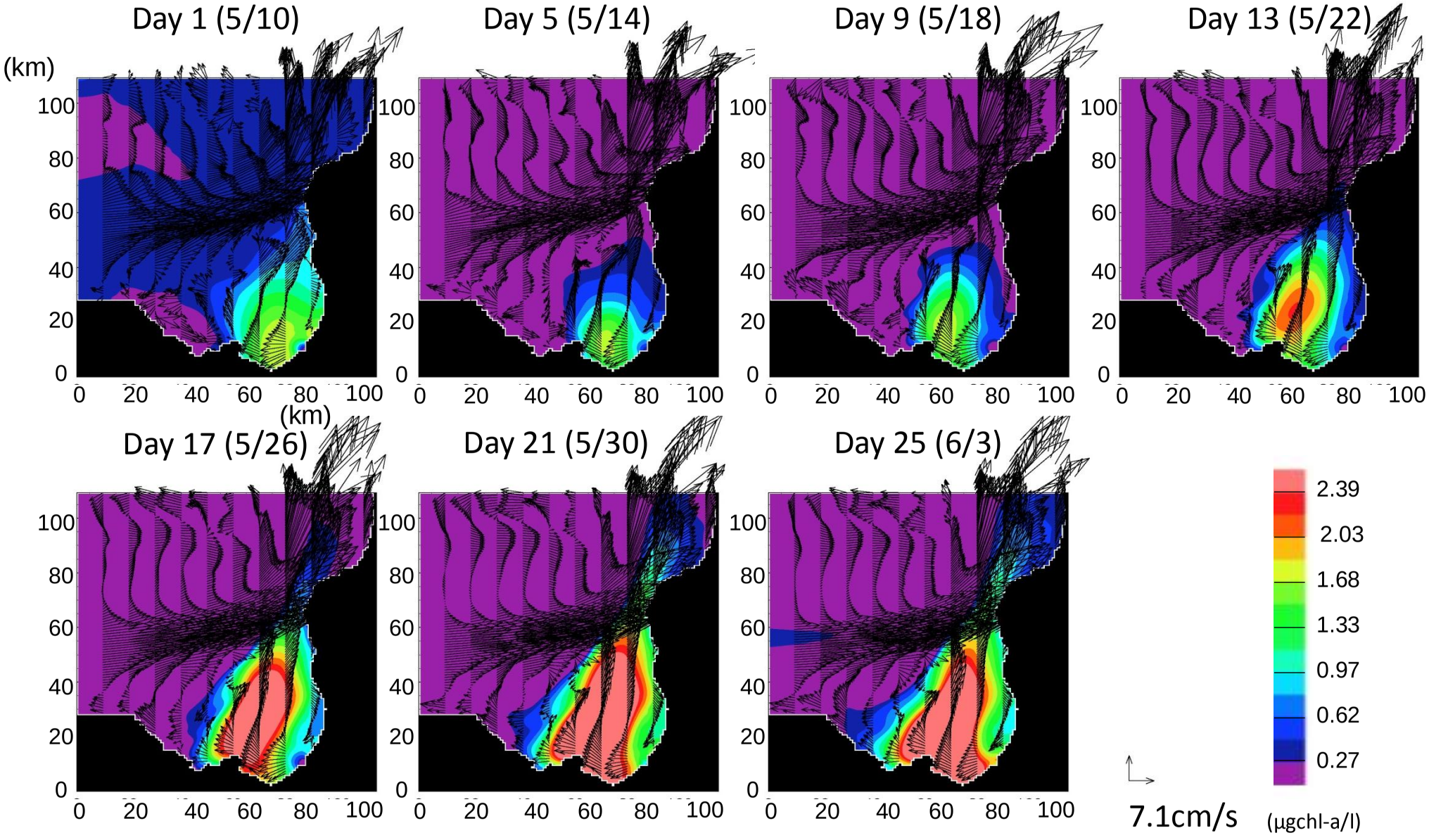

Fig. 3.5 (c): Same as (a) except that of phytoplankton.

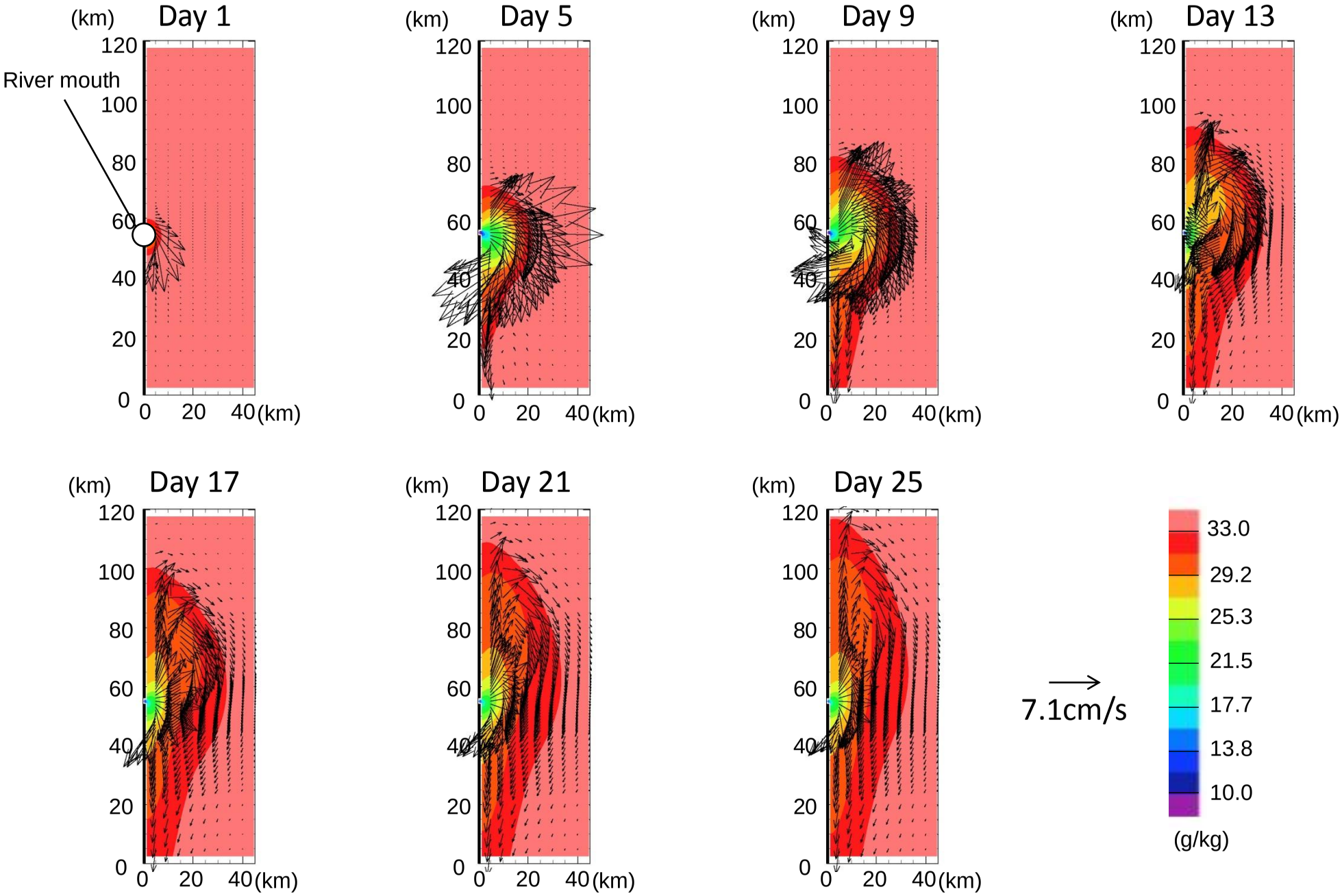

Fig. 3.6 (a): In the I-I case, the horizontal distributions of salinity in the surface layer (1 m depth), with current velocity field whose vectors are drawn at intervals of five grids.

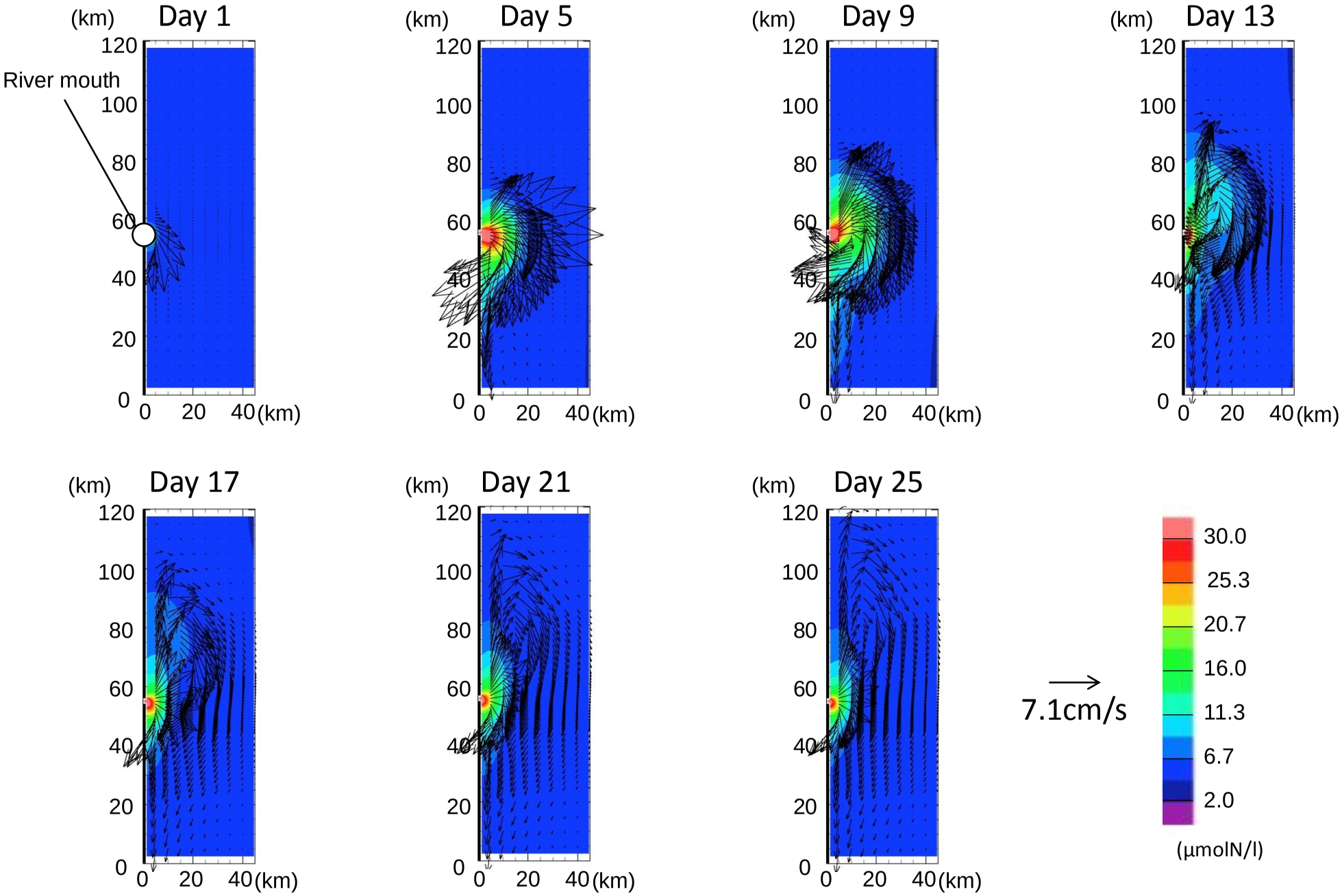

Fig. 3.6 (b): Same as (a) except that of nitrate.

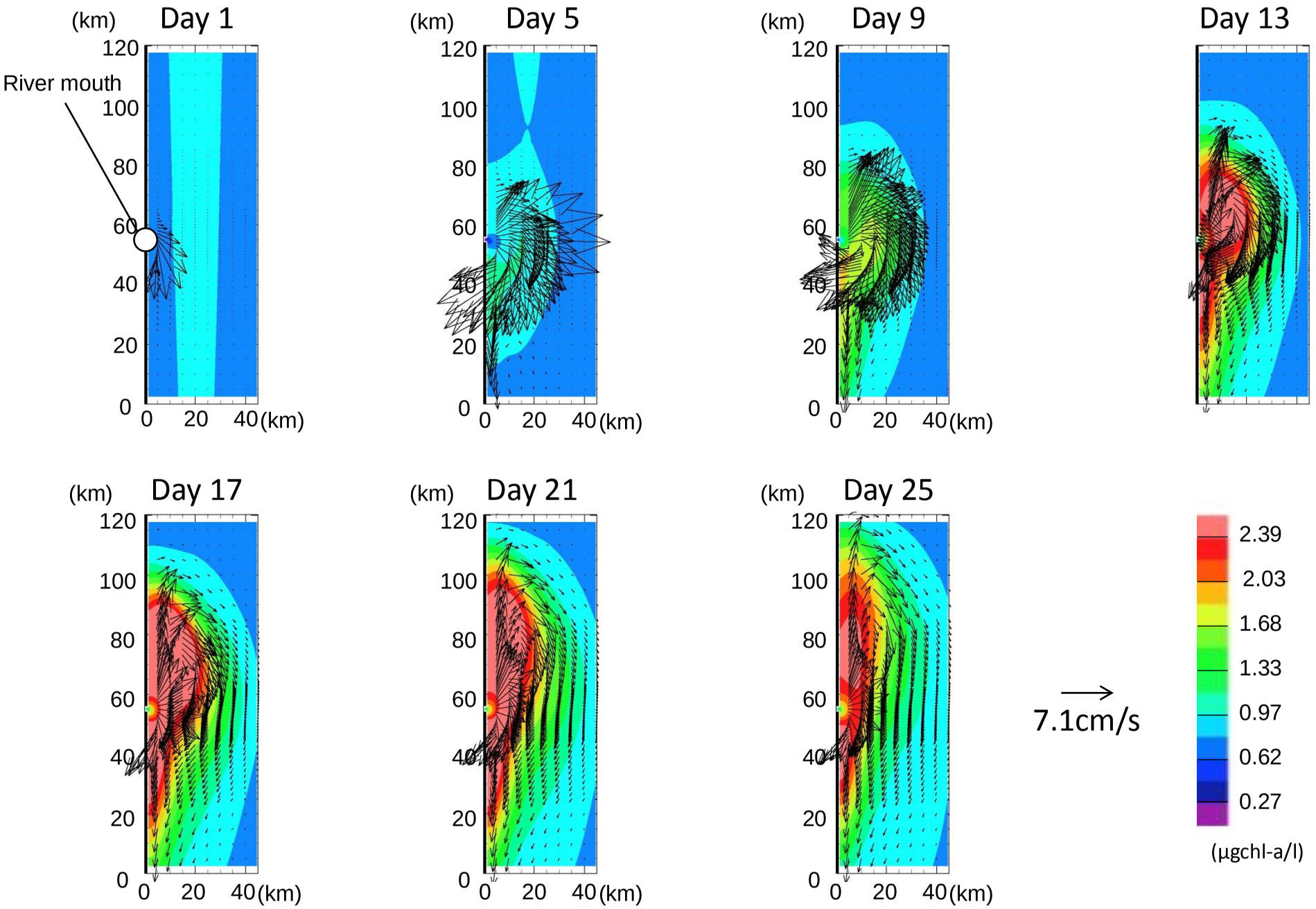

Fig. 3.6 (c): Same as (a) except that of phytoplankton.

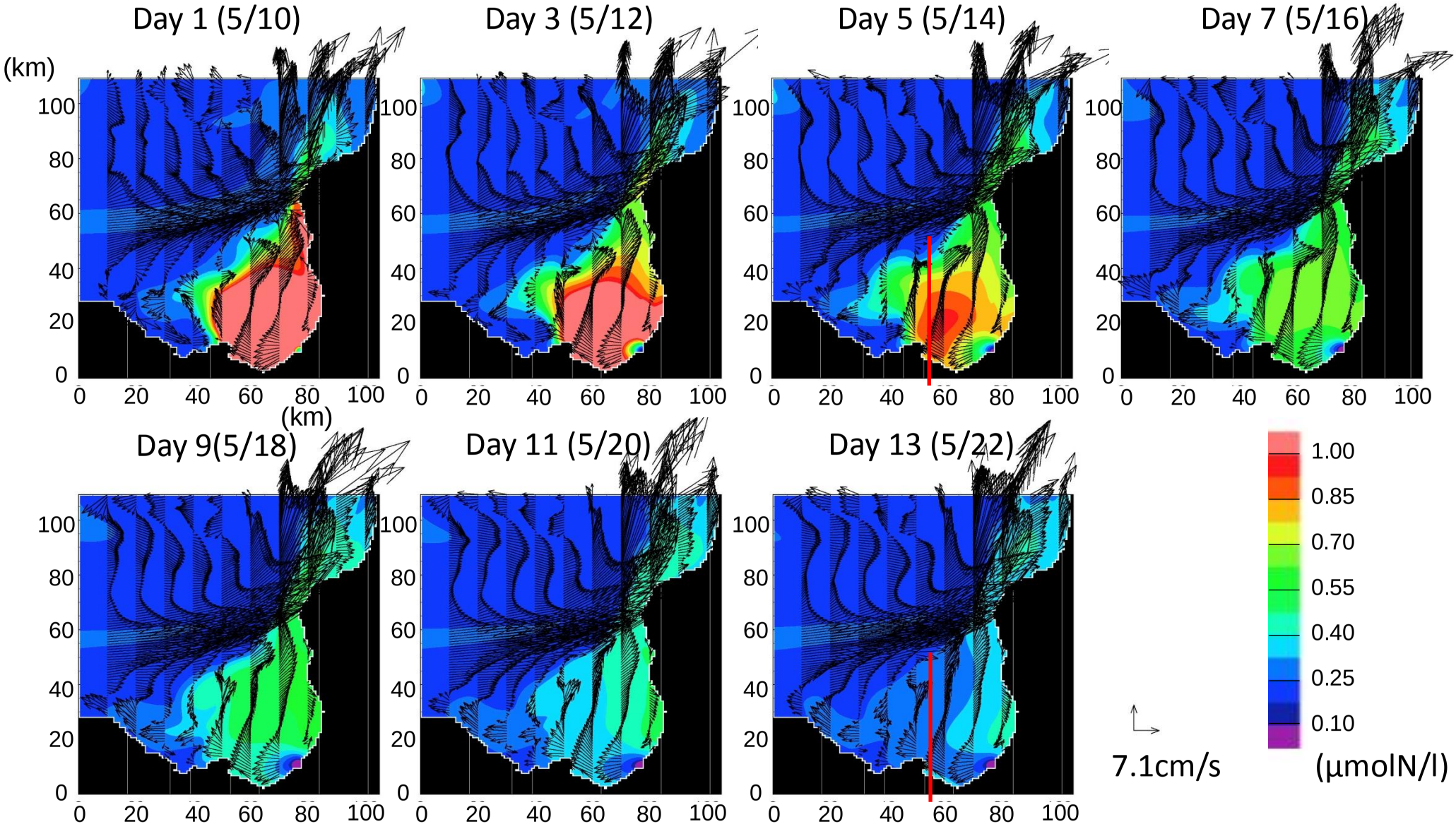

Fig. 3.7: Same as Fig. 3.5 except subsurface-originated nitrate. Red lines in Day 5 and Day 13 show the location of the vertical nearshore-to-offshore section detailed in Fig. 3.8.

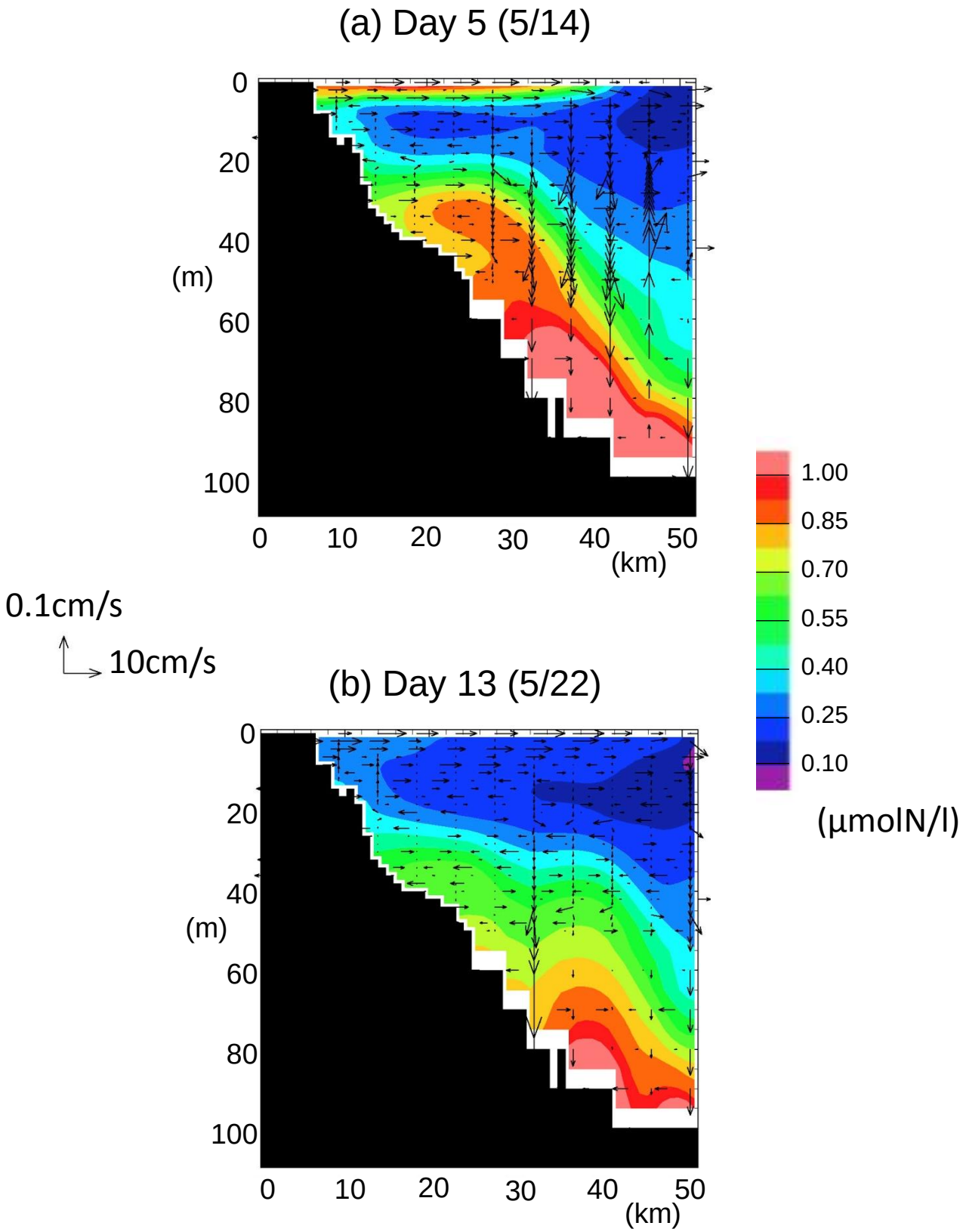

Fig. 3.8: (a) Subsurface-originated nitrate distribution and vertical circulation along the section shown as the red line in Fig. 3.7 (Day 5). (b) Same as (a) except that on Day 13.

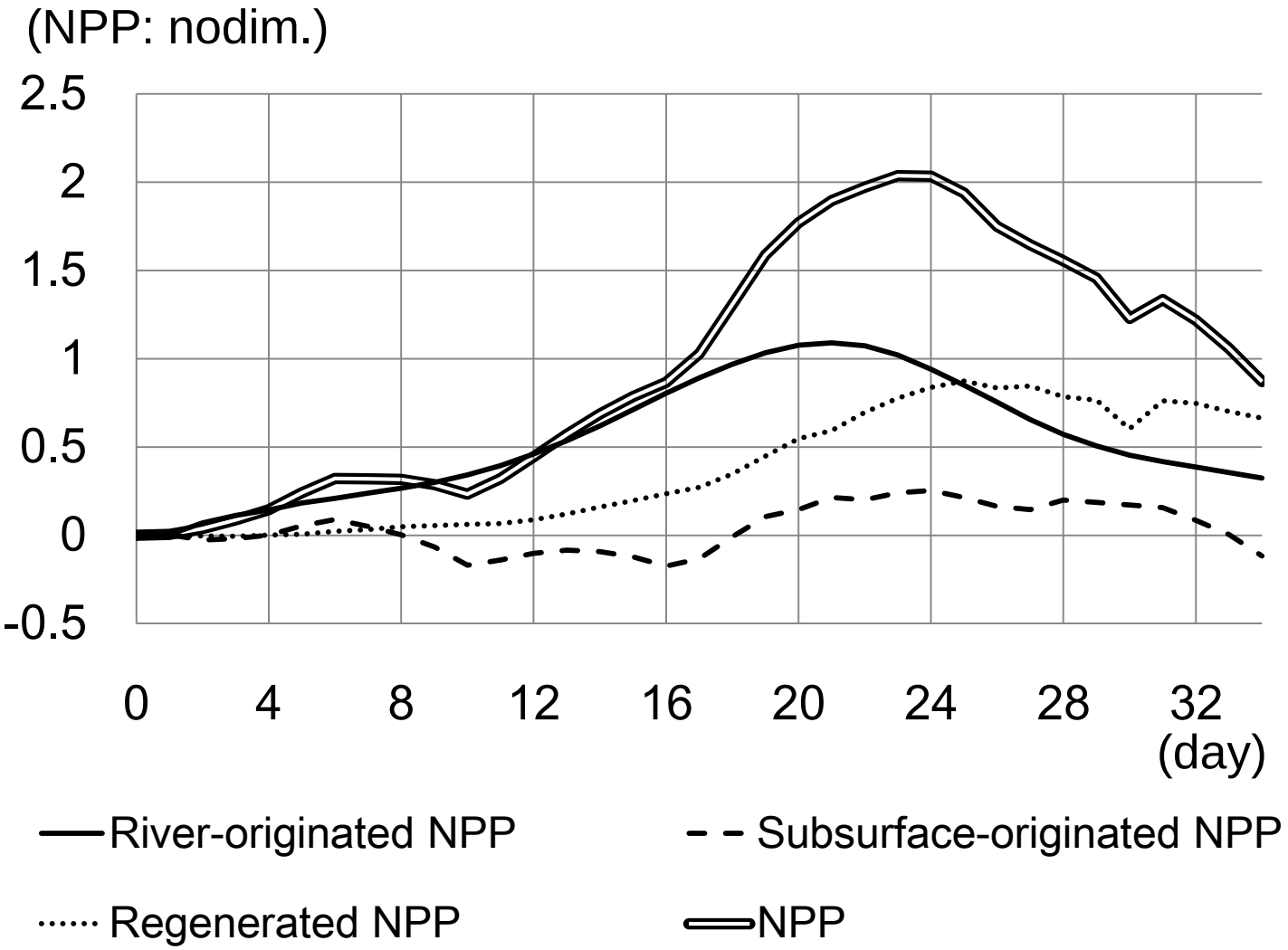

Fig. 3.9: Time series of normalized Net Primary Production, NPP, driven by river input in the calculation domain, that is, NPP in the Ishikari Bay case subtracted by that in the no flux case. NPP are categorized into three origins: river-originated (solid line), subsurface-originated (dashed line), and regenerated (dotted line) and normalized by the nitrate input, *i.e.*, nitrate of the daily mean in the Ishikari Bay case.

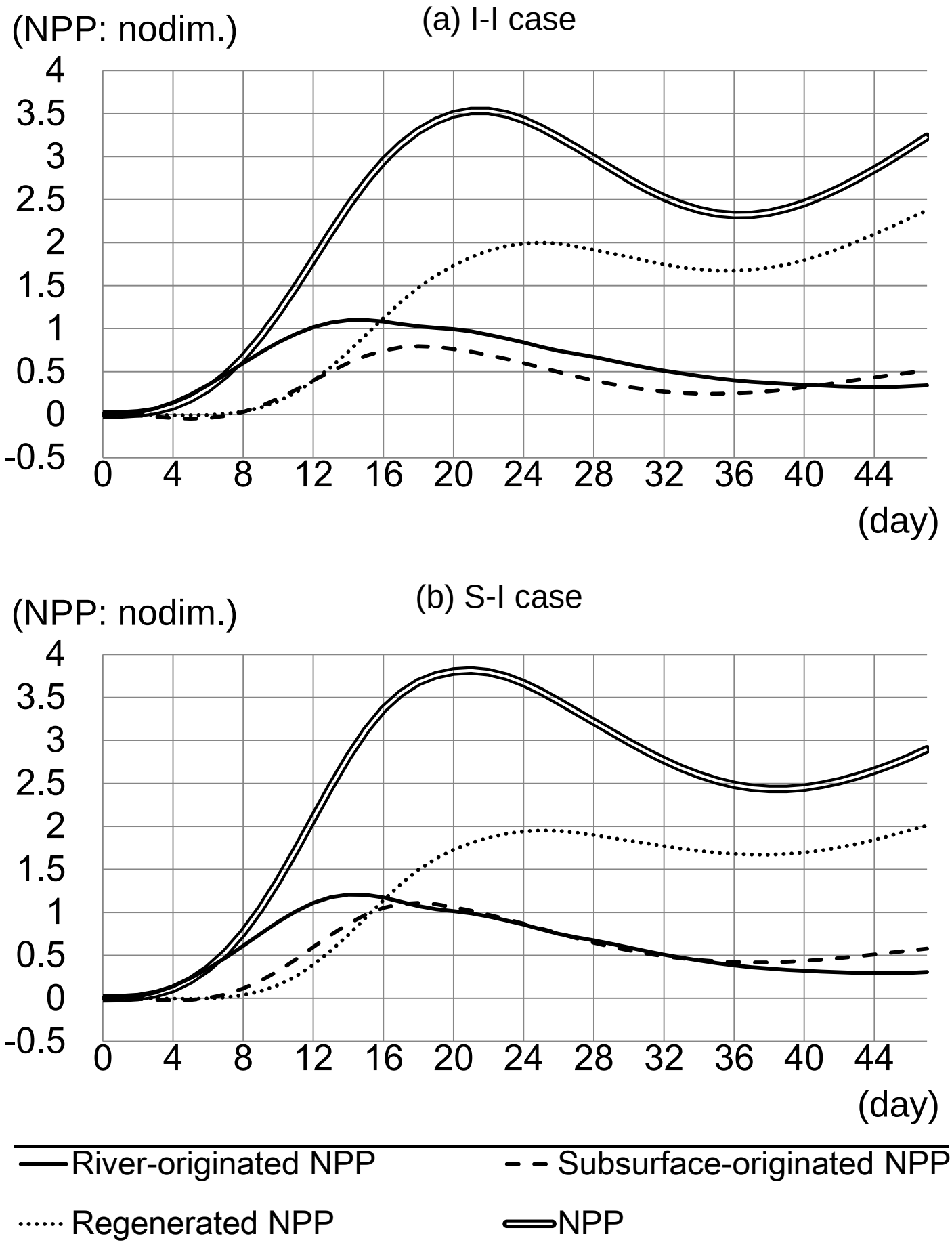

Fig. 3.10: (a) and (b) same as Fig. 3.9 except those in the I-I case and the S-I case, respectively.

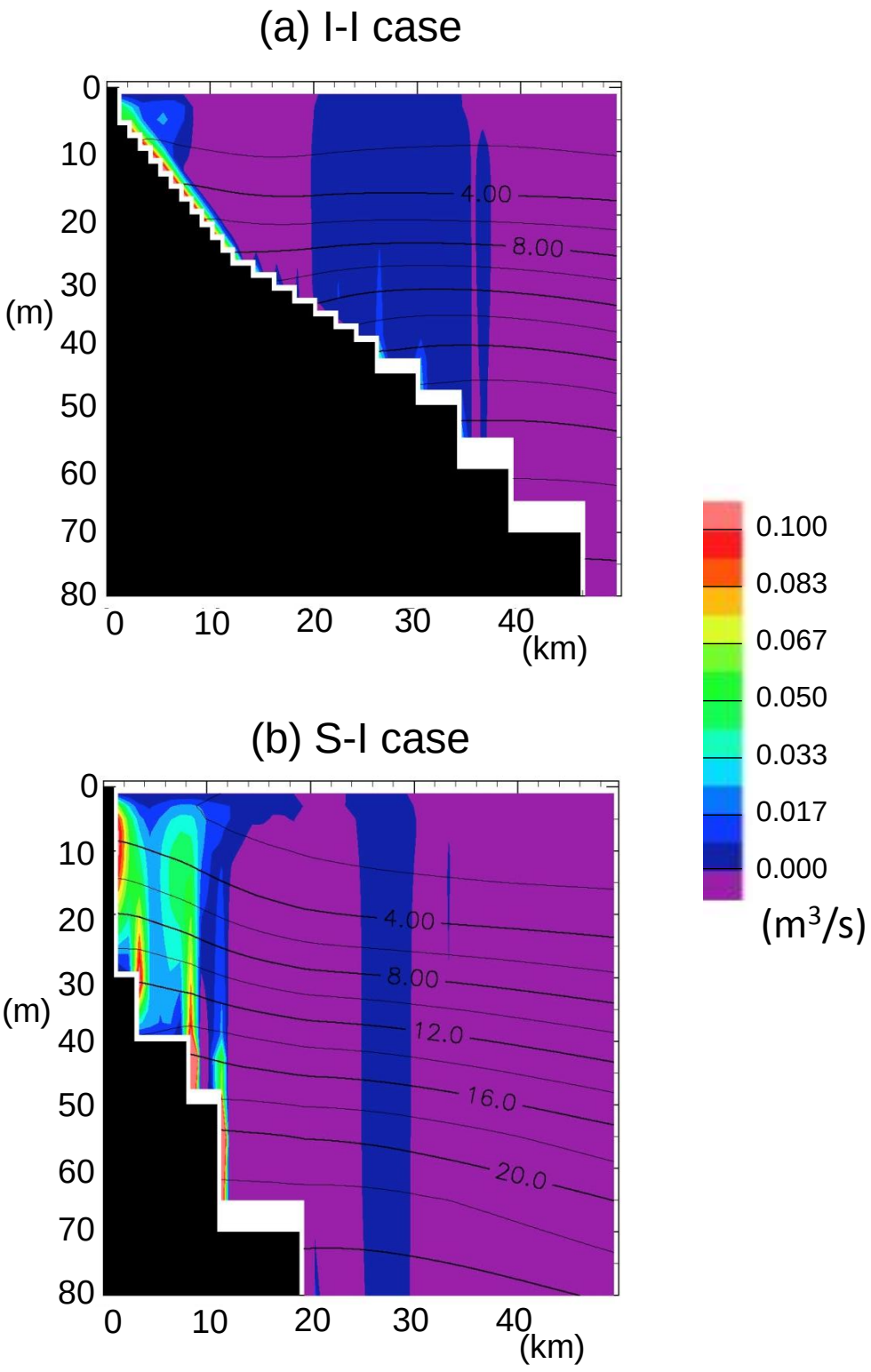

Fig. 3.11: (a) Distribution of vertical flow flux and subsurface-originated nitrate along the section at 10 km upstream from the river mouth in the I-I case (Day 19). (b) Same as (a) except that in the S-I case.

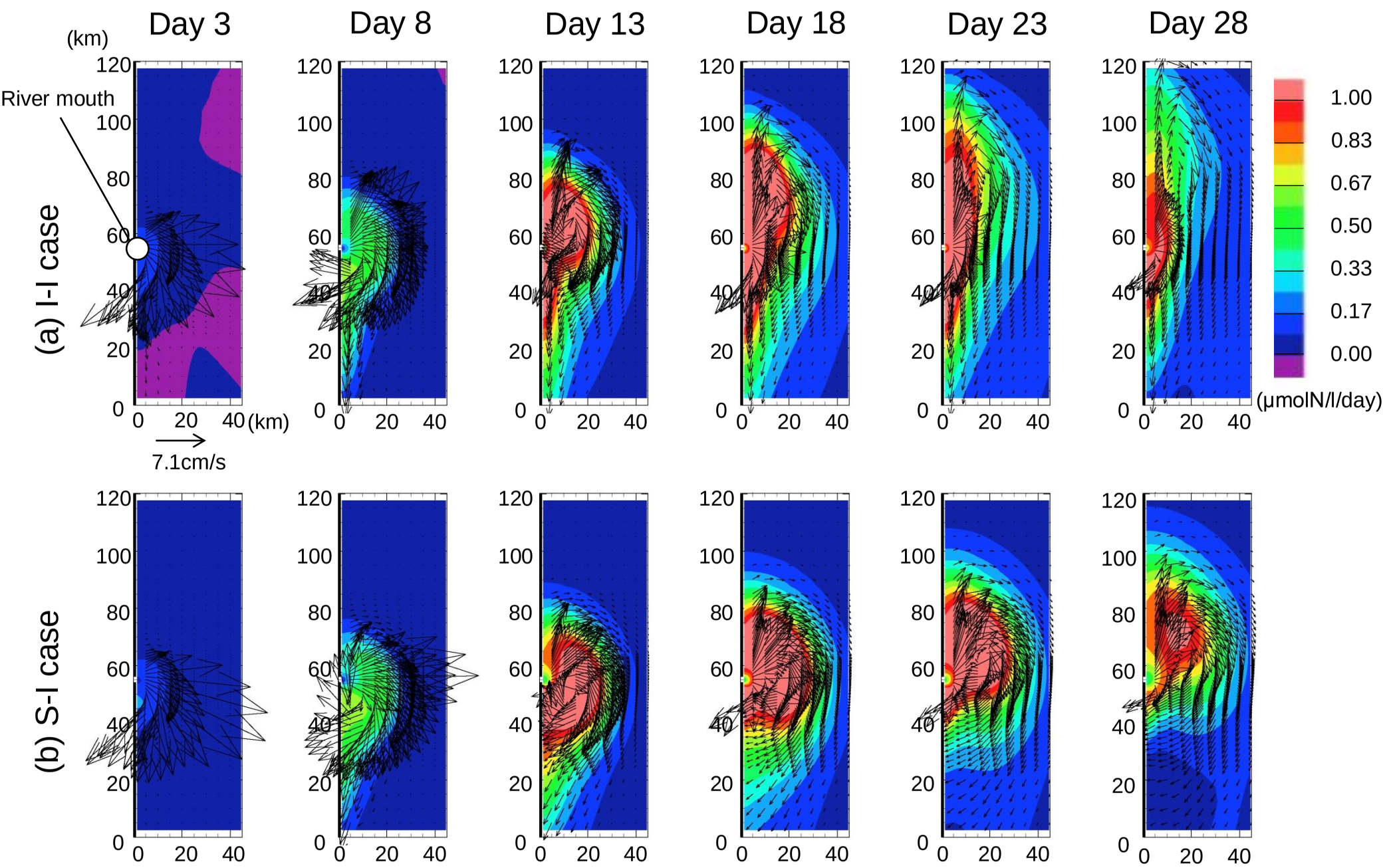

Fig. 3.12: Horizontal distributions of NPP in (a) the I-I case and (b) the S-I case in the surface layer (1 m depth), with current velocity field whose vectors are drawn at intervals of five grids.

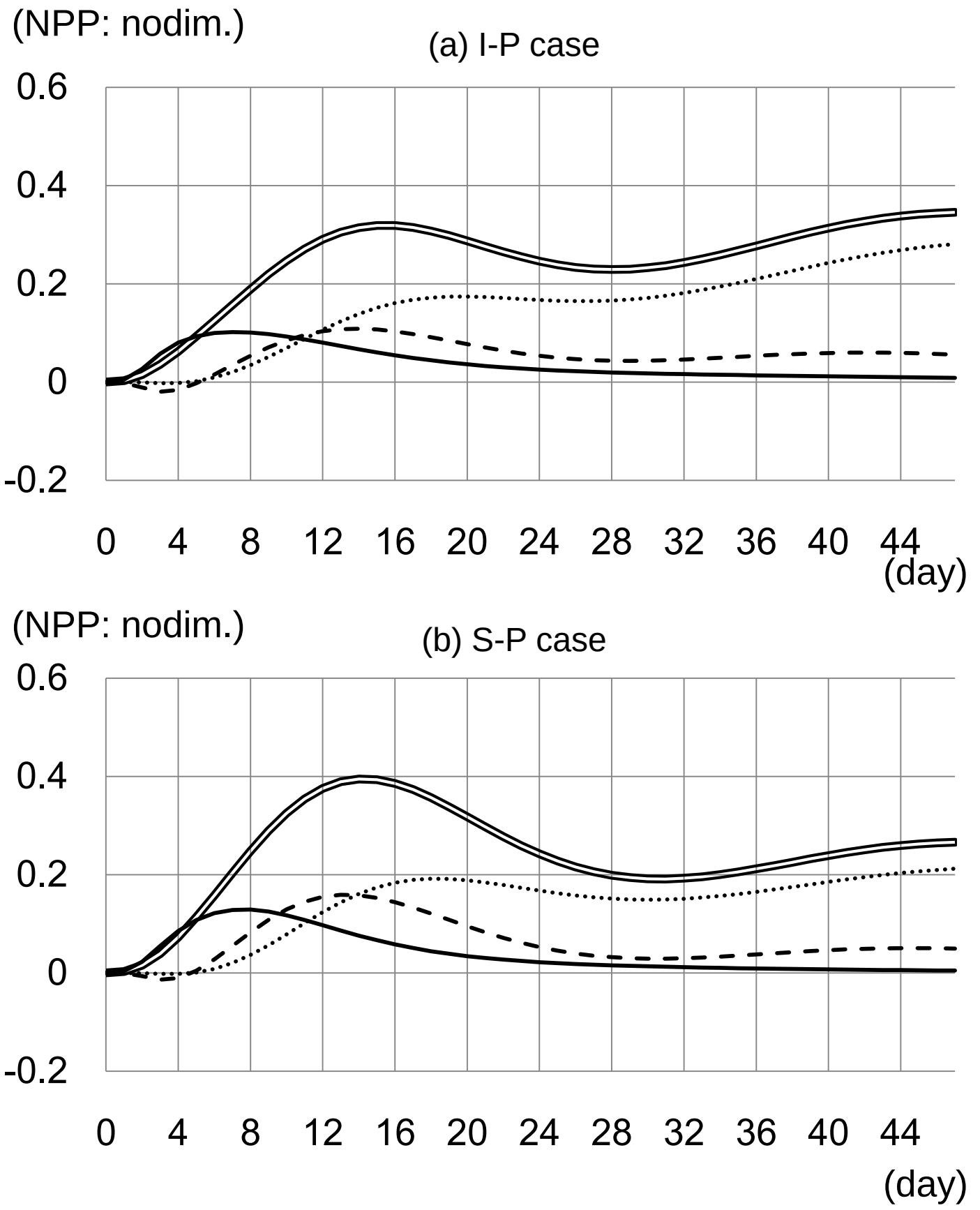

Fig. 3.13: Same as Fig. 3.9 except those in (a) the I-P case and (b) the S-P case.

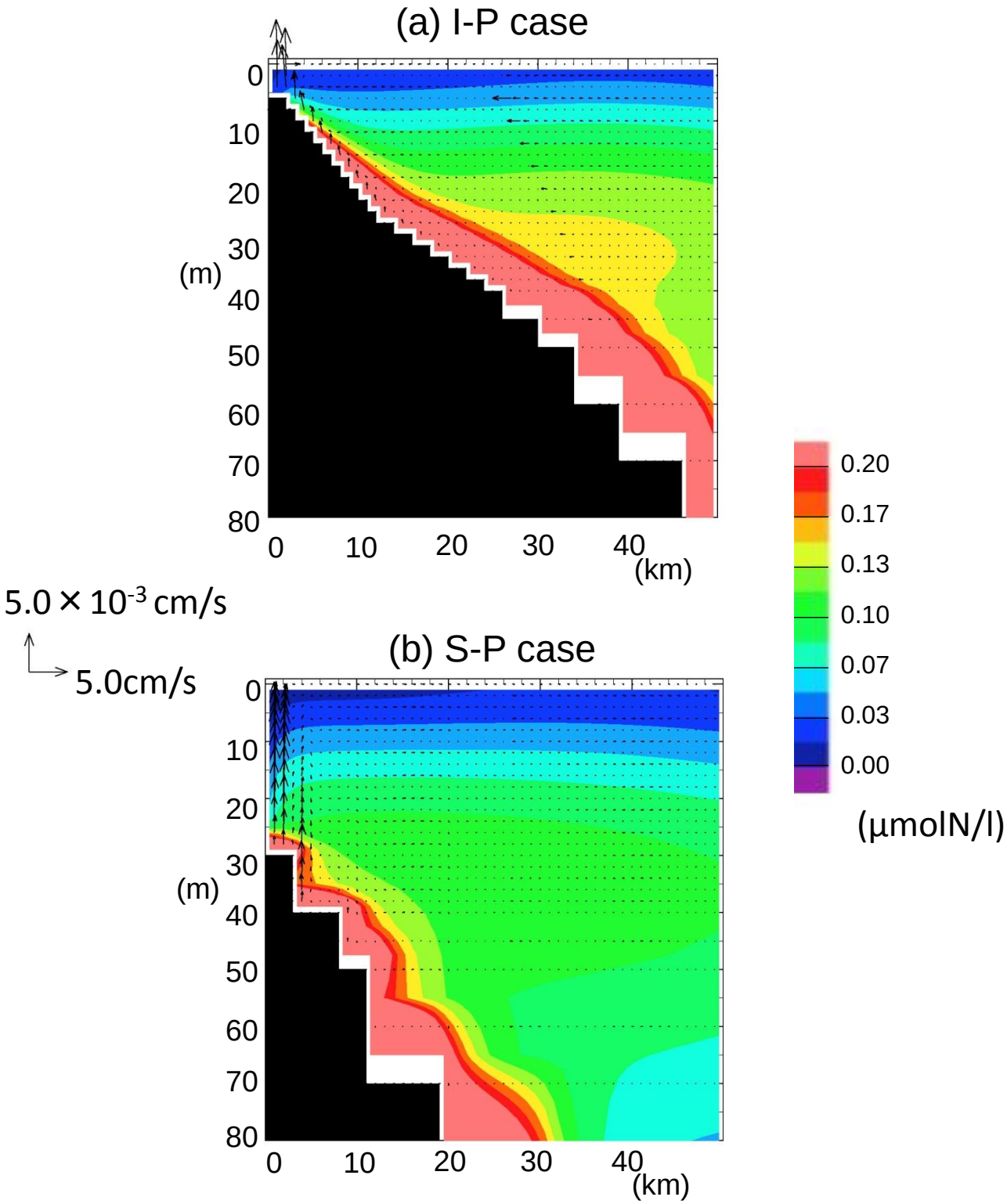

Fig. 3.14: (a) Detritus distribution and vertical circulation along the section on the river mouth in the I-P case (Day 34). (b) Same as (a) except that in the S-P case.

Chapter 4 General Conclusion

4.1 Where have we elucidated ROFI to?

We developed an ocean general circulation model (OGCM) including a simple ecosystem model to investigate the three-dimensional and daily temporal changes in phytoplankton blooms caused by riverine input such as flooding, and conducted quantitative studies focusing on primary production in ROFI.

In Chapter 2, we found that river does not only discharge nutrients to ROFI, but river also indirectly supplies nutrients with saline water from the subsurface to the surface by vertical circulation driven by the freshwater input. The direct and indirect nutrient supplies produce the shift of nitrate and phytoplankton maximum concentrations from the downstream (right-hand side of the river mouth) to the upstream (left-hand side of the river mouth) regions (D-U Shift). D-U Shift is categorized into three stages by the different nitrate origins: (1) phytoplankton increases using river-originated nitrate (RO-nitrate) in the downstream; (2) after RO-nitrate is exhausted, phytoplankton increases mainly using subsurface-originated nitrate (SO-nitrate) in the upstream, where nitrate is transported by upwelling associated with vertical circulation and horizontal anticyclonic gyre; and (3) after (SO-nitrate) is also exhausted, NPP (Net Primary Production) is kept high by regenerated nitrate (R-nitrate) in the upstream region. Several case studies (the only fresh water, SSM, *etc*.) were conducted, but the results are consistent with the above conclusion.

In Chapter 3, we conducted the realistic simulation of the Ishikari Bay to compare the conclusion in Chapter 2. The regions of salinity minimum and nitrate maximum are

located near the river mouth all the time, and the nitrate maxima do not shift as D-U Shift in Chapter 2. The phytoplankton maxima shift toward the left-hand side of the river mouth during the early time, but the shift does not keep going to the left-hand side all the time. This is because much SO-nitrate does not come from the subsurface to the surface layer after the middle simulated time, due to weak upwelling forced by vertical circulation in the left-hand side. We also conducted ideal setting-simulations to investigate the effects of bottom slope angle. The gentle angle of bottom slope weaken the vertical circulation and SO-nitrate supply from the subsurface, and the NPP is smaller than that of the steep angle case. Meanwhile, the NPP by R-nitrate become higher than that of the steep angle case, due to high concentration of detritus converted into R-nitrate on the bottom that is shallower in the gentle angle case.

It is natural that D-U Shift of phytoplankton maxima often occurs in the real situation like Ishikari Bay when high riverine input such as flooding. However, the conclusion in Chapter 2 that the shift is categorized into three stages by the different nitrate origins, RO-, SO- and R- nitrates in turn depends on the bottom slope angle and the way of inputs and the amounts of fresh water and nutrients. Recent simulation studies of global warming scenarios suggest that freshwater flux from rivers in the world would have greater fluctuations in magnitude (*e.g.*, Nijssen *et al*., 2001).

Horizontal fine resolution (1km~) set in this study enables to represent D-U Shift induced by horizontal and vertical circulation, and to have the detail spatial conclusion as the above. The fine resolution is practical for understanding ecosystem and biogeochemistry in ROFI. This study has elucidated primary production in a subarctic ROFI among comprehensive coastal regions, due to the biological parameters assumed in a subarctic region, so that different results from this study would be derived in the

case of other regions, for example, tropical region.

Numerical simulations are so helpful to understand a mechanism of phenomena, although numerical simulations are very difficult to reproduce the observed data. However, we must choose discussed topics under the given model setting, or set suitable model settings for topics we want. We should know the limitation of numerical simulations. In Chapter 3, for instance, we have focused on the dynamics for phytoplankton blooms such as the time sequence of nutrient origins, rather than matching to the observed data such as chlorophyll-a concentration. In this study, we cannot discuss long termed events such as seasonal variations of NPP or termination dynamics of phytoplankton blooms as a response to riverine input of nutrient, because these events are controlled by the other factors not considered in this study such as top-down control by zooplankton and physical forcing and/or processes.

In the respects of physical factor, we found that bottom slope angle and the way of freshwater input change the behaviour of plumes, nutrient supply from the subsurface with the change of vertical circulation, and the rate of regeneration. However, effects of coastal wind and background flow have not discussed yet. If wind stress was included, the D-U Shift would have a shorter distance but this phenomenon remains. Future studies are needed to investigate how variations of freshwater flux, geography as bottom slope angle and wind forcing change plankton blooms by flooding in ROFI.

4.2 For further studies

We found in this study that fresh water discharged from river is very important for ecosystem in ROFI, because horizontal and vertical circulations driven by geostrophic

adjustment and buoyancy spread nutrients from river over surface layer and generate nutrients supply from subsurface layer, respectively.

Recent studies show that large groundwater often exists under river systems (Fan *et al.*, 2013). Amazon River, for instance, has enormous ground water that is much broader at about 200 to 400 km wide, compared to the Amazon's width of about 1 to 10 km, and the studies concerning the ground water have been carried out (*e.g.*, Miguez-Macho and Fan, 2012; Pokhrel *et al.*, 2013). In Japan, Toyama Bay has a lot of submarine groundwater discharge (Kameyama *et al.*, 2005). Ecosystem and biogeochemical processes might be influenced by supplies of buoyancy by fresh water and nutrients from groundwater to the coastal region.

High SSM concentration also would affect the buoyancy of water from river during big flooding, because SSM increase the water density. In abyssal region, turbidity current is known as a tremendous transporter of SSM from continental slope to abyssal zone (Open University Course Team, 1989). The SSM concentration is proportional to the mass flux of river discharge to about the second power. The concentration would become equal to the initial salinity (33.5 g/kg), when the mass flux was about 14,000 m^3/s in equation (1), and the value is not impossible. The discharged high dense water might sink, gradually lighten with SSM removed from the water, and rise to the surface. The process is possible to help stirring coastal water with the buoyancy change.

Not a hydrostatic model used in this study but non-hydrostatic model is needed to estimate the both effects of submarine groundwater and high SSM water inputs on physical process, ecosystem and biogeochemical cycle. The effect is not appropriately estimated in recent global simulations, due to insufficient of resolution and computational resource. In future, we will use a non-hydrostatic model and begin with

small coastal region, and broaden the region to the global ocean for the unfinished dream that is solving ROFI's true colors.

Appendix Tide effects on phytoplankton blooms

Effect of tide has not been discussed in the above chapters. In the appendix, we conducted experiments with a simple tide process to confirm that the effect of tide on phytoplankton blooms.

The same ideal settings as the control case in Chapter 2 are applied except the tide process and periodic boundary condition toward y-direction (see Fig. 2.2). The tide process was incorporated, based on Isobe (2005) that represents the tide as a semidiurnal tidal wave that is ubiquitous in coastal and shelfwaters, according to the following equation:

$$\eta(x',\ t) = u_0\sqrt{\frac{H}{g}}e^{-x'/R}\cos\left(\frac{2\pi}{T_0}t\right) \qquad (5)$$

where η is the surface elevation, x' denotes the offshore distance from the coast, u_0 is the typical value of alongshore tidal-current amplitude (= 0.2 m/s), H is the depth, R is the external Rossby radii and T_0 represents the semidiurnal period (= 0.5 day). After a spin-up of 8 days with only the tide, we used the distributions and flows as initial conditions of the experiments driven by river input.

The tide-induced residual current flows along the coast from the upstream to the downstream (Compare Figure A.1 (a) with (b)). The extent of low salinity in the tide case is smaller than that in the no tide case all the time (Fig. A.1 (a), (b)), because the residual current increases the transport of fresh water to the downstream. The result is consistent with that of Isobe (2005). The area of high nitrate of the tide case is always

larger than that of the no tide case (Figure A.2 (a), (b)), especially the front of the tide case grows along the near coast. The area of phytoplankton bloom of the tide case is also larger than that of the no tide case, and D-U Shift occurs in the both cases (Figure A.3 (a), (b)). The shift in the tide case more proceeds to the upstream than that in the no tide case, due to the region of high nitrate extending to the upstream.

The vertical flow strengthened by tide along the coast supplies SO-nitrate (subsurface-originated nitrate) from the subsurface. Tide effect causes that the extent of upwelling and downwelling spreads to the upstream and to the downstream, respectively, and the upwelling and downwelling are strengthened along the near coast (Figure A.4 (a), (b)). The stronger upwelling of the tide case (*e.g.*, x = 1~10 km) transports high SO-nitrate from the subsurface to the surface layer in the upstream region (Figure A.5 (a)).

In the case that tide is included, the river plume of low salinity is horizontally suppressed. However, the extents of high nutrients and phytoplankton bloom more spread than that of no tide case, because tide strengthen vertical flow and supply subsurface water with high nutrients to surface layer. D-U Shifts of nitrate and phytoplankton also occur in the tide case, and the proceeding to the upstream is faster than that in the no tide case.

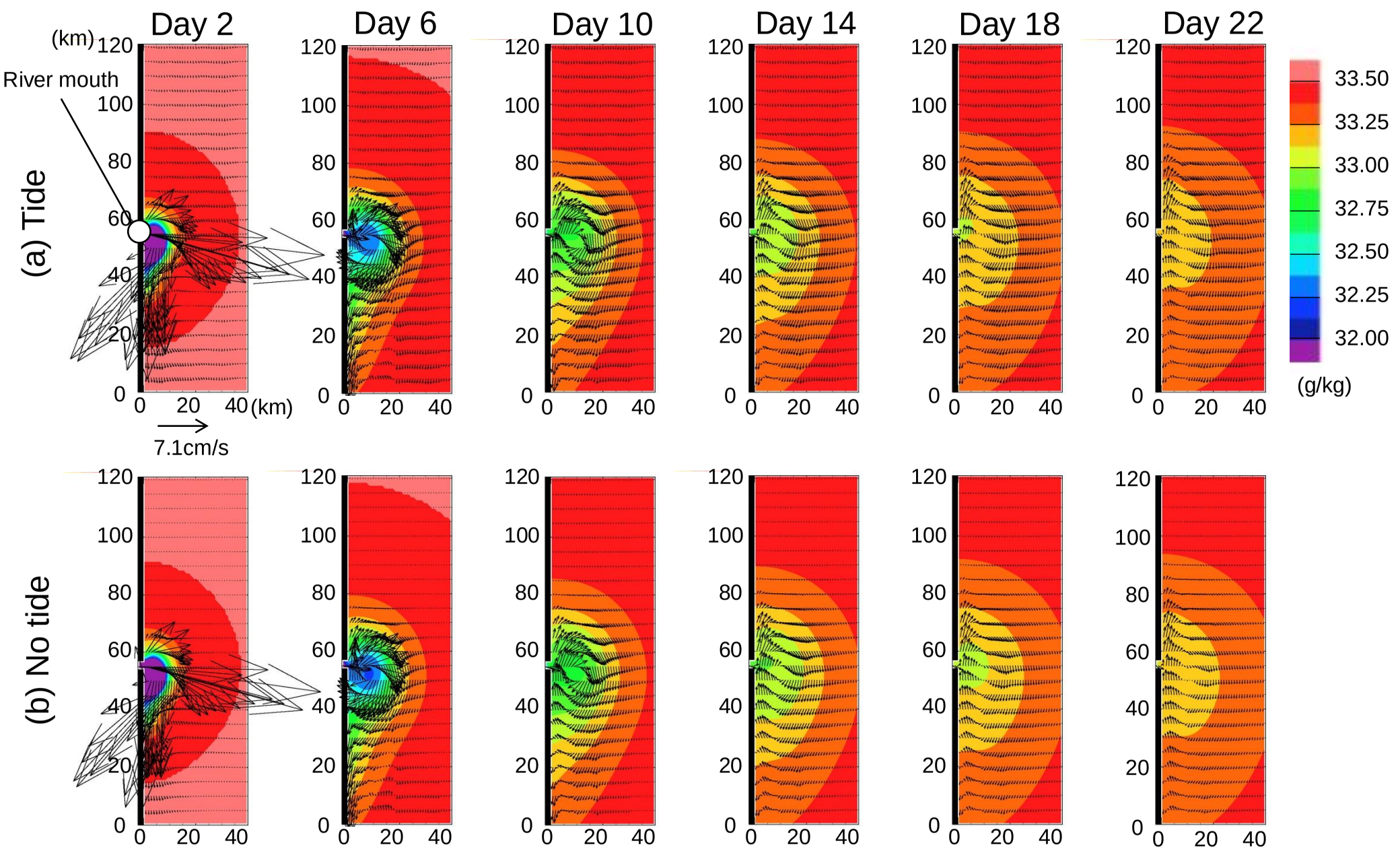

Fig. A.1: Horizontal distributions of salinity in (a) the tide case and (b) the no tide case in the surface layer (5 m depth), with current velocity field whose vectors are drawn at intervals of five grids.

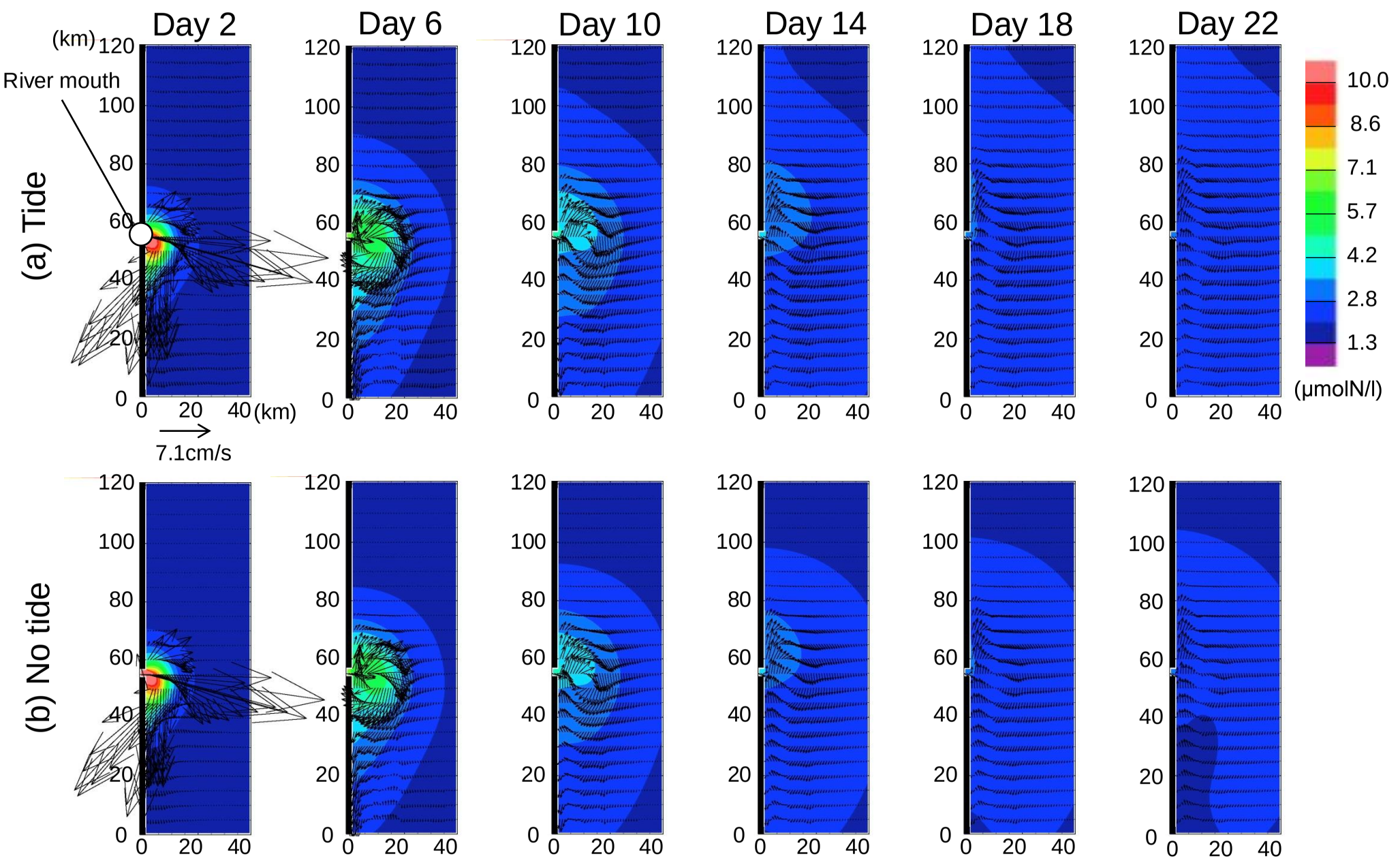

Fig. A.2: Same as Fig. A.1 except that of nitrate.

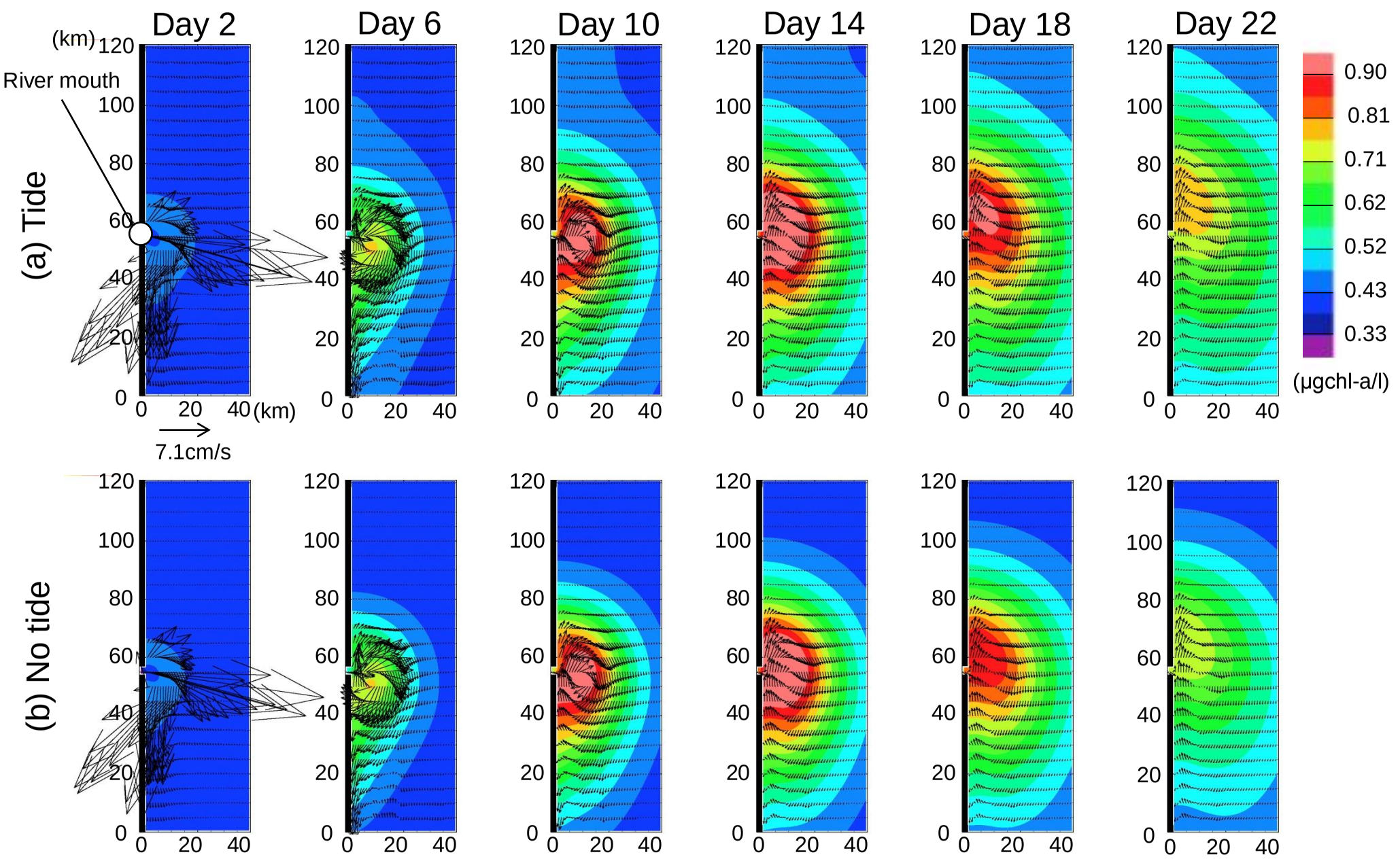

Fig. A.3: Same as Fig. A.1 except that of phytoplankton.

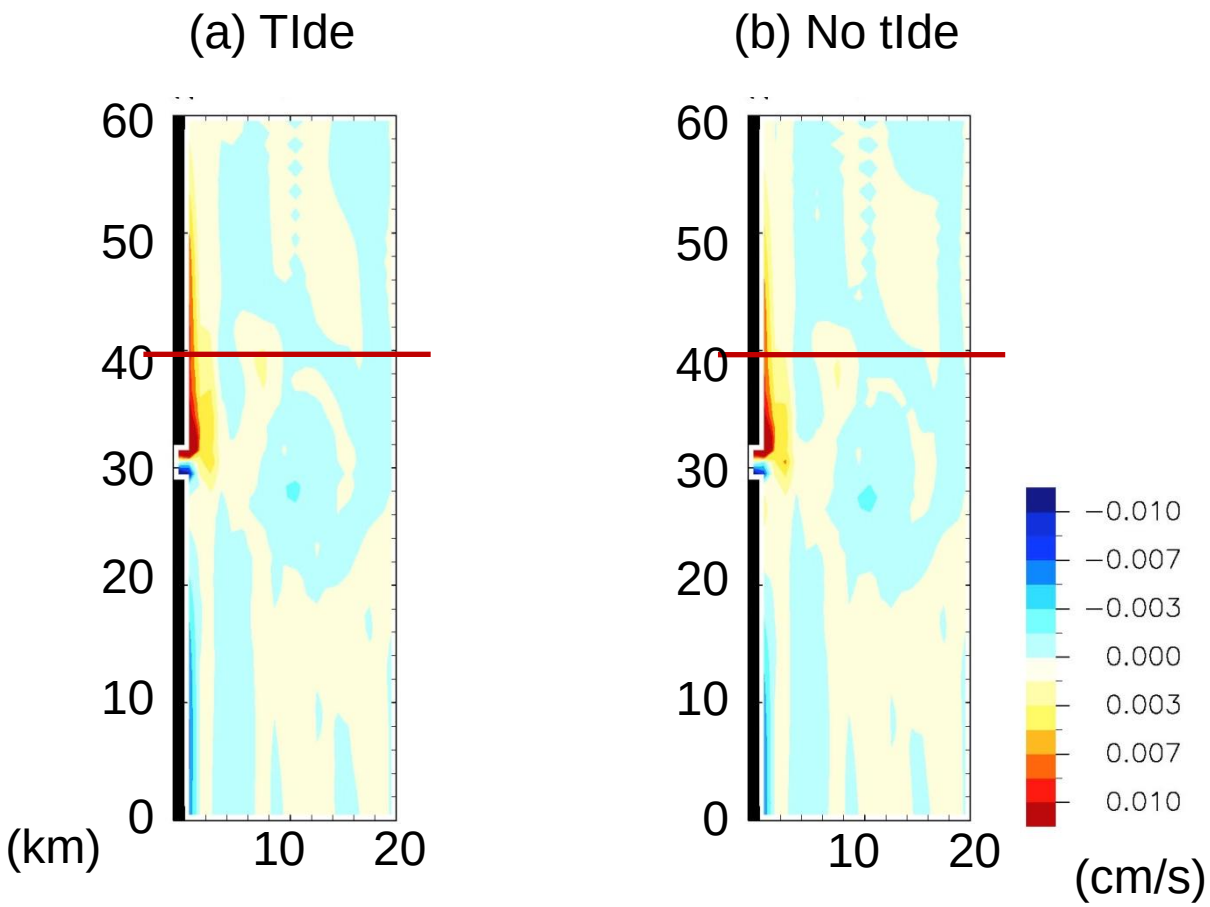

Fig. A.4: Horizontal distributions of vertical flow in (a) the tide case and (b) the no tide case over 10 m depth (Day 10). Red lines in (a) and (b) show the location of the vertical nearshore-to-offshore section detailed in Fig. A.5.

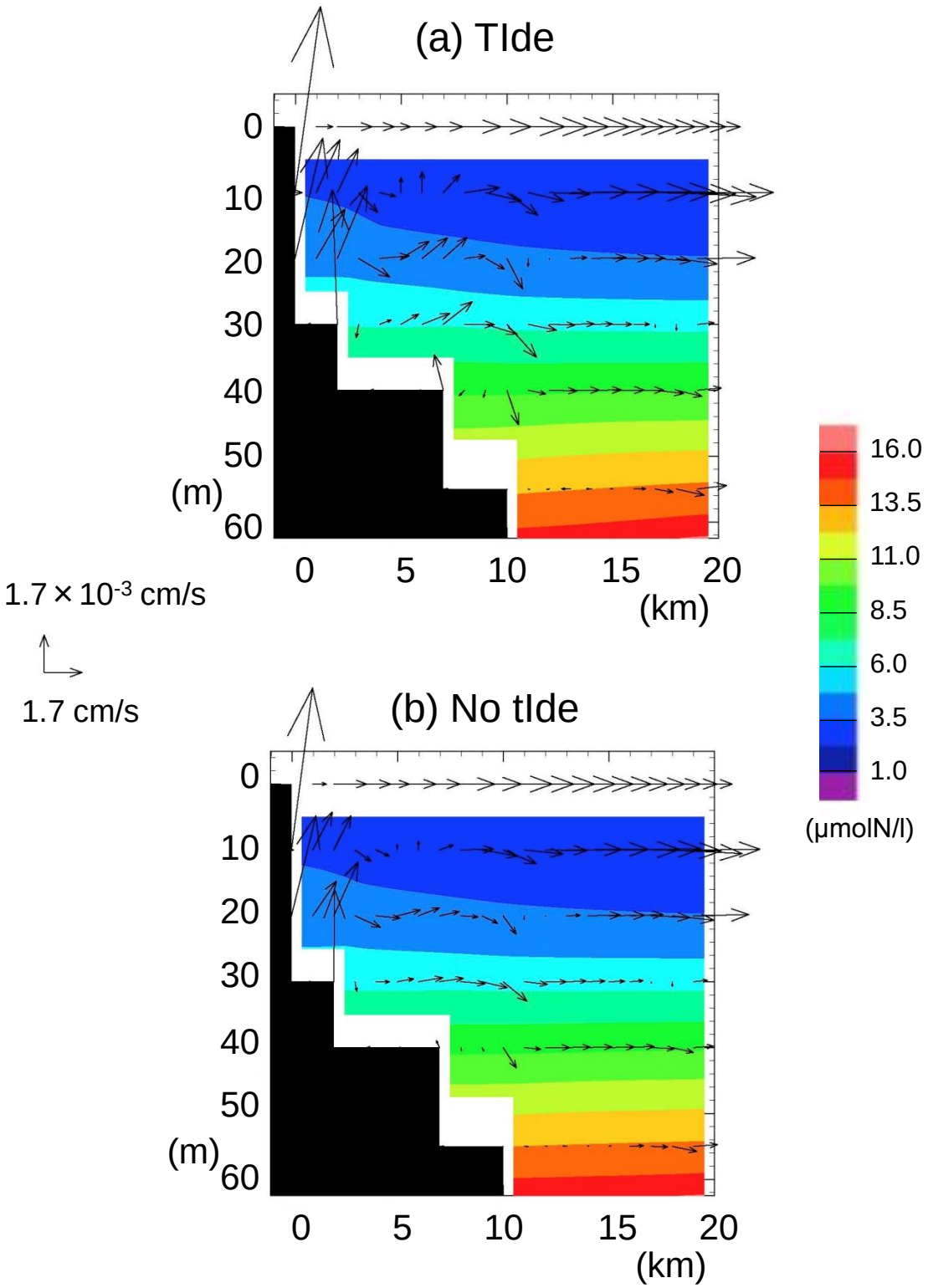

Fig. A.5: (a) Subsurface-originated nitrate distribution and vertical circulation along the section shown as the red line in Fig. A.4 (a). (b) Same as (a) except that in the no tide case.

Acknowledgements

I would like to express my deepest gratitude to my supervisor Prof. Yasuhiro Yamanaka who guides and supports me in my study and student life. I would express special obligation to Dr. Genta Mizuta for helping with the model settings and discussions many times.

The member of this dissertation committee provided many insightful comments: Prof. Yamanaka, Prof. Humio Mitsudera, Dr. Jun Nishioka and Dr. Goh Onitsuka. I am very grateful to Dr. Atsushi Kubokawa, Dr. Isao Kudo and Dr. Tomohisa Irino for discussing the physics of river plumes, providing biogeochemical data in Ishikari Bay and providing the information on empirical coefficients in Tokachi River, respectively. I deeply thank to Dr. Yutaka Isoda of the Faculty of Fisheries Sciences, Hokkaido University for providing physical data in Ishikari Bay and discussing the physics of ROFI. I am also much appreciative of Prof. Youichi Tanimoto, Prof. Keiichiro Ohshima, Prof. Naoto Ebuchi, Prof. Fumio Hasebe, Dr. Yutaka Watanabe, Dr. Tomohiro Nakamura, Dr. Yasushi Fukamachi, Dr. Takeshi Horinouchi and Dr. Masatomo Fujiwara who gave me many insightful comments in academic conferences, informal seminars or personal communications.

I would like to thank the members and graduates of Division of Ocean and Atmospheric Sciences, Graduate School of Environmental Science, Hokkaido University: Dr. Takafumi Hirata, Dr. Kazuhiro Misumi, Dr. Naosuke Okada, Dr. Yoshio Masuda, Dr. Hiroshi Sumata, Dr. Masahito Shigemitsu, Dr. Kunihiro Aoki, Dr. Naoki Yoshie, Dr. Taketo Hashioka, Dr. Akitomo Yamamoto, Dr. Ryota Shibano, Dr. Xuanrui

Xiong and Mr. Junji Matsuda. And it was a very valuable experience to share our student life with Dr. Yoichi Inai, Mr. Kouhei Kai, Dr. Satoshi Omiya, Mr. Hirotaka Sasaki, Mr. Yasunori Sue and other harmonious classmates and underclassmen.

Yasuhiro Hoshiba was supported by the Grant-in-Aid for the Global COE Program from MEXT and by Development of mitigation and adaptation techniques to global warming in the sectors of agriculture, forestry, and fisheries as a research assistant.

References

Agboola, J. I., S. Yoshi and I. Kudo (2009): Seasonal change of riverine nutrients and distribution of chlorophyll a in Ishikari Bay, subarctic oligotrophic coastal environment of Japan. *La mer*, **47**, 1-17.

Agboola, J. I., M. Uchimiya, I. Kudo, K. Kido and M. Osawa (2010): Dynamics of pelagic variables in two contrasting coastal systems in the western Hokkaido coast off Otaru port, Japan. Estuar., coast. shelf sci., **86**, 477-484.

Beardsley, R. C., R. Limeburner, D. Hu, K. Le and G. A. Cannon (1985): Discharge of the Changjiang (Yangtze River) into the East China Sea. *Cont. Shelf Res*., **4**, 57–76.

Beman, J. M., K. R. Arrigo and P. A. Matson (2005): Agricultural runoff fuels large phytoplankton blooms in vulnerable areas of the ocean. *Nature*, **434**, 211-214.

Bowden, K. F. (1983): Physical Oceanography of Coastal Waters. *John Wiley*, 302 pp.

Chapman, D. C. and S. J. Lentz (1994): Trapping of a coastal density front by bottom boundary layer. *J. Phys. Oceanogr*., **24**, 1464–1479.

Chao, S.-Y. and W. C. Boicourt (1986): Onset of estuarine plumes. *J. Phys. Oceanogr*., **16**, 2137–2149.

Costanza, R., R. d'Arge, R. de Groot, S. Farber, M. Grasso, B. Hannon *et al*. (1997): The value of the world's ecosystem services and natural capital. *Nature*, **387**, 253-260.

Fan, Y., H. Li and G. Miguez-Macho (2013): Global Patterns of Groundwater Table Depth. *Science*, **339**, 940-943.

Garvine, R. W. (2001): The impact of model configuration in studies of buoyant coastal discharge. *J. Mar. Res.*, **59**, 193-225.

Griffies, S. M. and R. W. Hallberg (2000): Biharmonic friction with a Smagorinsky-like viscosity for use in large-scale eddy-permitting ocean models. *Mon. Wea. Rev.*, **128**, 2935–2946.

Hasumi, H. (2002): Sensitivity of the global thermohaline circulation to interbasin freshwater transport by the atmosphere and the Bering Strait throughflow. *J. Climate*, **15**, 2516-2526.

Ileva, N. Y., H. Shibata, F. Satoh, K. Sasa and H. Ueda (2009): Relationship between the riverine nitrate-nitrogen concentration and the land use in the Teshio River watershed, North Japan. *Sustain. Sci.*, **4**, 189-198.

Isobe, A. (2005): Ballooning of river-plume bulge and its stabilization by tidal currents. *J. Phys. Oceanogr.*, **35**, 2337-2351.

Kaiser, M. J., M. J. Attrill, S. Jennings, D. N. Thomas, D. K. A. Barnes, A. S. Brierley, J. G. Hiddink, H. Kaartokallio, N. V. C. Polunin and D. G. Raffaelli (2005): Marine Ecology: Processes, Systems, and Impacts. *Oxford Univ. Press*, 501 pp.

Kameyama, S., U. Tsunogai, T. Gamo, J. Zhang, M. Suzuki and Y. Koyama (2005): Geochemical studies on submarine groundwater discharges in Toyama Bay using methane as a tracer (*in Japanese with English abstract*). *Geochemistry*, **39**, 131-140.

Kubokawa, A. (1991): On the behavior of outflows with low potential vorticity from a sea strait. *Tellus*, **43A**, 168-176.

Kudo, I., T. Yoshimura, C. W. Lee, M. Yanada and Y. Maita (2007): Nutrient regeneration at bottom after a massive spring bloom in a subarctic coastal

environment, Funka Bay, Japan. *J. Oceanogr.*, **63**, 791-801.

Kusuda, T. (2003): Aquatic environment in estuaries (*in Japanese*). Journal of Japan River Association '*KASEN*', **680**, 20-26.

Kusuda, T., K. Koga and Y. Awaya (1978): Aggregation of clay particles in salty water (*in Japanese*). *Journal of Water and Waste*, **20**, 295-300.

Le, V. S., T. Yamashita, T. Okunishi, R. Shinohara and M. Miyatake (2006): Characteristics of suspended sediment material transport in the Ishikari Bay in snowmelt season. *Applied Ocean Res.*, **28**, 275-289.

Leonard, B. P. (1979): A stable and accurate convective modeling procedure based upon quadratic upstream interpolation. *Comput. Methods Appl. Mech. Eng.*, **19**, 59–98.

Leonard, B. P., M. K. MacVean and A. P. Lock (1993): Positivity-preserving numerical schemes for multidimensional advection. *NASA Tech. Memo.* 106055, 62 pp.

Lihan, T., S. Saitoh, T. Iida, T. Hirawake and K. Iida (2008): Satellite-measured temporal and spatial variability of the Tokachi River plume. Estuar., coast. shelf sci., **78**, 237-249.

Magome, S. and A. Isobe (2003): Current structure and behavior of the river plume in Suo-Nada. *J. Oceanogr.*, **59**, 833-843.

Matano, P. R. and E. D. Palma (2010): The upstream spreading of bottom-trapped plumes. *J. Phys. Oceanogr.*, **40**, 1631-1650.

McCreary, J. P., S. Zhang and S. R. Shetye (1997): Coastal circulations driven by river outflow in variable-density 1½-layer model. *J. Geophys. Res.*, **102**, 15535-15554.

Mellor, G. L. and T. Yamada (1982): Development of a turbulence closure model for

geophysical fluid problems. *Rev. Geophys. Space Phys.*, **20**, 851-875.

Miguez-Macho, G. and Y. Fan (2012): The role of the groundwater in the Amazon water cycle: 1. Influence on seasonal streamflow, flooding and wetlands. *J. Geophys. Res.-Atm*, **117**, D15113.

Murty, V. S. N., Y. V. B. Sarma, D. P. Rao and C. S. Murty (1992): Water characteristics, mixing and circulation in the Bay of Bengal during southwest monsoons. *J. Mar. Res.*, **50**, 207–228.

Nijssen, B., G. M. O'Donnell, A. F. Hamlet and D. P. Lettenmaier (2001): Hydrologic sensitivity of global rivers to climate change. *Climatic Change*, **50**, 143-175.

Nof, D. and T. Pichevin (2001): The ballooning of outflows. *J. Phys. Oceanogr.*, **31**, 3045-3058.

Open University Course Team (1989): Ocean chemistry and deep-sea sediments. *Linacre House, Jordan Hill, Oxford* OX2 8DP, UK.

Pimenta, F. M., A. D. Kirwan and P. Huq (2011): On the transport of buoyant coastal plumes. *J. Phys. Oceanogr.*, **41**, 620-640.

Piola, A. R., S. I. Romero and U. Zajaczkovski (2008): Space-time variability of the Plata plume inferred from ocean color. *Cont. Shelf Res.*, **28**, 1556–1567.

Pokhrel, Y. N., Y. Fan, G. Miguez-Macho, Pat J.-F. Yeh and Shin-Chan Han (2013): The role of groundwater in the Amazon water cycle: 3. Influence on terrestrial water storage computations and comparison with GRACE. *J. Geophys. Res.-Atm*, **118**, 3233–3244.

Rattray, M. and D. V. Hansen (1962): A similarity solution for circulation in an estuary. *J. Mar. Res.*, **20**, 121-133.

Simpson, J. H. (1997): Physical processes in the ROFI regime. *J. Mar. Systems*, **12**,

3-15.

Tachibana, H., K. Yamamoto, K. Yoshizawa and Y. Magara (2001): Non-point pollution of Ishikari River, Hokkaido, Japan. *Water Sci. and Technol.*, **44(7)**, 1-8.

Tsujino, H., H. Hasumi and N. Suginohara (2000): Deep pacific circulation controlled by vertical diffusivity at the lower thermocline depths. *J. Phys. Oceanogr.,* **30**, 2853-2865.

Unoki, S. (1993): Coastal physical oceanography (*in Japanese*). *Tokai University Press*, 672 pp.

Usui, T., S. Nagao, M. Yamamoto, K. Suzuki, I. Kudo, S. Montani, A. Noda and M. Minagawa (2006): Distribution and sources of organic matter in surficial sediments on the shelf and slope off Tokachi, western North Pacific, inferred from C and N stable isotopes and C/N ratios. *Mar. Chem.,* **98**, 241-259.

Walker, N. D., G. S. Fargion, L. J. Rouse and D. C. Biggs (1994): The great flood of summer 1993: Mississippi River discharge studied. *EOS Trans. AGU,* **75**, 409.

Weingartner, T. J., S. Danielson, Y. Sasaki, V. Pavlov and M. Kulakov (1999): The Siberian Coastal Current: A wind and buoyant-forced Arctic coastal current. *J. Geophys. Res*., **104**, 29697–29713.

Yamamoto, T. and T. Hashimoto (2007): Estuarine circulation and primary production (*in Japanese with English abstract*). *Bull. Coast. Oceanogr.*, **44**, 137-145.

Yankovsky, A. E. (2000): The cyclonic turning and propagation of buoyant coastal discharge along the shelf. *J. Mar. Res.,* **58**, 585–607.

Yoshida, K., K. Domon and T. Watanabe (1977): Physical and chemical conditions on the inshore fishing grounds in Ishikari Bay (*in Japanese with English abstract*).

Sci. Rep. Hokkaido Fish. Exp. Stn., **34**, 1-6.

Yoshikawa, C., Y. Yamanaka and T. Nakatsuka (2005): An ecosystem model including nitrogen isotopes: perspectives on a study of the marine nitrogen cycle. *J. Oceanogr.*, **61**, 921-942.

Yoshimura, T. and I. Kudo (2011): Seasonal phosphorus depletion and microbial response to the change in phosphorus availability in a subarctic coastal environment. *Mar. Chem.*, **126**, 182-192.

A-line data home page by Fisheries Research Agency, Hokkaido and Tohoku Institute. http://hnf.fra.affrc.go.jp/a-line/data/nutri/Data_aline0001-0710.csv. Accessed 28 September 2012

Ishikari River discharge from Water Information System. Ministry of Land, Infrastructure and Transport, Japan. http://www1.river.go.jp/cgi-bin/DspWaterData.exe?KIND=7&ID=301031281101100&BGNDATE=20070131&ENDDATE=20071231&KAWABOU=NO. Accessed 14 October 2013

Tokachi River discharge from Water Information System. Ministry of Land, Infrastructure and Transport, Japan. http://www1.river.go.jp/cgi-bin/DspWaterData.exe?KIND=7&ID=301081281107070&BGNDATE=20060131&ENDDATE=20061231&KAWABOU=NO. Accessed 14 September 2012